ACS Catalysis

pubs.acs.org/acscatalysis Review

Oxidative Dehydrogenation of Propane to Propylene with Soft Oxidants via Heterogeneous Catalysis

Xiao Jiang, Lohit Sharma, Victor Fung, Sang Jae Park, Christopher W. Jones, Bobby G. Sumpter, Jonas Baltrusaitis, and Zili Wu*

Cite This: *ACS Catal.* 2021, 11, 2182−2234

Read Online

ABSTRACT: Oxidative dehydrogenation of propane to propylene can be achieved using conventional, oxygen-assisted dehydrogenation of propane (O_2−ODHP) or via the use of soft oxidants, such as CO_2, N_2O, S-containing compounds, and halogens/halides. The major roles of soft oxidants include inhibiting overoxidation and improving propylene selectivity, which are considered to be current challenges in O_2-assisted dehydrogenation. For both CO_2− and N_2O−ODHP reactions, significant efforts have been devoted to developing redox-active (e.g., chromium, vanadate, iron, etc.), nonredox-type main group metal oxide (e.g., group IIIA, gallium), and other transition metal/metal oxide catalysts (e.g., molybdenum, palladium platinum, rhodium, ruthenium, etc.), as well as zeolite-based catalysts with adjustable acid−base properties, unique pore structures, and topologies. Metal sulfides have shown promising performance in DHP, whereas the development of suitable catalysts has lagged for SO_2- or S-assisted ODHP. Recently, significant efforts have been focused on homogeneous and heterogeneous ODHP using halogens (e.g., Br_2, I_2, Cl_2, etc.) and hydrogen halides (e.g., HCl and HBr) for the development of facile processes for C_3H_6 synthesis. This Review aims to provide a critical, comprehensive review of recent advances in oxidative dehydrogenation of propane with these soft oxidants, particularly highlighting the current state of understanding of the following factors: (i) relationships between composition, structure, and catalytic performance, (ii) effects of the support, acidity, and promoters, (iii) reaction pathway and mechanistic insights, and (iv) the various roles of soft oxidants. Theoretical and computational insights toward understanding reaction mechanisms and catalyst design principles are also covered. Future research opportunities are discussed in terms of catalyst design and synthesis, deactivation and regeneration, reaction mechanisms, and alternative approaches.

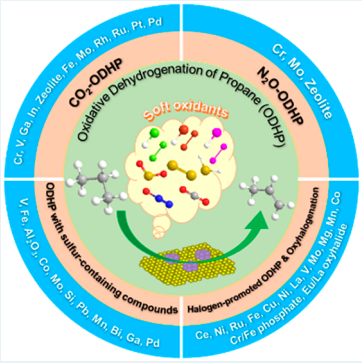

KEYWORDS: *oxidative dehydrogenation of propane, soft oxidants, propane, propylene, carbon dioxide, nitrous oxide, sulfur/halogen-containing compounds*

1. INTRODUCTION

Propylene (C_3H_6) is a crucial organic feedstock for a large number of chemicals in the petrochemical industry.[1] However, it is currently faced with a serious supply deficit because of the rapid growth in market demand for C_3H_6 derivatives.[2] At present, propylene is mainly produced by steam cracking and fluid catalytic cracking (FCC) of naphtha, light diesel, and other oil byproducts, as well as direct dehydrogenation of propane (DHP).[3] Yet, the dehydrogenation process suffers from two inherent drawbacks: (i) the endothermicity-induced thermodynamic limit for C_3H_8 conversion that demands high-energy input and (ii) the rapid catalyst deactivation because of coke formation.[4] Alternatively, oxidative dehydrogenation of propane (ODHP) is attractive because of its exothermicity, which makes it free from the thermodynamic restraint at lower temperatures.[5] Presently, oxygen (O_2) has been widely used as an oxidant for ODHP. Though major progress has been made by using redox-active transition metal oxide catalysts, such as vanadium[1,6] and molybdenum,[6] the presence of O_2 can cause overoxidation of olefins to carbon oxides (CO_x), resulting in the inefficient use of the reactant and low process selectivity.[1,6] Most recently, hexagonal boron nitride (h-BN) has emerged as an outstanding catalyst for O_2−ODHP with high C_3H_6 selectivity (e.g., 79% selectivity with 14% C_3H_8 conversion at 490 °C) and well-suppressed overoxidation.[7] To date studies have mainly focused on low-temperature activity[8] and probing possible active sites and mechanisms, including surface oxy-functionalization, peculiar kinetic features, and radical chemistry in the gas phase.[9,10] Despite potential advantages, concerns of process flammability due to the presence of O_2 exist and might impair practical implementa-

Received: September 11, 2020
Revised: January 11, 2021
Published: February 4, 2021

https://dx.doi.org/10.1021/acscatal.0c03999
ACS Catal. 2021, 11, 2182−2234

Table 1. Reactions Involved in ODHP with Soft Oxidants and Corresponding Changes in Enthalpy and Gibbs Free Energy (Calculated by HSC Chemistry)

CO_2−ODHP	chemical equation	$\Delta H_{25°C}$ (kJ mol^{-1})	$\Delta G_{25°C}$ (kJ mol^{-1})
direct dehydrogenation of propane (DHP)	$C_3H_8 \leftrightarrow C_3H_6 + H_2$ (2-1)	124	86
reverse water-gas shift (RWGS)	$CO_2 + H_2 \leftrightarrow CO + H_2O$ (2-2)	41	29
CO_2−ODHP	$C_3H_8 + CO_2 \leftrightarrow C_3H_6 + CO + H_2O$ (2-3)	164	115
dry reforming of propane (DRP)	$C_3H_8 + 3CO_2 \leftrightarrow 6CO + 4H_2$ (2-4)	621	383
reverse Boudouard reaction	$CO_2 + C \leftrightarrow 2CO$ (2-5)	172	120
propane decomposition I	$C_3H_8 \leftrightarrow 3C + 4H_2$ (2-6)	104	23
propane decomposition II	$C_3H_8 \leftrightarrow CH_4 + 2C + 2H_2$ (2-7)	29	−27
propane cracking	$C_3H_8 \leftrightarrow C_2H_4 + CH_4$ (2-8)	82	41
propylene decomposition	$C_3H_6 \leftrightarrow 3C + 3H_2$ (2-9)	−20	−63
coke formation	$C_3H_8 + 3CO_2 \leftrightarrow 2C + 2H_2 + 2H_2O + 4CO$ (2-10)	359	201
O_2−ODHP	$C_3H_8 + 1/2O_2 \leftrightarrow C_3H_6 + 2H_2O$ (2-11)	−188	−142
N_2O−ODHP	chemical equation	$\Delta H_{25°C}$ (kJ mol^{-1})	$\Delta G_{25°C}$ (kJ mol^{-1})
N_2O decomposition	$N_2O \leftrightarrow N_2 + 1/2O_2$ (2-12)	−82	−104
N_2O−ODHP	$C_3H_8 + N_2O \leftrightarrow C_3H_6 + H_2O + N_2$ (2-13)	−199	−246
SO_2−/S_2(H_2S)−ODHP	chemical equation	$\Delta H_{25°C}$ (kJ mol^{-1})	$\Delta G_{25°C}$ (kJ mol^{-1})
SO_2−ODHP	$C_3H_8 + 1/3SO_2 \leftrightarrow C_3H_6 + 1/3H_2S + 2/3H_2O$ (2-14)	55	22
H_2S partial oxidation	$H_2S + 1/2O_2 \leftrightarrow 1/2S_2 + H_2O$ (2-15)	−157	−155
S_2−ODHP	$C_3H_8 + 1/2S_2 \leftrightarrow C_3H_6 + H_2S$ (2-16)	39	13
H_2S oxidation	$H_2S + 1/2SO_2 \leftrightarrow H_2O + 3/2S$ (2-17)	−73	−45
halogen (X_2)-promoted ODHP and oxyhalogenation	chemical equation	$\Delta H_{25°C}$ (kJ mol^{-1})	$\Delta G_{25°C}$ (kJ mol^{-1})
Cl_2 dehydrogenation	$C_3H_8 + Cl_2 \leftrightarrow C_3H_6 + 2HCl$ (2-18)	−60	−104
Cl_2 regeneration	$2HCl + 1/2O_2 \leftrightarrow Cl_2 + H_2O$ (2-19)	−57	−38
Br_2 dehydrogenation	$C_3H_8 + Br_2 \leftrightarrow C_3H_6 + 2HBr$ (2-20)	21	−24
Br_2 regeneration	$2HBr + 1/2O_2 \leftrightarrow Br_2 + H_2O$ (2-21)	−138	−119
I_2 dehydrogenation	$C_3H_8 + I_2 \leftrightarrow C_3H_6 + 2HI$ (2-22)	115	70
I_2 regeneration	$2HI + 1/2O_2 \leftrightarrow I_2 + H_2O$ (2-23)	−232	−212
C_3H_8 oxychlorination	$C_3H_8 + HCl + 1/2O_2 \leftrightarrow C_3H_7Cl + H_2O$ (2-24)	−176	−161
dehydrochlorination	$C_3H_7Cl \leftrightarrow C_3H_6 + HCl$ (2-25)	58	18
C_3H_8 oxybromination	$C_3H_8 + HBr + 1/2O_2 \leftrightarrow C_3H_7Br + H_2O$ (2-26)	−190	−174
dehydrobromination	$C_3H_7Br \leftrightarrow C_3H_6 + HBr$ (2-27)	72	32
C_3H_8 oxyiodination	$C_3H_8 + HI + 1/2O_2 \leftrightarrow C_3H_7I + H_2O$ (2-28)	−195	−179
dehydroiodination	$C_3H_7I \leftrightarrow C_3H_6 + HI$ (2-29)	78	37

tion.[5,11] To address this issue, an alternative approach is to introduce soft oxidants to replace O_2 for ODHP, such as CO_2, NO_x, and S-containing compounds, as well as halogen/halides. Furthermore, the combination of these soft oxidants in ODHP offers avenues to directly utilize them for chemical conversion to reduce or mitigate acid-gas emissions, thereby adding environment-sustainability-energy benefits to ODHP reactions. For example, an approach of H_2-free CO_2 conversion through the ODHP process using renewable energy could potentially help to reduce CO_2 emissions.[12]

There have been several excellent reviews regarding ODHP with CO_2 as an oxidant.[6,13−16] Most of them have concentrated on the feasibility of utilizing CO_2 as an oxidant for multiple reactions but fewer focused on the details of the ODHP reaction. Also, there has been little covered regarding the development of catalysts for other soft oxidant-assisted ODHP. In addition, the growing "propylene gap" between market demand and productivity and the continuously increasing concerns of environmental burden motivate the need for developing alternative approaches using soft oxidants for sustainable chemical production. All of these factors necessitate a timely analysis and summary of the literature to highlight current progress in catalyst development for alkane conversion utilizing soft oxidants.[17] Therefore, the present Review describes state-of-the-art catalysts that have been developed for the ODHP reaction with soft oxidants and provides an overview of the relationship between catalyst composition, structure, and catalytic performance by extrapolating the reported kinetic and characterization results. Major soft oxidants including CO_2, N_2O, and S-containing compounds, and halogen/halides are reviewed. Among these, CO_2-/NO_x-assisted ODHP reactions have been mostly studied, with significant efforts aimed at developing supported metal oxide catalysts including redox-type transition metal

https://dx.doi.org/10.1021/acscatal.0c03999
ACS Catal. 2021, 11, 2182−2234

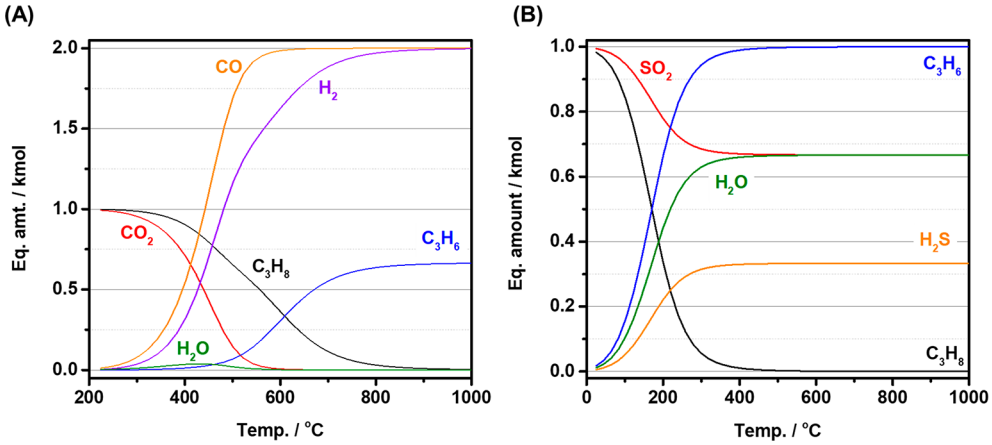

Figure 1. Thermodynamic equilibrium plots. Equilibrium product amounts for CO_2−ODHP (A) and SO_2−ODHP (B), along with temperatures. Equilibrium calculations were performed using HSC Chemistry 6 software by utilizing a Gibbs free energy minimization algorithm. Conditions: C_3H_8/CO_2 = 1/1, C_3H_8/SO_2 = 1/1, and ambient pressure.

oxides (e.g., chromium, vanadium, and iron)[5,18−20] and main group metal oxides with nonredox property (e.g., gallium).[5] Catalytic performance has been found to strongly depend on the dispersion of active species and the nature of the support.[1] Based on the variation of these aspects, the roles of CO_2 and N_2O also differ among catalysts.[21−24]

In sharp contrast to CO_2 and N_2O, sulfur-assisted DHP and ODHP have not been well studied in the context of active sites, structure, composition, or reaction mechanism, despite these soft oxidants being potential promoters for the reaction. Additionally, sulfur compounds, such as H_2S, are a common cocontaminant in natural gas.[25−27] Therefore, significant effort is needed to realize the feasibility of this chemistry. Recently, catalytic oxychlorination over metal phosphate (e.g., $CrPO_4$ and $FePO_4$) and rare earth metal oxides/oxychlorides (e.g., CeO_2 and EuOCl) has garnered more interest, as propylene yields up to 55% have been achieved at 500 °C. Oxychlorination chemistry is found to be largely correlated with the ability of catalyst to oxidize HCl to molecular Cl_2.

In the present Review, we start with a thermodynamic analysis of ODHP with various soft oxidants, then endeavor to cover the progress in ODHP with each soft oxidant, with emphasis on the following aspects: (i) the relationship between composition, structure, and catalytic performance, presenting the composition-induced molecular structure and active sites of catalysts in correlation with observed kinetic behavior; (ii) the influence of the nature of the support and its acidity on the activity and selectivity; and (iii) mechanistic insights, using the relationship between catalyst composition, structure, and catalytic performance in conjunction with theoretical calculations to provide an overview of the working principles of ODHP reactions for different soft oxidants. In addition, this Review underlines various roles of different soft oxidants in these reactions, such as shifting reaction equilibria, reoxidizing catalysts, removing coke, serving as cocatalyst, and possessing competitive adsorption against C_3H_8. A perspective on future research opportunities is also provided at the very end.

2. THERMODYNAMIC ANALYSIS OF OXIDATIVE DEHYDROGENATION OF PROPANE WITH SOFT OXIDANTS

2.1. Thermodynamic Analysis. *2.1.1. CO_2−ODHP.* For the reaction between CO_2 and propane, as listed in Table 1, isotope-labeling experiments reveal the presence of parallel-consecutive reaction networks consisting of direct dehydrogenation (eq 2-1), reverse water−gas shift (eq 2-2), and oxidative dehydrogenation of propane with CO_2 (eq 2-3).[28] As is well-known, one major advantage of O_2−ODHP is its thermodynamic favorability due to its exothermicity (eq 2-11).[29] However, this advantage is no longer relevant in the case of CO_2−ODHP because all major reactions are endothermic. One of the roles of CO_2 is to shift the equilibrium of the ODHP reaction (eq 2-3) to the product side by consuming produced H_2 via the RWGS (eq 2-2), thereby resulting in enhanced C_3H_8 conversion.[22] Meanwhile, dry reforming of propane (DRP, eq 2-4) can also occur and dominate in the same temperature range (Figure 1A). DRP is thermodynamically less restrained than dry reforming of ethane and methane.[12] Of note, since the CO_2−ODHP reaction is a volume-increasing process, adding inert gas such as He and N_2 allows a further enhancement of the equilibrium C_3H_8 conversion.[30] In relation to the effect of C_3H_8/CO_2 ratios, a high CO_2 partial pressure leads to higher C_3H_8 conversion, yet presents a detrimental impact on C_3H_6 production.[30] This stems from the existing competition between DRP and CO_2−ODHP. Therefore, it would be desirable to kinetically inhibit DRP and improve ODHP, which becomes a major challenge in designing efficient catalysts for CO_2−ODHP.[30]

Other side reactions, such as propane decomposition and cracking, as well as propylene decomposition (eqs 2-6−2-9), show less thermodynamic restraint and can readily occur, especially at higher temperatures. Among them, propylene decomposition (eq 2-9) is thermodynamically more favorable than propane decomposition (eq 2-6).[31] Undoubtedly, these reactions have negative impacts on activity and selectivity to the target product propylene at high temperatures in both ODHP and DHP. In addition, the decomposition reactions are one of the major causes of severe catalyst deactivation through coking, with the extent varying depending on the catalysts used. For example, the decomposition reaction (eq 2-

https://dx.doi.org/10.1021/acscatal.0c03999
ACS Catal. 2021, 11, 2182−2234

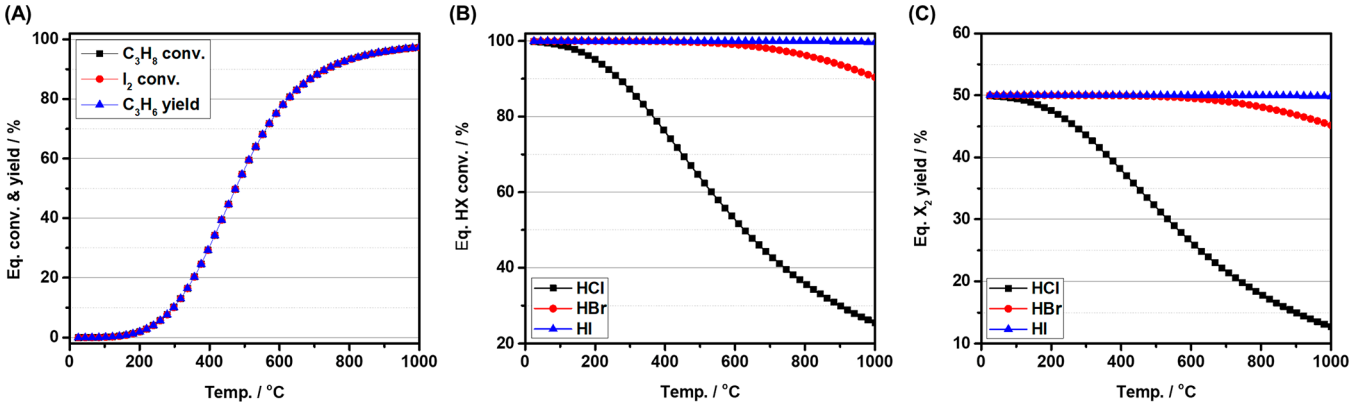

Figure 2. Thermodynamic equilibrium plots. Equilibrium conversion and yield of I-promoted C_3H_8 dehydrogenation reaction (A) as a function of temperature; equilibrium halide (HX) conversion (B) and halogen yield (X_2) (C) of halide oxidation along with temperatures. Conditions: C_3H_8/halide = 2/0.5, C_3H_8/I_2 = 1/1 (stoichiometric ratio, as shown in Table 1), and ambient pressure.

7) dominates and causes severe deactivation in the case of Fe−Ce solid solution catalysts,[29] while the cracking reaction (eq 2-8) may occur on precious Pt catalysts.[32,33] Coke formation (eq 2-10) is one of the major causes of deactivation of the catalysts for CO_2−ODHP.[34] This reaction is endothermic and not a spontaneous reaction at room temperature because of its highly positive Gibbs free energy. However, it becomes spontaneous starting from ∼400 °C (i.e., $\Delta G_{400°C} = -6.5$ kJ mol^{-1}), resulting in catalyst deactivation in turn. In addition, propane hydrogenolysis[32,33] and CO_2 methanation[29] are also reported side reactions during CO_2−ODHP reaction on different catalysts, yet they are scarcely studied. These thermodynamic analyses highlight the critical role of catalysts in kinetically controlling these side reactions.

The reverse Boudouard reaction (eq 2-5) is a side reaction that has been extensively studied for CO_2−ODHP. Its occurrence can aid coke removal, therefore inhibiting coking and improving stability.[23] This is considered one of the positive roles of utilizing CO_2 as an oxidant and is discussed in detail in section 3.5.3.

2.1.2. N_2O−ODHP. Nitrous oxide (N_2O) is also a soft oxidant that has been used widely in ODHP. Two parallel reactions are involved, including N_2O decomposition to O_2 and N_2 (eq 2-12) and the N_2O-assisted ODHP reaction (eq 2-13).[19,35,36] As listed in Table 1, these reactions are exothermic and spontaneous at room temperature. Similar to O_2−ODHP, this reaction route is free of thermodynamic restraint.

2.1.3. ODHP in the Presence of Sulfur-Containing Compounds. Sulfur-containing compounds can serve as either soft oxidants or promoters for ODHP reactions. SO_2 is a potential oxidant for the ODHP reaction (eq 2-14), but the reaction is endothermic and not spontaneous at room temperature (Table 1).[37,38] In comparison to CO_2−ODHP, SO_2−ODHP requires less energy and becomes spontaneous at ∼300 °C (i.e., $\Delta G_{300°C} = -2.1$ kJ mol^{-1}), lower than that for CO_2−ODHP (i.e., $\Delta G_{700°C} = -1.9$ kJ mol^{-1}). An alternative is to use S_2 as an oxidant, and it can be generated/regenerated in situ with the introduction of H_2S in the feed gas.[39,40] In this reaction, H_2S partial oxidation to form S_2 is the initial step (eq 2-15), followed by C_3H_8 dehydrogenation to C_3H_6 with S_2 being reduced to H_2S (eq 2-16). Notably, the thermodynamic restraint of S_2−ODHP is lower than that of N_2O−ODHP (i.e., $\Delta G_{175°C} = -0.4$ kJ mol^{-1}). Considering the exothermicity and spontaneity of H_2S partial oxidation (Table 1), the $S_2(H_2S)$−ODHP reaction can readily occur in the temperature range that has been examined in the literature (400−950 °C). S_2 can be regenerated through partial H_2S oxidation to complete the reaction cycle. Inspired by the Claus Process in the industry,[41] the use of SO_2 has been proposed to oxidize H_2S for S recovery (eq 2-17), which does not pose a thermodynamic limit (Table 1).[42] Despite the thermodynamic feasibility of using molecular sulfur for ODHP, it presents problems because of the temperature sensitivity of sulfur polymorphs. To obtain reactive, diradical species S_2, high temperatures (i.e., 648−800 °C) are required.[43,44] However, thermal cracking of C_3H_8 may occur at such high temperatures, making this reaction more challenging.

2.1.4. Halogen(X_2)-Promoted ODHP and Oxyhalogenation. Halogens have been known as effective promoters for oxidative dehydrogenation of hydrocarbons.[45,46] As listed in Table 1, a halogen can react with C_3H_8 by abstracting hydrogen to form hydrogen halide (eqs 2-18, 2-20, and 2-22), followed by regeneration of the halogen via oxidation with O_2 (eqs 2-19, 2-21, and 2-23).[43] Cl_2-promoted ODHP (eq 2-18) is exothermic and spontaneous at room temperature; therefore, it is free from thermodynamic restraint. Br_2-promoted ODHP is slightly endothermic but still spontaneous at room temperature (eq 2-20). Despite such difference, the thermodynamic restraint is negligible, as 100% C_3H_8 conversion and C_3H_6 yield can be achieved starting from 25 °C (not shown here). Differently, I_2-promoted ODHP is endothermic and not a spontaneous reaction at room temperature (eq 2-22). As presented in Figure 2A, the conversion and yield start to increase at ∼200 °C, gradually rise with temperature, and ultimately reach ∼100% at 1000 °C. Although Cl_2-promoted ODHP is more thermodynamically favorable, the reaction is always fast and nonselective toward the formation of propylene, and there is a risk of explosion under some conditions.[47] On the other hand, I_2-promoted ODHP suffers from limited recycling efficiency of expensive I_2, hampering its industrial implementation.[47] By contrast, Br_2-promoted ODHP is more feasible from a practical point of view, yet a high C_3H_8/Br ratio is necessary to avoid the formation of 2,2-$C_3H_6Br_2$.[47] As reported, the activity of the ODHP reaction in the presence of a halogen relies heavily on the ease with which the hydrogen halide is oxidized back to the halogen.[43] As presented in Figure 2B and 2C, clearly, HI oxidation is thermodynamically more favorable

https://dx.doi.org/10.1021/acscatal.0c03999
ACS Catal. 2021, 11, 2182−2234

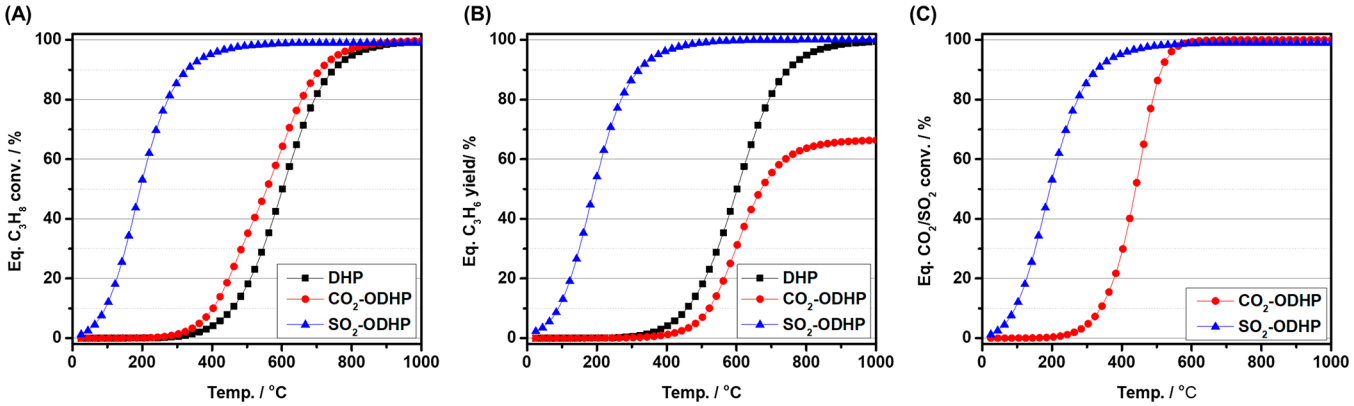

Figure 3. Thermodynamic equilibrium plots. Equilibrium C_3H_8 conversion (A), C_3H_6 yield (B), and CO_2/SO_2 conversion (C) of DHP, SO_2−ODHP, and CO_2−ODHP as a function of temperatures. Conditions: C_3H_8/CO_2 = 1/1, C_3H_8/SO_2 = 1/0.33, and 1 atm.

than the rest, rendering it an outstanding candidate among the halogens in the case of the halo-dehydrogenation reaction.

An alternative is to integrate the functionalization of C_3H_8 and the regeneration of halogen-based compounds in one step via propane oxyhalogenation, followed by the formation of propylene through dehydrohalogenation (eqs 2-24−2-29).[48,49] Dehydrohalogenation requires energy input, but these reactions possess no thermodynamic restraint as a whole, as the total reaction is analogous to O_2−ODHP in eq 2-11. Besides, dehydrohalogenation becomes spontaneous at mild reaction temperatures, such as with HCl at ∼175 °C (i.e., $\Delta G_{175°C}$ = −2.0 kJ mol^{-1}), with HBr at ∼275 °C (i.e., $\Delta G_{275°C}$ = −2.1 kJ mol^{-1}), and with HI at ca. 300 °C (i.e., $\Delta G_{300°C}$ = −1.1 kJ mol^{-1}). Different to halogen-promoted ODHP, the evolution of a halogen via halide oxidation should be suppressed during oxyhalogenation, especially in the gas phase reaction, as it triggers undesired reaction paths including polyhalogenation, coking, cracking, and combustion.[50] In this context, HI is less favorable among halides in oxyhalogenation of propane, whereas HCl is a better candidate. This can also be reflected from the lower values in the changes of enthalpy and Gibbs free energy (Table 1).

2.2. Comparison between ODHP Reaction with Various Soft Oxidants. For ODHP reactions with various soft oxidants discussed above, O_2-/N_2O-assisted ODHP, as well as Cl_2-promoted ODHP and oxyhalogenation, reactions are exothermic and spontaneous, leading to no thermodynamic limit. The remaining reactions including CO_2-/SO_2-assisted and Br_2-/I_2-promoted ODHP reactions are endothermic, whereas the later reactions are thermodynamically more favorable than the former ones if the halogen regeneration reactions are taken into consideration. Between CO_2- and SO_2-assisted ODHP reactions, the former reaction is the least favorable, as CO_2 is both thermodynamically and chemically stable.

Figure 3 compares equilibrium C_3H_8 conversion and C_3H_6 yield for the cases of CO_2− and SO_2−ODHP under their respective stoichiometric ratio, as well as those of the direct dehydrogenation reaction. As presented in Figure 3A, both SO_2− and CO_2−ODHP exhibit higher C_3H_8 conversion than exhibited for direct dehydrogenation, especially for SO_2−ODHP, which displays a rapid increase in C_3H_8 conversion at low temperatures (i.e., 25−200 °C). Such prominence can also be reflected from the highest C_3H_6 yield in Figure 3B, demonstrating the promising role of SO_2 as a soft oxidant for selective C_3H_8 dehydrogenation to C_3H_6. By contrast, CO_2−ODHP shows no conversion between 25 and 200 °C and can only occur at ∼300 °C and above, analogous to the DHP reaction. Although it shows a slight enhancement in C_3H_8 conversion between ∼300 and 800 °C, the C_3H_6 yield of CO_2−ODHP decreases in comparison to that of DHP. High temperatures can trigger both RWGS and DRP reactions because of their endothermicity, which promotes C_3H_8 conversion. Yet, the initiation of these two reactions also results in production of more undesired CO as a carbonaceous product, in turn, reducing the C_3H_6 yield. As shown in Figure 3C, SO_2−ODHP also presents limited thermodynamic restraint, as it shows a similar, rapid increase in SO_2 conversion, reaching the highest value at a lower temperature than CO_2−ODHP. Combined with the above observations, SO_2−ODHP is thermodynamically easier than CO_2−ODHP, along with limited thermodynamic restraint at low temperatures (i.e., 25−200 °C).

3. OXIDATIVE DEHYDROGENATION OF PROPANE WITH CARBON DIOXIDE

To verify the feasibility of CO_2−ODHP, early screening tests were conducted on metal oxides that are active for DHP and O_2−ODHP, including transition metal oxides (Fe_2O_3 and Cr_2O_3) and main-group metal oxides (Ga_2O_3, Al_2O_3, and SiO_2).[51,52] Among them, Ga_2O_3, Fe_2O_3, and Cr_2O_3 exhibit activity, and the C_3H_6 yield decreases in the sequence of $Ga_2O_3 > Fe_2O_3 \geq Cr_2O_3 \gg Al_2O_3 > SiO_2 \sim$ none. For SiO_2 and Al_2O_3-supported counterparts, Cr_2O_3 performs better than the other two metal oxides in terms of both C_3H_8 conversion and C_3H_6 yield and selectivity (Table 2). Continuous efforts have been put forth to clarify the relationship of catalytic performance and essential factors for enhancements, primarily focusing on metal oxide dispersion (e.g., active site configuration, redox properties, etc.) and the nature of the support (e.g., textural property, acid−base property, etc.).[53]

Of note, deactivation is rapid on individual metal oxides, especially on Ga_2O_3 (∼75% from 0.17 to 0.75 h on stream) and Cr_2O_3 (∼78% within the same time range).[52] Carbon deposition and reduction in active sites might be responsible for such rapid deactivation, the dominance of which depends on the nature of metal oxide, roles of CO_2, and reaction mechanisms. Hence, unraveling the deactivation mechanisms and seeking solutions for catalyst regeneration are another area that has been extensively studied. In addition, there are

https://dx.doi.org/10.1021/acscatal.0c03999
ACS Catal. 2021, 11, 2182−2234

Table 2. Summary of Activity Performance of CrOx-Based and Reference Catalysts for CO_2−ODHP Reaction

catalyst	temp (°C)	C_3H_8/CO_2 ratio	conversion (%)		yield (%)	selectivity (%)				ref
			C_3H_8	CO_2	C_3H_6	C_3H_6	C_2H_6	C_2H_4	CH_4	
Cr_2O_3[a]	650	1: 3.6	4.3	1.5	4.3	100	0	0	0	51
$(Cr_2O_3)_5/\gamma\text{-}Al_2O_3$[a]	650	1: 3.6	21.1	9.1	18.3	86.7	0	0	13.3	51
$(Cr_2O_3)_5/TiO_2$[a]	650	1: 3.6	4.8	1.8	4.8	100	0	0	0	51
$(Cr_2O_3)_5$/MCM-41[a]	650	1: 3.6	24.9	4.0	22.2	89.3	0	0	10.7	51
$(Cr_2O_3)_5/ZrO_2$[a]	650	1: 3.6	46.5	24.7	35.4	76.1	0.3	0.3	23.6	51
$(Cr_2O_3)_5/SiO_2$[a]	650	1: 3.6	27.0	5.5	23.0	85.0	2.6	2.6	2.4	51
$(Fe_2O_3)_5/SiO_2$[a]	650	1: 3.6	21.6	1.0	6.9	31.8	37.6	37.6	30.6	51
$(Cr_2O_3)_5/SiO_2$[b]	650	1: 3.6	27.0	5.5	23.0	85.0	2.6	2.6	12.4	51
$(Cr_2O_3)_5\text{-}K_{0.1}/SiO_2$[b]	650	1: 3.6	24.8		19.8	80.0				51
$(Cr_2O_3)_5\text{-}K_{0.2}/SiO_2$[b]	650	1: 3.6	22.3		22.3	100.0				51
$(Cr_2O_3)_5\text{-}K_{0.4}/SiO_2$[b]	650	1: 3.6	31.3		28.6	91.2				51
$(Cr_2O_3)_5\text{-}K_{0.8}/SiO_2$[b]	650	1: 3.6	17.4		15.5	89.1				51
$(Cr_2O_3)_5\text{-}K_{1.0}/SiO_2$[b]	650	1: 3.6	3.0		2.1	70.0				51
$(Cr_2O_3)_5\text{-}Ni_{1.0}/SiO_2$[b]	650	1: 3.6	16.2	15.6	16.2	100.0	0	0	0	51
$(Cr_2O_3)_5\text{-}La_{0.4}/SiO_2$[b]	650	1: 3.6	23.4	5.9	21.1	90.0	0	0	10.0	51
$(Cr_2O_3)_5\text{-}Fe_{5.0}/SiO_2$[b]	650	1: 3.6	20.5	7.2	20.5	100.0	0	0	0	51
$Cr_{3.4}$/SBA-1[c]	550	1: 5	33.2	4.6	29.2	87.9	2.9	3.3	5.9	54
$Cr_{3.4}$/SBA-15[c]	550	1: 5	27.2	3.4	24.3	89.3	2.4	3.5	4.7	54
$Cr_{3.4}/SiO_2$-a[c]	550	1: 5	23.2	3.3	20.9	90.3	1.7	3.1	4.9	54
$Cr_{3.4}/SiO_2$-p[c]	550	1: 5	15.4	2.1	14.3	92.6	1.3	2.5	3.6	54
$(Cr_2O_3)_{0.5}/SiO_2$[d]	600	1: 2	22		~17.16	78		14		55
$(Cr_2O_3)_{1.0}/SiO_2$[d]	600	1: 2	35		~30.45	87		8		55
$(Cr_2O_3)_{3.0}/SiO_2$[d]	600	1: 2	42		~36.54	87		7		55
$(Cr_2O_3)_{5.0}/SiO_2$[d]	600	1: 2	47		~40.89	87		8		55
$(Cr_2O_3)_{7.5}/SiO_2$[d]	600	1: 2	43		~38.70	90		7		55
$(Cr_2O_3)_{0.5}/SiO_2$[d]	650	1: 2	32		~21.44	67		27		55
$(Cr_2O_3)_{1.0}/SiO_2$[d]	650	1: 2	42		~31.50	75		18		55
$(Cr_2O_3)_{3.0}/SiO_2$[d]	650	1: 2	58		~43.50	75		18		55
$(Cr_2O_3)_{5.0}/SiO_2$[d]	650	1: 2	63		~47.88	76		17		55
$(Cr_2O_3)_{7.5}/SiO_2$[d]	650	1: 2	53		ca. 39.75	75		18		55
5%Cr-TUD-1	550	~4: 1	~24	3.5	~17	~90	~2	~2	~6	11
	600	~4: 1	~37	5.6	~31	~81	~10	~10	~10	11
Cr_{10}/SBA-15[e]	600	1: 1	~10	~5	~9	~90				56
$Ni_{0.5}\text{-}Cr_{10}$/SBA-15[e]	600	1: 1	~19	~13	~17	~90				56
Cr_2O_3/SiO_2[f]	400	1: 7	1.9	0	1.9	100	0	0	0	57
	450	1: 7	6.9	0.3	6.7	96.5	0	0	3.5	57
	500	1: 7	15.6	0.8	14.7	94.7	1.0	1.7	2.7	57
	550	1: 7	25.3	1.9	24.0	94.6	1.0	1.9	2.5	57
$Cr_{3.4}$/MCM-41-DHT[g]	550	1: 5.6	~28		26	~92				58
$Cr_{3.4}$/MCM-41-TIE[g]	550	1: 5.6	~29		26	~91				58
Cr_1/SBA-1[h]	550	1: 5	17.0	1.4	15.8	92.7	1.5	3.1	2.7	59
Cr_2/SBA-1[h]	550	1: 5	25.7	2.8	23.2	90.4	2.2	3.2	4.2	59
Cr_3/SBA-1[h]	550	1: 5	30.5	4.0	27.1	88.7	2.8	3.2	5.3	59
Cr_5/SBA-1[h]	550	1: 5	37.2	6.1	31.8	85.4	3.1	3.3	8.2	59
Cr_7/SBA-1[h]	550	1: 5	37.7	6.7	32.0	85.0	3.3	3.3	8.4	59
Cr_{10}/SBA-1[h]	550	1: 5	37.0	6.4	31.7	85.6	3.0	3.2	8.2	59
Cr_{15}/SBA-1[h]	550	1: 5	36.0	6.2	30.9	85.8	3.1	3.1	8.0	59
$(Cr_2O_3)_2/ZrO_2$[i]	550	1: 2	30.7		16.7	54.5		0.92	6.59	60
$(Cr_2O_3)_2/\gamma\text{-}Al_2O_3$[i]	550	1: 2	9.67		7.68	79.4			3.35	60
$(Cr_2O_3)_2/SiO_2$[i]	550	1: 2	19.1		14.7	76.7		2.83	1.93	60
$(Cr_2O_3)_2$/SBA-15[i]	550	1: 2	24.2		20.3	83.9		3.33	1.82	60
c-Cr_5/t-ZrO_2[j]	550	1: 2.6	41		25.4	62			38	61
m-Cr_5/t-ZrO_2[j]	550	1: 2.6	58		30.2	52			48	61
c-Cr_{15}/t-ZrO_2[j]	550	1: 2.6	59		32.5	55			45	61
m-Cr_{15}/t-ZrO_2[j]	550	1: 2.6	58		33.1	57			43	61
$Cr_{3.4}/SiO_2$[k]	600	1: 7	27.7	3.2	25.2	90.8	1.5	4.5	3.2	62
$Cr_{3.4}/SiO_2$ (w/o CO_2)[k]	600		20.7		19.0	92.0	0.4	4.6	3.0	62
$Cr_{3.4}/Al_2O_3$[k]	600	1: 7	29.7	5.5	23.9	80.5	1.2	8.2	10.1	62
$Cr_{3.4}/Al_2O_3$ (w/o CO_2)[k]	600		50.8		47.4	93.4	1.8	1.7	3.1	62

https://dx.doi.org/10.1021/acscatal.0c03999
ACS Catal. 2021, 11, 2182−2234

Table 2. continued

catalyst	temp (°C)	C_3H_8/CO_2 ratio	conversion (%)		yield (%)	selectivity (%)				ref
			C_3H_8	CO_2	C_3H_6	C_3H_6	C_2H_6	C_2H_4	CH_4	
$Cr_{6.8}/Ga_2O_3$[l]	600	1: 7	~49		~33	~68				63
	600		~39		~28	~72				63
$Cr_{6.8}$/MCM-41[m]	550	1: 5	~40	~6	34.9	88.5	~3	~2.5	~6.2	64
Cr_5/MSU-x[n]	450	1: 3	7.0	3.1	6.5	92.2	0	0	7.8	65
	500	1: 3	18.4	8.7	16.8	91.3	2.4	0.4	5.9	65
	550	1: 3	32.8	13.8	28.8	87.8	3.4	1.3	7.5	65
	600	1: 3	50.4	20.7	42.1	83.5	4.5	2.8	9.5	65
$Cr_{0.04}$-SBA-1°	500	1: 5	12.9	1.3	11.8	91.7	1.8	2.3	4.1	66
	550	1: 5	26.7	3.4	24.1	90.2	2.0	3.5	4.3	66
	600	1: 5	39.4	6.2	34.1	86.6	2.3	6.0	5.1	66
	650	1: 5	55.2	9.9	42.3	76.7	2.8	12.8	7.7	66
$Cr_{5.0}$/AC[p]	550	1: 5	39.8		34.5	86.7	1.6	2.8	7.5	67
$Cr_{10}O_x/SiO_2$[q]	496	1: 1	4.9	1.1	3.9	79				68
$Ru_{0.5}Cr_{10}O_x/SiO_2$[q]	496	1: 1	5.8	2.1	~4.5	~78				68
$Ru_{0.75}Cr_{10}O_x/SiO_2$[q]	496	1: 1	7.0	3.1	~5.8	~82.5				68
$Ru_{1.0}Cr_{10}O_x/SiO_2$[q]	496	1: 1	9.0	5.6	7.7	85				68
$Ru_{2.0}Cr_{10}O_x/SiO_2$[q]	496	1: 1	6.4	7.9	~4.5	~70				68
$Ru_{3.0}Cr_{10}O_x/SiO_2$[q]	496	1: 1	4.5	11.5	1.8	39				68
$Cr_{1.27}$-MSU-x[r]	600	1: 1	~44		~38	~86				69
$Cr_{1.27}$/MSU-x[r]	600	1: 1	~36		~30	~84				69
$Cr_{0.25}/SiO_2$-MVS[s]	600	1: 2	30.2		26	87.2		7.4		70
$Cr_{0.5}/SiO_2$-MVS[s]	600	1: 2	43.9		37	85.1		7.4		70
$Cr_{1.3}/SiO_2$-MVS[s]	600	1: 2	47.3		39	83.2		7.8		70
$Cr_{6.0}/SiO_2$-MVS[s]	600	1: 2	85.1		69	80.8		7.6		70
Cr_{10}/SiO_2-MVS[s]	600	1: 2	80.6		63	77.6		7.5		70
Cr_7/MSS-1[t]	600	1: 4	~55	13.3	45.1	~82				71
Cr_7/MSS-2[t]	600	1: 4	~71	15.3	55.7	~79				71
Cr_7/MSS-3[t]	600	1: 4	~48	10.5	41.4	~86				71
Cr_7/MSS-4[t]	600	1: 4	~43	5.7	37.8	~87				71
$Cr_2O_3-ZrO_2$[u]	550	1: 2	33.6		28.4	84.6	0	0.5	14.9	72
$Cr_2O_3-ZrO_2$-110[v]	550	1: 2	44.3		37.3	84.3	0	0.5	15.2	72
$Cr_2O_3-ZrO_2$-150[v]	550	1: 2	51.1		41.7	81.7	0	0.5	17.8	72
$Cr_2O_3-ZrO_2$-180[v]	550	1: 2	53.3		42.1	79.0	0	0.5	20.5	72
7Cr-ZrO_2[w]	550	1: 2	68		40.5	ca. 59.6				73
$Cr_{0.25}$-SiO_2[x]	600	1: 2	38	4	31	81	7	11	0	21
$Cr_{0.5}$-SiO_2[x]	600	1: 2	50	9	37	75	8	9	0.5	21
$Cr_{1.0}$-SiO_2[x]	600	1: 2	62	16	45	73	8	8	2.8	21
$Cr_{2.0}$-SiO_2[x]	600	1: 2	71	19	47	66	13	7	2.5	21
$Cr_{0.25}$-SiO_2[y]	600	1: 2	57		32	56	11	19	0.3	21
$Cr_{0.5}$-SiO_2[y]	600	1: 2	70		37	53	15	18	1.2	21
$Cr_{1.0}$-SiO_2[y]	600	1: 2	77		35	46	9	18	3.6	21
$Cr_{2.0}$-SiO_2[y]	600	1: 2	82		35	43	14	18	7.3	21
$(Cr_2O_3)_5/Al_2O_3$[z]	550	1: 1			3.3	92.9	0.5	1.6	5.0	74, 75
$(Cr_2O_3)_5$/AC[z]	550	1: 1			9.3	93.6	1.3	2.1	3.0	74, 75
$(Cr_2O_3)_5/SiO_2$[z]	550	1: 1			9.1	94.0	1.8	1.6	2.6	74, 75
$(Cr_2O_3)_5/Al_2O_3$[aa]	550	1: 1			~1.4					74, 75
$(Cr_2O_3)_5$/AC[aa]	550	1: 1			~3.5					74, 75
$(Cr_2O_3)_5/SiO_2$[aa]	550	1: 1			~6.1					74, 75

[a]Values in the subscript are Cr loadings in weight basis. [b]Values in the subscript of Cr_2O_3 and K represent loadings of Cr and K in weight basis, respectively. [c]Cr loading is 3.4 wt. %. SiO_2-a and SiO_2-p are commercial silica materials from Sigma-Aldrich and POCh. [d]Values in subscript are Cr loadings. [e]Cr and Ni loadings are 10 and 0.5 wt. %. [f]Cr loading was 0.92 wt. %. Data were collected at TOS = 0.2 h. [g]Cr loading is 3.4 wt. %. DHT and TIE represent the methods to prepare the catalysts and stand for direct hydrothermal synthesis and template-ion exchange, respectively. [h]Values in the subscript represent Cr loadings. Data were collected at TOS = 10 min. [i]Cr_2O_3 loading is 2 wt. %. [j]Cr loading is 5 wt. %. m and c stand for microwave-assisted hydrothermal method and conventional hydrothermal method, respectively. Data were collected at TOS = 5 min. [k]Cr loading is 3.4 wt. %. Data were collected at TOS = 0.2 h. [l]Cr loading is 6.8 wt. %. [m]Cr loading is 6.8 wt. %, and catalysts are prepared by incipient wetness impregnation (IWI). Data were collected at TOS = 0.17 h. [n]Cr_2O_3 loading is 5 wt. %. [o]Values in the subscript represent Cr/Si molar ratio. [p]Cr loading is 5 wt. %. [q]Values in the subscript of Ru and Cr stand for loadings of Ru and Cr, respectively. Data were collected at TOS = 50 min. [r]Cr loading is 1.27 wt. %. Cr-MSU-x and Cr/MSU-x are prepared by $(N^0\ M^{n+})I^0$ pathway and IWI, respectively. [s]Values in the subscript represent Cr loadings in wt. %. MVS stands for metal vapor synthesis. [t]Cr loading is fixed at 7 wt. %. Data were collected at TOS = ~10 min. [u]Catalyst is prepared by coprecipitation method, and Cr loading is 10 wt. %. Data were collected at TOS = 10 min. [v]Values in the subscript represent Cr

https://dx.doi.org/10.1021/acscatal.0c03999
ACS Catal. 2021, 11, 2182−2234

Table 2. continued

loading in wt. %. Data were collected at TOS = 20 min. [w]7Cr means the Cr content in the form of Cr/(Cr + Zr) = x/100, molar ratio. [x]Values in the subscript represent Cr loading in wt. %. Data were collected at TOS = 20 min. O_2 is fed in the feed gas with the $C_3H_8/CO_2/CO$ at 5: 10: 1. [y]Catalysts are prepared by hydrothermal treatment at temperatures (110, 150, and 180 °C) after coprecipitation, and Cr loadings are 10 wt. %. [z]Data were collected at TOS = ∼30 min. [aa]Data were collected at TOS= 6 h.

other challenges to be addressed, such as the competitive adsorption between CO_2 and C_3H_6 and elusive reaction mechanisms.

On the basis of the achievements in these areas, this section mainly covers the progress in (i) developing fundamental understanding of the relationship between catalyst composition, structure, and activity with representative redox-active and nonredox metal oxide catalysts (i.e., loading-dependent evolution of active sites during reaction, support/promoter nature), (ii) catalyst deactivation and regeneration, and (iii) the roles of CO_2 in affecting reaction paths, modifying catalyst surfaces, and coke removal.

3.1. Redox-Type Catalysts. *3.1.1. Chromium (Cr)-Based Catalysts. 3.1.1.1. Identification of Active Cr Sites and Redox Cycles. Cr Content-Dependent Evolution of Cr Sites.* For supported Cr catalysts, the generation and dispersion of Cr species at lower oxidation states (i.e., Cr^{3+}/Cr^{2+}) are of importance in attaining high C_3H_6 yield in CO_2−ODHP, the structural evolution of which relies heavily on Cr coverage and textural properties of the support.[5] Table 3 summarizes the surface density of commonly used redox-active metal oxides on supports. On SiO_2-supported Cr catalysts, the loading-dependent evolution of Cr species follows the sequence of grafted Cr^{6+} → dispersed Cr^{6+} oxide → microcrystalline Cr^{3+} → crystalline α-Cr_2O_3 with increasing Cr loading.[76] α-Cr_2O_3 is the most thermodynamically stable chromium oxide phase, yet inactive for catalysis because of its high resistance to reduction and oxidation.[54] Generally, a monolayer Cr coverage is the threshold for the optimal Cr-dependent activity. Below monolayer coverage, the C_3H_6 yield usually increases with an increase in Cr content; but beyond this threshold, the excess redox Cr species cannot be attached with the support so that unstable Cr species may decompose to nonredox crystalline α-Cr_2O_3 particles with no activity.[54] An analogous monolayer "threshold" is also known for supported VO_x catalysts for the O_2−ODHP reaction.[77]

Table 3. Monolayer Surface Coverages of Supported Metal Oxide Catalysts (atoms nm^{-2})[78,79]

	Al_2O_3	TiO_2	ZrO_2	Nb_2O_5	SiO_2
Re	2.3	2.4	3.3		0.54
Cr	4.0	6.6	9.3		0.6
Mo	4.6	4.6	4.3	4.6	0.3
W	4.0	4.2	4.0	3.0	0.1
V	7.3	7.9	6.8	8.4	0.7
Nb	4.8	5.8	5.8		0.3

Reproduced with the permission from ref 78. Copyright 1996 Elsevier B.V

The variation of Cr structures is also sensitive to Cr loadings, which can determine the activity. Botavina et al. have prepared a series of Cr_2O_3/SiO_2 catalysts with a wide range of Cr loadings (0.5−7.5 wt. %) and have attained comparable activity to that required by industrial processes (e.g., conversion ≥ 50% and olefin ≥ 90%).[55] $(Cr_2O_3)_5/SiO_2$ (5 wt. % Cr loading) exhibits the best performance in C_3H_8 conversion and C_3H_6 selectivity, while $(Cr_2O_3)_{7.5}/SiO_2$ with a higher Cr loading leads to reductions in both (Table 2). Diffuse reflectance UV−vis results reveal the evolution of Cr structures along with the loadings: (i) Cr(VI) is in the form of mono-, di-, and polychromates for all fresh catalysts and (ii) Cr(III) only exists in the form of (α-Cr_2O_3) at higher Cr loadings (i.e., ≥ 3.0 wt. %). The prominent activity on $(Cr_2O_3)_5/SiO_2$ correlates to well-dispersed mono- and dichromates; yet high Cr loadings give rise to the formation of extended polychromate structures that are less active.

Redox Cycle. As shown in Figure 4, there exists a clear correlation of C_3H_6 yield with the number of redox sites, corroborating the important role of redox Cr species in assuring high C_3H_6 yield in CO_2−ODHP.[22] However, the redox cycles are not unambiguously established. There are two major types of redox cycles that have been proposed, namely, $Cr^{6+} \leftrightarrow Cr^{3+}/Cr^{2+}$ and $Cr^{3+} \leftrightarrow Cr^{2+}$. The former redox cycle is proposed on MCM-41- (Figure 5), TUD-1-,[11] and Al_2O_3-supported Cr catalysts,[80−82] while the latter is known on Ni-promoted[56] (Figure 5) and unpromoted CrO_x/SiO_2.[57] On the basis of these supported Cr catalysts, one can postulate a potential correlation of the nature of the support with Cr reducibility, as well as with Cr loading-dependent dispersion. Major progress has been made in unveiling the later correlation. However, the support effect has been scarcely studied.

On Cr-MCM-41 with high Cr dispersion, CO_2 enables the completion of the redox cycle by reoxidizing the reduced $Cr(III)O_6$ to $Cr(VI)O_4$, though the oxidation efficiency is not comparable to O_2 (Figure 5).[58] In contrast, Michorczyk et al. reported a redox cycle of $Cr^{3+} \leftrightarrow Cr^{2+}$ on CrO_x/SiO_2 below a monolayer Cr coverage (0.34 Cr nm^{-2}, see Table 3).[57] As shown in Table 2, C_3H_8 conversion increases with the rise of reaction temperatures, and C_3H_6 selectivity is higher than 94%. Meanwhile, CO_2 conversion is evident, yet the values are not comparable to those of C_3H_8 conversion. In situ diffuse reflectance spectroscopy (DRS) spectra reveal that the reoxidation of Cr^{3+} to Cr^{6+} (eq 3-1) hardly occurs during regeneration, even if the catalyst is exposed to an excess of CO_2. Hence, the redox-property scenario in O_2−ODHP (i.e., $Cr^{6+} \rightarrow Cr^{3+}/Cr^{2+}$) is unlikely replicated in CO_2−ODHP (eq 3-2). Given their capability to catalyze both DHP and RWGS reactions,[83] CrO_x might take part in the reaction through the redox cycle of $Cr^{3+} \rightarrow Cr^{2+}$ with H_2, formed via RWGS (eq 3-3), as the reducing agent, followed by reoxidation of Cr^{2+} to Cr^{3+} by CO_2 (eq 3-4). Of note, such a case might only happen below a monolayer coverage, because the migration of Cr^{3+} species to form stable Cr_2O_3 clusters is slow, giving rise to the further reduction of $Cr^{3+} \leftrightarrow Cr^{2+}$.

$$Cr_2O_3 + 3CO_2 = 2CrO_3 + 3CO \quad (3\text{-}1)$$

$$Cr_2O_3 + 1.5O_2 = 2CrO_3 \quad (3\text{-}2)$$

$$Cr^{3+}O^- + H_2 = Cr^{2+} + H_2O \quad (3\text{-}3)$$

$$Cr^{2+} + CO_2 = Cr^{3+}O^- + CO \quad (3\text{-}4)$$

https://dx.doi.org/10.1021/acscatal.0c03999
ACS Catal. 2021, 11, 2182−2234

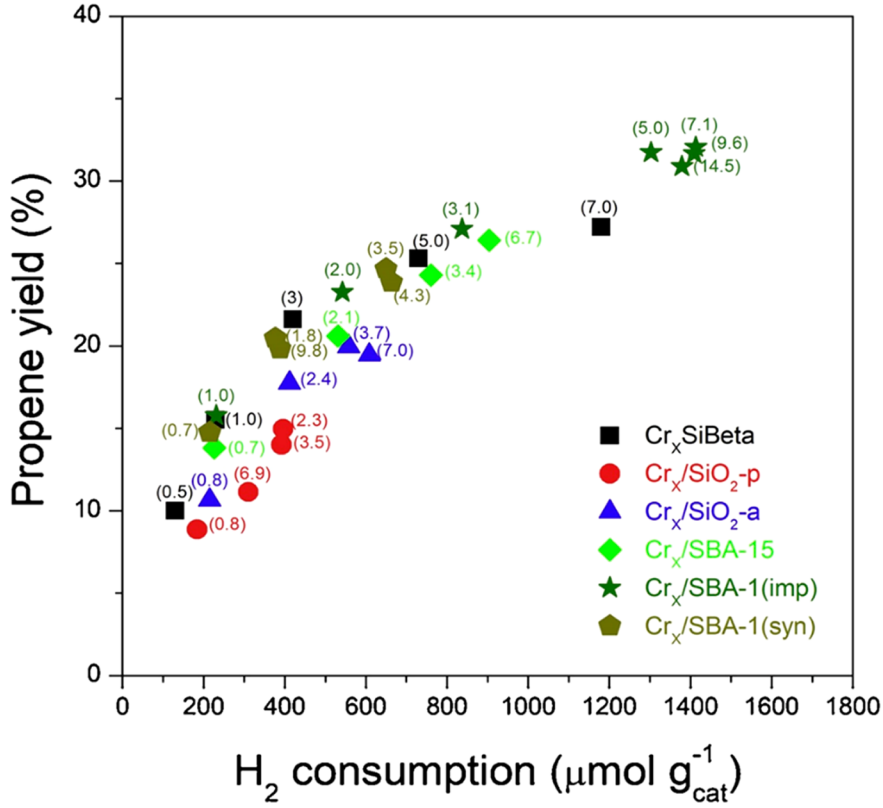

Figure 4. Variation of propylene yield with hydrogen consumption (proportional to number of Cr redox species) for several different CrO_x-based catalysts in CO_2−ODHP. Hydrogen consumption was calculated per catalysts weight based on H_2-TPR experiments. Sample notations: Cr_x/SBA-1(imp), Cr_x/SBA-15, Cr_x/SiO_2-a (silica support from Aldrich), and Cr_x/SiO_2-p (silica support from Polish Chemical Reagents) catalysts obtained by impregnation; Cr_x/SBA-1(syn) prepared by Cr incorporation during SBA-1 synthesis. In the figure, the values in the brackets indicate total Cr content in the catalysts. Reproduced with permission from ref 22. Copyright 2020 Elsevier B.V.

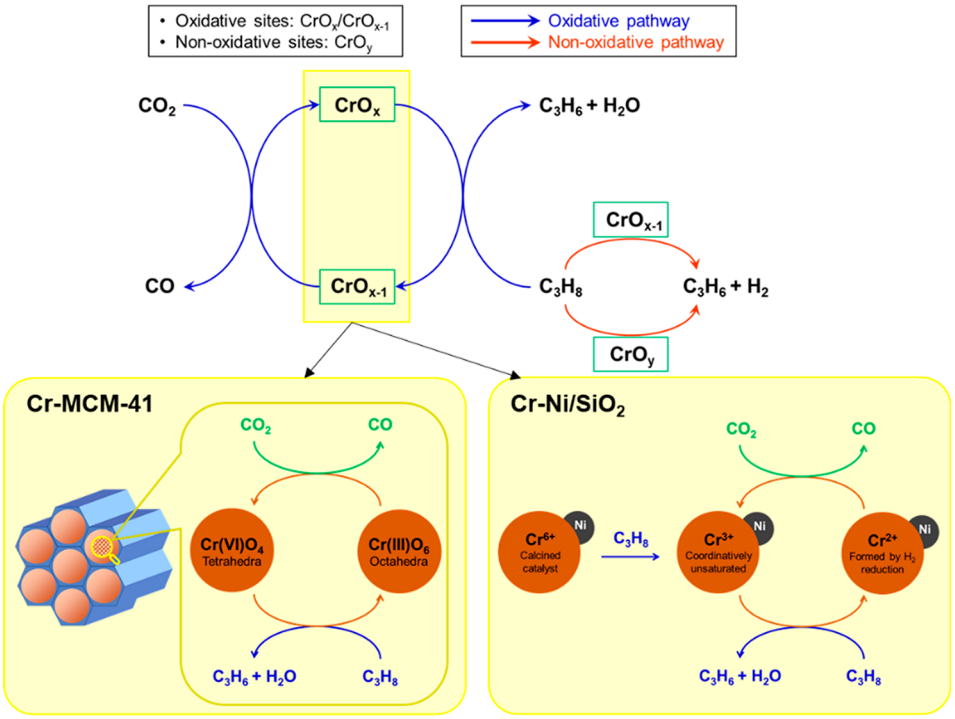

Figure 5. Proposed redox and nonredox reaction pathways and their relationship with Cr active sites in CO_2−ODHP on supported Cr catalysts. Reproduced with the permission from ref 59. Copyright 2012 Elsevier B.V. Proposed redox cycles of Cr sites on Cr-MCM-41 and Cr−Ni/SiO_2 for CO_2−ODHP were adapted on from refs 80 and 81 and ref 56, respectively.

https://dx.doi.org/10.1021/acscatal.0c03999
ACS Catal. 2021, 11, 2182−2234

Comprehensive reaction paths have been proposed by incorporating both redox and nonredox sites.[59] As illustrated in Figure 5, the oxidized CrO_x and reduced CrO_{x-1} sites are proposed as the major active sites responsible for C_3H_8 dehydrogenation. Generally, the C_3H_6 yield increases with the concentration of Cr^{6+} species, indicative of their crucial role as precursors to form active species. At the initial stage, the reduction of Cr^{6+} species leads to the generation of Cr^{2+}/Cr^{3+} species (i.e., CrO_{x-1}), which triggers the C_3H_6 formation through a nonoxidative pathway. Also, the nonredox Cr^{3+} sites (CrO_y), formed through Cr^{3+} oxide agglomeration, may contribute to the nonoxidative pathway, though insignificantly. Alternatively, the presence of CO_2 contributes to the completion of the redox cycle, namely, $CrO_x \leftrightarrow CrO_{x-1}$, enabling C_3H_6 formation through the oxidative pathway. The presence of a redox cycle can boost the H_2 consumption via RWGS and therefore promote C_3H_6 formation by shifting the equilibrium of the ODHP to the product side.

3.1.1.2. Effects of Support. The nature of the support is important in affecting the dispersion and evolution of Cr species, therefore determining the intrinsic activity. Among support materials, metal oxides have been widely used, such as Al_2O_3, ZrO_2, CeO_2, TiO_2, and SiO_2. For better Cr dispersion, ordered, mesoporous materials, such as SBA-1/SBA-15/MCM-41, and carbon-based supports with tunable surface functional groups are also promising candidates. To clarify the support effect, the following aspects have been explored, including (i) metal−support interaction, (ii) acid−base properties in the adsorption and activation of reactant molecules, and (iii) textural properties and their correlation with dispersion of Cr species and mass transfer.

Metal Oxides. In an early work led by Ge et al., the prominent activity of Cr_2O_3/SiO_2 has been confirmed via screening tests on Cr_2O_3, Cr_2O_3/SiO_2, Cr_2O_3/γ-Al_2O_3, Cr_2O_3/ZrO_2, Cr_2O_3/TiO_2, and Cr_2O_3/MCM-41 (Table 2).[51] Relatively weak metal−support interaction appears to benefit C_3H_6 formation, such as SiO_2.[60] In the presence of CO_2, the partially oxidized Cr_2O_3 surface and the boundaries of Cr_2O_3 and SiO_2, are responsible for the improved C_3H_6 yield.[74,75] Although high CO_2 conversion can be achieved on the ZrO_2-supported counterpart, its strong basicity leads to lower C_3H_6 selectivity but higher selectivity toward CO and CH_4.[51,60,61] Competitive adsorption between CO_2 and C_3H_8 occurs on supports with amphoteric property, such as γ-Al_2O_3, leading to decreased catalytic performance (Table 2), especially at higher CO_2 partial pressures.[62,82] MCM-41-supported Cr catalysts exhibit comparable activity to the SiO_2-supported counterpart, which is associated with its ordered mesoporous structure with large surface area and pore volume.[51] Such prominence is also evident on SBA-15 and SBA-1 (Table 2).[54] The ordered mesoporous structure and large surface area not only helps to improve Cr surface density but also the dispersion of the Cr^{6+} species, thereby benefiting C_3H_6 formation.

Because of the high activity of Ga_2O_3 in CO_2−ODHP (discussed in section 3.2.1), it has been applied as support for Cr catalysts with expectation of synergistic effect. Michorczyk et al. have prepared Cr_2O_3/β-Ga_2O_3 with various loadings for CO_2−ODHP.[63] The CO_2-promoting effect is observed on $Cr_{6.8}/\beta$-Ga_2O_3 at temperatures higher than ∼570 °C (Table 2). Adding Cr neutralizes the acid sites on β-Ga_2O_3, leading to coking resistance through a CO_2-induced reverse Boudouard reaction.

Ordered, Mesoporous Silica (MCM-41, MSU-x, SBA-15/SBA-1, and TUD-1). As mentioned above, the redox properties and appropriate dispersion of Cr species on the surface are important for CO_2−ODHP. To achieve high activity and selectivity, introducing mesoporous silica as a support offers avenues to tune these factors. The materials that have been explored include MCM-41, MSU-x, SBA-15/SBA-1, and TUD-1.

MCM-41, a typical mesoporous molecular sieve, features well-ordered channels, controllable uniform pore size (2−10 nm), and large surface area, and can be incorporated by heteroatoms, such as Cr, into the wall substituting Si^{4+} and forming isolated active centers.[84] Direct hydrothermal synthesis (DHT) and template-ion exchange (TIE) methods are effective in tuning the locations and coordination environments of the incorporated metal cations.[84−86] Wang et al. have prepared Cr-incorporated MCM-41 catalysts by both DHT and TIE methods, and found different Cr species in the calcined forms.[58] DHT results in monochromate species on the wall surface of MCM-41, while TIE produces a large quantity of polychromate species other than monochromate. Despite such differences, both catalysts are reduced from Cr^{6+} to Cr^{3+} oxide clusters during reaction, which explains their analogous activity and selectivity (Table 2). X-ray absorption (XANES and EXAFS) spectroscopic measurements reveal the reduction of $Cr(VI)O_4$ in tetrahedral coordination in the formed monochromate species to $Cr(III)O_6$ octahedra during the reaction, in which $Cr(VI)O_4$ is more active than $Cr(III)O_6$.[80,81] CO_2 enables the completion of the redox cycle by participating in the reoxidation of $Cr(III)O_6$ to $Cr(VI)O_4$ in Cr-MCM-41 (Figure 5). In a later work, Piotr et al. have also found prominent activity and selectivity on MCM-41-supported CrO_x catalysts with optimal Cr loading at 6.8 wt. % (Table 2).[64] Similarly, well-dispersed Cr species play a pivotal role in promoting the catalytic performance; yet differently, a redox cycle of $Cr^{2+} \leftrightarrow Cr^{3+}$ is proposed (Figure 5), analogous to the scenario reported by Yun et al.[56] and Ohishi et al.[87]

MSU-x features high surface area (600−1000 $m^2\ g^{-1}$ and 3−5 nm pore size) and 3D wormlike channels, which can potentially improve the dispersion of Cr species and facilitate the diffusion of reagent molecules.[88] For these reasons, Liu et al. have prepared Cr-MSU-x catalysts with a wide range of Cr loadings (i.e., 1−20 wt. %) for CO_2−ODHP.[65] C_3H_8 conversion reaches the highest at Cr = 5 wt. % at 550 °C (Table 2). At 600 °C, C_3H_8 conversion is as high as 50%, and C_3H_6 selectivity is 83.5%. A Cr loading-dependent transformation of Cr sites has been evident in the calcined catalysts, such as Cr(VI) in monochromate → V(VI) in di/trichromates → crystalline/amorphous α-Cr_2O_3. The trade-off between active Cr(VI) and α-Cr_2O_3 with elevated Cr loading determines the optimized Cr loading at 5 wt. %, and coordinatively unsaturated Cr(III) ions are active sites responsible for dehydrogenation.

A comparative study, led by Zhang et al., finds that a SBA-15-supported Cr catalyst exerts better catalytic performance and stability than γ-Al_2O_3, SiO_2, and ZrO_2-supported counterparts for CO_2−ODHP (Table 2).[60] Such prominent activity and coking resistance are associated with the preservation of active Cr(III) species in the presence of CO_2, weak metal−support interactions, and the high surface area of the support. Similarly, SBA-1 is also a promising candidate not only because of its high surface area, narrowed

https://dx.doi.org/10.1021/acscatal.0c03999
ACS Catal. 2021, 11, 2182−2234

pore size, and 3D channels but also due to its characteristic cubic mesoporous phase, which is mechanically more stable than materials with hexagonal mesopores.[89,90] This is valuable for industrial applications where catalyst shaping processes are necessary. Michorczyk et al. have prepared Cr-SBA-1 catalysts via a direct synthesis method using cetyltrimethylammonium bromide (CTAB), ammonium dichromate, and tetraethyl orthosilicate as surfactant, Cr precursor, and Si source, respectively.[66] The as-prepared catalysts present characteristic 3D pore structures, though the incorporation of Cr results in limited perturbation of the structural order. The catalytic performance varies depending on the Cr/Si molar ratios and reaches optimal performance at Cr/Si = 0.04 (Table 2). The same group has also continued their work by exploring the Cr loading-dependent evolution of Cr species on Cr/SBA-1 catalysts.[59] Incipient wetness impregnation (IWI) is used to prepare the catalysts because this allows a higher density of active sites, while preserving the pore structure. Cr^{6+}, dispersed Cr^{5+}, and crystalline α-Cr_2O_3 have been observed on Cr/SBA-15 catalysts in the calcined form, with Cr loading increasing from 1 to 15 wt. %. Cr^{6+} species in the form of mono- and dichromates present in all catalysts, regardless of Cr loadings; Cr^{5+} species exist at Cr loading below 7 wt. %; inactive α-Cr_2O_3 species can be detected at a Cr loadings higher than 5 wt. %. As compared in Table 2, the catalytic performance reaches maximum at Cr = 7 wt. % and barely changes with elevated Cr loadings, which is associated with the dominance of inactive α-Cr_2O_3 species. Similarly, activity performance is a function of well-dispersed Cr^{2+}/Cr^{3+} sites and the redox cycle, the formation of which stems from the rapid reduction of Cr^{6+} species upon contact with C_3H_8.

To better disperse CrO_x species and facilitate mass transfer within the pores, TUD-1, with high surface area and unique 3D mesoporous network structure, has been introduced as support.[11] To ascertain the formation of CrO_x with small, uniform crystals, a microwave irradiation method is used to prepare the catalysts. 5%Cr/TUD-1 exhibits higher C_3H_8 conversion at ∼24% and C_3H_6 selectivity at ∼90% at 550 °C (Table 2), while good stability at 8 h on stream is observed on 7%Cr/TUD-1. High catalytic performance can be attributed to the unique 3D mesoporous structure enabling the encapsulation of CrO_x particles with high dispersion.

Activated Carbons (ACs). ACs are also promising support materials because of their high surface area and abundant surface oxygen functional groups (OFGs) with tunable acid−base properties. Kuśtrowski et al. have introduced HNO_3-activated AC with high surface area support for Cr catalysts and obtained optimal catalytic performance at Cr = 5 wt. % (Table 2).[67] Carbonyl and carboxyl species, known as respective basic and acid OFGs on the surface of AC, are identified as additional active sites in the reaction. Their gradual reduction with time on stream (TOS) is linked with the fast deactivation other than coking.

3.1.1.3. Effects of Promoter. CO_2 has been proposed to participate in the redox cycles of $Cr^{2+} \rightarrow Cr^{3+}$[59,64] or $Cr^{3+} \rightarrow Cr^{6+}$;[56,80,91] however, its oxidation potential is rather weak. Besides, CO_2 is quite inert and not easily activated by CrO_x.[59] The addition of O_2 in the reactants as a co-feed with CO_2 has been initially proposed to overcome these issues, yet the selectivity drops.[55] An alternative is to introduce promoters to facilitate CO_2 activation on the Cr_2O_3 catalysts and to improve its oxidizing ability for selective and stable performance.

Alkali Metal Oxides. Because of their basic property, alkali metal oxides have been widely used as promoters for CO_2 adsorption and activation in CO_2 hydrogenation reactions.[92] Ge et al. have prepared K-promoted Cr_2O_3/SiO_2 with various K loadings for CO_2−ODHP.[51] The addition of K results in the reduction of C_3H_8 conversion in comparison to unpromoted Cr_2O_3/SiO_2, though a higher C_3H_6 selectivity is obtained (Table 2). According to characterization results, K addition modifies the Cr_2O_3 surface by decreasing its redox potential and surface acidity, resulting in the drop in C_3H_8 conversion. Similar impacts are evident on Li-/Na-promoted Cr_2O_3/SiO_2 catalysts, except that the stability of C_3H_6 yield can be improved by K.[93] IR results show that a substantial part of protons in hydroxyl groups on the surface of Cr_2O_3/SiO_2 are replaced by alkali metal ions, the loss of which accounts for the drop in activity on promoted catalysts.

Transition Metals (Ru and Ni). Ru is a potential promoter because of its high activity in CO_2 hydrogenation.[94,95] Jin et al. have prepared Ru-promoted Cr_2O_3/SiO_2 and clarified the Ru loading-dependent reactivity in CO_2−ODHP.[68] C_3H_8 conversion presents a volcano-like trend that maximizes at Ru = 1 wt. % with almost doubled C_3H_8 conversion and improved C_3H_6 selectivity in comparison to the unpromoted counterpart (Table 2). A proper amount of Ru plays an important role in optimizing activity and selectivity because it can balance the RWGS and C_3H_6 reforming.

Ni is also a potential candidate because of its activity in CO_2 activation for CO_2 reforming reactions[96,97] and RWGS.[98−100] Yun et al. have prepared Ni-promoted CrO_x/SBA-15 catalysts for CO_2−ODHP.[56] In the calcined form, NiO and CrO_x distribute in the vicinity of one another, and the presence of Ni can affect the Cr species by converting them to nickel chromate. The Ni-promoted catalyst outperforms the unpromoted counterpart in both activity and stability (Table 2). Particularly, CO_2 conversion has been significantly improved. The major role of Ni is to facilitate CO_2 dissociation to CO and an adsorbed O* next to the Ni site, which can subsequently regenerate Cr^{3+} via reoxidation.

3.1.1.4. Innovation in Preparation Methods. Dispersion and types of Cr^{6+} species in the calcined catalysts are crucial in determining the catalytic performance, and can be generally tuned by pH, ligand effect, and surfactant. Synthetic approaches include $(N^0M^{n+})I^0$ pathway,[69] metal vapor synthesis method,[70] and sol−gel method.[71] Efforts are also devoted to improving selectivity while preserving activity of CrO_x/ZrO_2 catalysts, as they present outstanding C_3H_8 conversion and C_3H_6 yield, though CH_4 is dominant (section 3.1.1.2). Synthetic methods revolve around tuning the surface acid−base properties, crystalline structure, and textural properties. Developed synthetic approaches include hydrothermal methods[61] and acid−base pairs.[101]

$(N^0M^{n+})I^0$ Pathway Driven by Electrostatic Driving Force. Dispersion of Cr^{6+} species and crystallite size are sensitive to pH during the synthesis.[69] At pH < 2, Cr species are present in the forms of tri- and tetrachromates ($Cr_3O_{10}^{2-}$ and $Cr_4O_{13}^{2-}$, respectively), which are highly polymerized and susceptible to forming inactive crystalline α-Cr_2O_3; at 2 < pH < 6, the formation of smaller Cr anions, such as dichromate ($Cr_2O_7^{2-}$), is favored, leading to better Cr dispersion; at pH > 8, isolated CrO_4^- is stable but hardly leads to high activity for CO_2−ODHP. To obtain highly dispersed Cr species with desired types, Baek et al. have introduced a $(N^0M^{n+})I^0$ pathway to prepare MSU-x-supported Cr catalysts at pH =

https://dx.doi.org/10.1021/acscatal.0c03999
ACS Catal. 2021, 11, 2182−2234

4, in which N^0 is a nonionic poly(ethylene oxide) surfactant, M^{n+} is the metal cation, and I^0 is an electrically neutral silica precursor, and the assembly process of metal cations is driven by electrostatic control.[69] Chromium(III) acetate hydroxide ($(CH_3CO_2)_7Cr_3(OH)_2$) is used to offer both Cr^{3+} cations and electrostatic driving force, as well as helping to disperse the precursor molecules through the steric effect of ligands. The as-prepared catalysts present a mesopore structure resembling 3D wormhole-like holes with high surface areas (e.g., 730−903 $m^2\ g^{-1}$), pore volumes (e.g., 0.71−1.03 $cm^3\ g^{-1}$), and narrow pore size (e.g., 3.9−4.5 nm). Optimal catalytic performance is achieved at Cr = 1.27 wt. %, which also outperforms the catalyst prepared by IWI with the same Cr loading (Table 2). The H_2-TPR profiles reveal the presence of isolated and polymeric Cr^{6+} species in the calcined catalysts, which are designated as "hard" and "soft" Cr^{6+} species, respectively, based on their reducibility. Soft Cr^{6+} species are crucial to achieve high catalytic performance, while hard species have a negative impact on activity. During the reaction, these soft Cr^{6+} species-derived coordinatively unsaturated Cr^{3+} species promote RWGS and C_3H_6 formation through the redox cycle of $Cr^{3+} \leftrightarrow Cr^{6+}$.

Metal Vapor Synthesis Method. The metal vapor synthesis (MVS) method enables the co-condensation of metal vapor with the vapor of weakly stabilizing organic ligands during the preparation, the well-defined organometallic species or solvent-stabilized metal clusters are formed, which is conducive to prepare supported metal catalysts on a wide range of organic and inorganic support materials.[102−105] On Cr-based catalysts, this method allows high Cr dispersion even at quite high loadings, particularly useful for the support with limited surface area. Botavina et al. have prepared Cr/SiO_2 catalysts by the MVS method with a wide range of Cr loadings, namely, 0.25−10 wt. %.[70] An optimal Cr loading is obtained at 6.0 wt. % (Table 2), at which both C_3H_8 conversion and C_3H_6 yield have been substantially increased by ∼1.8- and ∼1.7-fold, respectively, in comparison to $Cr_{0.25}/SiO_2$, while the reduction of C_3H_6 selectivity is merely 7.3%.

Sol−Gel Method. Wang et al. have prepared CrO_x-doped mesoporous silica sphere (Cr/MSS) catalysts by one-pot synthesis via a sol−gel method, and systematically investigated the influence of adding active precursors on the morphology, pore structure, and active species, as well as their correlation with catalytic performance.[71] Generally, all synthetic procedures entail the first step of preparing a surfactant solution (CTAB and triethanolamine, $TEAH_3$) and the second step of adding a Si source. The catalysts are categorized into three groups, namely, MSS-1, MSS-2, and MSS-3, representing adding the Cr precursor in the first step, second step, and after the second step, respectively. For Cr/MSS-2, adding the Cr precursor concurrently with the Si source exerts well-dispersed Cr species on the micelle-silica walls with the gradual generation of silica walls, and no Cr species enter the core of the silica sphere. Such a feature results in high dispersion of Cr species with more isolated chromates, enhanced medium acid sites, and well-retained pore structure of the silica sphere. Therefore, Cr/MSS-2 exhibits the highest C_3H_8 conversion and C_3H_6 yield, with slightly lower C_3H_6 selectivity among three catalysts, and also outperforms the benchmark Cr/MSS-4, prepared by IWI (Table 2).

Hydrothermal Method. Oliveira et al. have prepared Cr/ZrO_2 via a microwave-assisted hydrothermal method, a facile, time-efficient method to prepare oxides with smaller crystallites through fast nucleation.[61] The incorporation of microwave results in the formation of smaller tetragonal *t*-ZrO_2 crystallite. At lower Cr content (i.e., 5 wt. %), m-Cr/ZrO_2, prepared by the microwave-assisted hydrothermal method, displays higher activity in C_3H_8 conversion and C_3H_6 yield than c-Cr/ZrO_2, prepared by a conventional hydrothermal method, but lower C_3H_6 selectivity, as well as faster deactivation (Table 2). Wu et al. have investigated the temperature effects of hydrothermal treatment on the catalytic performance on Cr−Zr bimetallic oxides, and obtained optimal activity and selectivity on the catalyst treated at 180 °C (Table 2).[72] At this temperature, more Cr^{6+} species, a precursor of active species Cr^{3+}/Cr^{2+} species, are formed, leading to the substantially enhanced activity with well-retained high selectivity.

Acid−Base Pair. The "acid−base pair" concept is a self-adjusted process that has been widely used to prepare ordered, mesoporous multimetal oxides,[101] in which the pH of the desired sol−gel reaction is adjusted by a self-generated reaction medium between two or more inorganic species with the correct acidity.[106] Xie et al. have prepared Cr oxide-modified mesoporous ZrO_2 (Cr-ZrO_2) via the acid−base pair pathway.[73] The as-prepared bimetallic oxides feature mesoporous structures resembling 3D wormholes. The crystalline structure of ZrO_2 shifts from a monoclinic to tetragonal, then to disordered crystals with the increased Cr content, which in turn affects the dispersion of Cr species. 7Cr-ZrO_2 presents more abundant well-dispersed Cr^{6+} species and isolated Cr^{6+} species, which are precursors for the formation of active Cr^{3+}/Cr^{2+} species during reaction, thereby leading to the highest initial activity and selectivity (Table 2).

3.1.1.5. Deactivation and Regeneration. Coke deposition and reduction of active sites are major reasons for deactivation of Cr-based catalysts. Coking is relatively easier to reverse by reoxidation; moreover, the presence of CO_2 can help to remove coke in situ through a reverse Boudouard reaction or to inhibit the coking process.[73] Regeneration in air or CO_2 at high temperatures (i.e., 550−650 °C) is widely applied, through which most of the activity and selectivity are usually recoverable. For example, regeneration in O_2 at 600 °C for 5 min can completely restore the activity of CrO_x/ZrO_2, and such recovery is repeatable after 4 cycles.[67] Differently, using CO_2 as a regeneration oxidant only allows a complete recovery in the second cycle, beyond which, however, it cannot prevent the catalyst from further deactivation. Alternatively, co-feeding O_2 in CO_2−ODHP can promote the removal of coke during the reaction, but it is accompanied by a drastic decrease in C_3H_6 selectivity and C_2−C_3 olefin selectivity.[55]

By contrast, a complete recovery of active sites is rather challenging yet is still achievable if a proper method is used to prepare well-dispersed Cr species. As aforementioned (section 3.1.1.4), Baek et al. have introduced a $(N^0M^{n+})I^0$ pathway to prepare MSU-x-supported Cr catalysts with highly dispersed Cr species.[69] The activity can be completely recovered under simple oxidation in air at 650 °C, retaining its repeatability after 6 cycles.

From a practical point of view, increasing Cr loading while preserving high dispersion is necessary to attain comparable catalytic performance that meets industrial requirements. However, the formation of inactive crystalline α-Cr_2O_3 is inevitable at higher Cr loadings, the presence of which limits the activity and is also detrimental to stability. To overcome

https://dx.doi.org/10.1021/acscatal.0c03999
ACS Catal. 2021, 11, 2182−2234

this issue, Botavina et al. have prepared highly dispersed Cr–SiO_2 catalysts by direct one-pot hydrothermal synthesis.[21] By following the procedure of MCM-41 synthesis, the as-prepared catalysts exhibit MCM-41-type mesoporous structure with high surface area (600–1000 m^2 g^{-1}). Long-term tests demonstrate better stability of $Cr_{2.0}$–SiO_2 in C_3H_8 conversion after 900 min on stream in the joint presence of CO_2 and O_2 (Figure 6A), but accompanied by a lower C_3H_6 yield than the

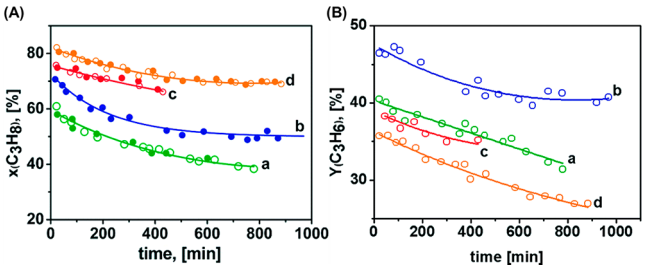

Figure 6. Changes of C_3H_8 conversion (A) and C_3H_6 yield (B) versus reaction time during ODHP and DHP reactions on $Cr_{2.0}$–SiO_2 catalyst (T = 600 °C, GHSV = 200 h^{-1}) in the as-prepared state (open symbols) and after reaction and subsequent treatment in O_2 at 600 °C for 6 h (solid symbols: after 5–8 runs): (a) C_3H_8: N_2 = 15: 85 (green curve; solid symbol: after 5 runs), (b) C_3H_8: CO_2: N_2 = 15: 30: 55 (blue curve; solid symbol: after 8 runs), (c) C_3H_8: O_2: N_2 = 15: 3: 82 (red curves; solid symbols: after 5 runs), and (d) C_3H_8: CO_2: O_2: N_2 = 15: 30: 3: 52 (orange curves; solid symbols: after 8 runs). Reproduced with the permission from ref 21. Copyright 2016 Royal Society of Chemistry.

other reaction conditions (Figure 6B). The improved stability originates from the trade-off between the reduced C_3H_6 yield and increased C_2H_4 yield (Table 2). Notably, a relatively well-retained yield is obtained under the condition of CO_2 alone (Figure 6B). Spectroscopic studies (diffuse reflectance electronic spectroscopy and X-ray absorption near edge spectroscopy) reveal that the average oxidation state of Cr in CO_2–ODHP is 2+, which is lower than that (i.e., Cr^{3+}) in the presence of co-fed O_2. This is indicative of a lower probability of forming crystalline α-Cr_2O_3 if CO_2 is the only oxidant. Apparently, the combination of the soft oxidant CO_2 and well-dispersed Cr species in the 3D pore structure with high surface area is effective in avoiding fast deactivation and in prolonging the catalyst lifetime.

As discussed in section 3.1.1.2, the unique pore structure and large surface area of mesoporous support materials are effective in confining the growth of Cr species and affecting dispersion and structure of Cr species. However, the preservation of pore structure and porosity under reaction conditions is challenging. Michorczyk et al. find that the irreversible degradation of the pore structure after multiple cycles leads to decreased selectivity on $Cr_{0.04}$-SBA-1.[66] An option to preserve the unique pore structure is to control the Cr loading at a lower level, however, this sacrifices the activity. Choosing proper synthetic methods to prepare catalysts provides solutions to overcome this issue. Michorczyk et al. have prepared Cr/SBA-1 catalyst by IWI.[59] Compared to the Cr-SBA-1 prepared by direct synthesis method, the pore structure of IWI-prepared catalysts is preserved to a larger degree, significantly alleviating the irreversible deactivation caused by pore collapse.

3.1.2. Vanadium(V)-Based Catalysts. 3.1.2.1. Identification of Active V Sites and Redox Cycle. VO_x is another redox-active metal oxide that has been extensively studied in the O_2–ODHP reaction, and the overoxidation still impairs the effort to achieve high C_3H_6 selectivity. Early attempts have tried to neutralize the sites for overoxidation on vanadate catalysts. Adding CO_2 in the feed gas of C_3H_8/O_2 is a promising approach, as it enables a decrease of surface molecular oxygen species that account for overoxidation by tuning adsorption–desorption equilibria on basic oxidizing sites.[107,108]

Similar to CrO_x, catalytic performance of VO_x depends on its structure, dispersion, and interaction with the support.[1] Depending on the ratio of metal loading and surface area of support, four types of VO_x species are present during reaction, including monovanadate, oligomeric vanadate, polyvanadate, and V_2O_5 crystallite.[77,109] Figure 7 illustrates the evolution of surface VO_x configurations as a function of surface V density on VO_x/Al_2O_3. Monovanadate VO_x species are proposed as active sites (see Table 3 for monolayer surface density on various metal oxide supports). The oxygen of V=O (vanadyl) groups of the monomeric VO_x species are reported to account for propylene formation.[115] As the vanadia surface density increases, oligomeric species appear to emerge and are considered more active for propylene synthesis than the monomeric species.[77] Bulk V_2O_5 favors overoxidation, thus reducing C_3H_6 selectivity.[77,110,111] Noteworthily, there is another type of proposed active site at submonolayer V coverages, in which the bridging V–O-support bond is critical for O_2–ODHP.[1] Its strength appears to associate to the ODHP reaction kinetics, as evidenced from the variations in apparent activation energy among vanadium catalysts supported on NbO_5, SiO_2, Al_2O_3, ZrO_2, CeO_2, and TiO_2. However, this scenario is scarcely reported in CO_2–ODHP.

Results of isothermal reduction confirm that CO_2 cannot reoxidize the catalyst completely to V_2O_5 but is capable of oxidizing V_2O_3 to V_2O_4.[28] Redox mechanisms have been proposed on the silsesquioxane cluster with an isolated V^{5+}–O–V^{3+} pair via density functional theory (DFT) calculations

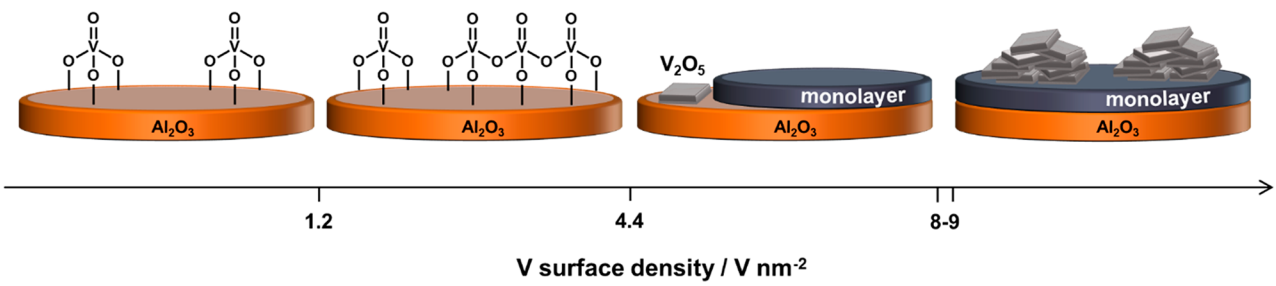

Figure 7. Schematic illustration of surface V density-dependent configurational evolutions of VO_x species on VO_x/Al_2O_3 catalysts.[77,109]

https://dx.doi.org/10.1021/acscatal.0c03999
ACS Catal. 2021, 11, 2182–2234

for the entire reaction network including CO_2−ODHP, DHP, and RWGS.[28] As illustrated in Figure 8, V^{4+} plays an important role in the activation of the secondary C−H bond of C_3H_8 (RDS) by hydrogen abstraction in both CO_2−ODHP and DHP routes. Yet the regeneration of active V sites differs, in which V^{3+} can be reoxidized through the dissociative CO_2 adsorption, while the regeneration in DHP follows the path of hydrogen migration from the bridge oxygen to V^{3+} → hydrogen migration from the vanadyl oxygen (V^{5+}−O−H) to bridge oxygen → desorption of H_2. In RWGS, V^{4+} sites are involved in H_2 dissociation and water formation and desorption. CO_2 dissociation also occurs on reduced V^{3+} sites, reoxidizing V^{3+} sites through oxygen abstraction. Of note, alternative redox cycles have also been known, such as the $V^{5+} \leftrightarrow V^{4+}$ cycle on an oxidized diamond-supported VO_x catalyst.[112]

3.1.2.2. Effects of Support. Mesoporous silica has been introduced as support to prepare VO_x catalysts with high dispersion.[1] However, these materials have long, isolated channels and inefficient mass transfer, leading to low catalytic activity.[113] Therefore, mesoporous materials with short-range, ordered mesopores with highly dispersed VO_x species are desired. Xue et al. have prepared homogeneous, monodispersed 3D dendritic mesoporous silica nanospheres (3D dendritic MSNSs) and used them as support for VO_x catalysts.[114] The catalysts have been prepared via an oil−water biphase stratification reaction system that allows the delicate control of monolayer coverage and prohibit agglomeration of V species to V_2O_5. The as-prepared catalyst displays higher C_3H_6 selectivity and comparable C_3H_8 conversion in comparison to other catalysts in Table 4. Both conversion and selectivity can be completely recovered after simple reoxidation in air.

Diamond is another form of carbon that can be a potential support candidate, because its surface can be functionalized with various surface oxygen functional groups (OFGs), such as C−O−C ether type structures and C═O carbonyl type structures, through oxidative treatment in acids (HNO_3, HClO, H_2O_2, etc.) and oxidation in O_2.[115,116] Nakagawa et al. have introduced oxidized commercial diamond as a support and conducted comparative studies among different metal oxides and support materials for CO_2−ODHP.[112] Cr and V oxides supported on diamond display better catalytic performance than other metal oxides, including Ga, Mn, and Fe oxides (Table 4). Of note, the diamond-supported VO_x catalyst outperforms Al_2O_3-, SiO_2-, and activated carbon (AC)-supported VO_x catalysts in terms of VO_x surface area-based C_3H_6 formation rates.

3.1.2.3. Effects of Promoter. VO_x/SiO_2 possesses a lower monolayer coverage of VO_x (~3.3 V nm^{-2}) compared to more reactive oxide support materials such as Al_2O_3 (~7−8 V nm^{-2}).[117] To enrich the surface VO_x species with monovanadate and improve their retention against compression to form polymerized species or bulk V_2O_5, incorporating another metal component featuring a noninteracting nature offers avenues to achieve this goal.[30] Tungsten oxide (WO_x) is known to influence the dispersion of VO_x in this regard.[1,118,119] Ascoop et al. have introduced WO_x into VO_x/SiO_2 catalysts for CO_2−ODHP.[28] The highest C_3H_6 turnover frequency (TOF) is obtained at W/V = 0.1 molar ratio, while W/V = 0.6 achieves the highest C_3H_6 selectivity. The apparent activation energy (127−147 kJ mol^{-1}) appears to be independent of W/V molar ratios, demonstrating that

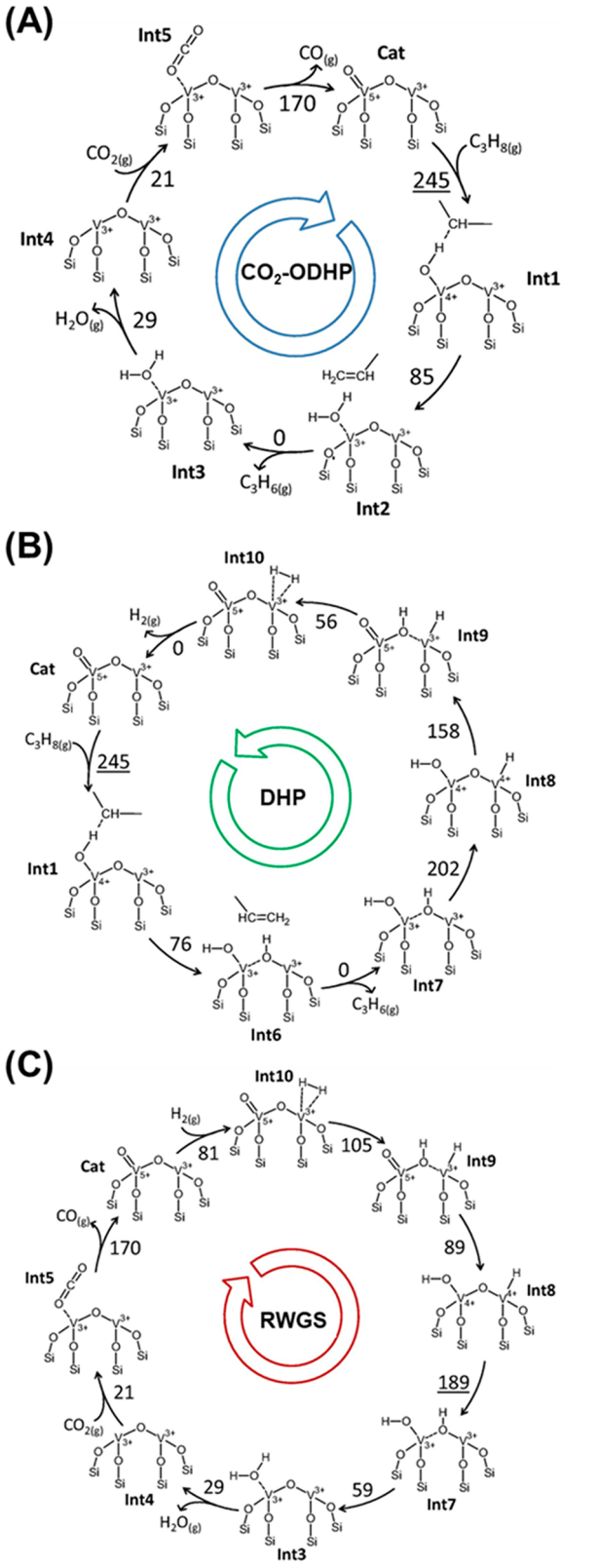

Figure 8. Catalytic cycles for CO_2−ODHP (A), DHP (B), and RWGS (C) on silsesquioxane cluster with an isolated V^{5+}−O−V^{3+}. Gibbs free energy barriers at 600 °C are reported in kJ mol^{-1} next to the reaction arrows. Underlined numbers correspond to the highest Gibbs free energy barriers of the catalytic cycle. Reproduced with the permission from ref 28. Copyright 2016 Elsevier B.V.

https://dx.doi.org/10.1021/acscatal.0c03999
ACS Catal. 2021, 11, 2182−2234

Table 4. Summarized Activity Performance of VO_x-Based and Reference Catalysts for CO_2−ODHP

catalyst	temp (°C)	C_3H_8/CO_2 ratio	conversion (%)		yield (%)	selectivity (%)				ref
			C_3H_8	CO_2	C_3H_6	C_3H_6	C_2H_6	C_2H_4	CH_4	
5% Cr/O−diamond	600	1: 5	19.7		11.8	59.9	7.3	7.3	5.4	112
V/O−diamond	600	1: 5	13.7		8.6	62.7	7.1	7.1	3.1	112
Ga/O−diamond	600	1: 5	9.1		3.4	37.7	13.0	13.0	3.9	112
Mn/O−diamond	600	1: 5	9.0		2.7	29.3	17.9	17.9	7.2	112
Fe/O−diamond	600	1: 5	6.6		1.6	23.8	13.1	13.1	4.1	112
O−diamond	550	1: 9	0.9		0.5	57.8	35.2	7.0	0.0	112
1% Cr/O−diamond	550	1: 9	1.6		0.9	53.9	20.5	4.7	20.9	112
3% Cr/O−diamond	550	1: 9	4.2		3.1	73.3	6.8	2.3	17.6	112
5% Cr/O−diamond	550	1: 9	4.0		3.5	86.8	7.8	2.9	2.5	112
10% Cr/O−diamond	550	1: 9	5.9		3.7	63.0	4.9	2.1	30.0	112
$V_{5.2}$-MSNS[a]	600	1: 4	19		16.9	89				114
V_7/Al_2O_3[b]	550	1: 3	6.72	3.28	6.50	96.7				30
Cr_4/Al_2O_3[b]	550	1: 3	5.18	1.32	4.65	89.8				30
Mo_5/Al_2O_3[b]	550	1: 3	2.19	0.40	2.11	96.3				30
W_7/Al_2O_3[b]	550	1: 3	0.55	0.10	0.50	90.9				30
V_7Cr_4/Al_2O_3[b]	550	1: 3	9.98	5.03	9.54	95.6				30
V_7Mo_5/Al_2O_3[b]	550	1: 3	10.08	3.34	9.74	96.6				30
V_7W_7/Al_2O_3[b]	550	1: 3	9.85	3.40	9.56	97.1				30
$V_{4.2}/SiO_2$[c]	600	1: 2	13.7		5.5	40.2		0.0	9.0	120
$V_{4.2}$/Na-SiO_2[c]	600	1: 2	3.4		0.0	0.0		85.5	8.2	120
$V_{6.9}/SiO_2$[c]	600	1: 2	29.2		6.3	21.4		0.0	9.7	120
$V_{6.9}$/Na-SiO_2[c]	600	1: 2	2.2		0.0	86.2		86.2	8.3	120

[a]Number in the subscript represents V loading on weight basis. MSNS stands for mesoporous silica nanosphere. [b]Numbers in the subscript represent loading of metal oxides (V_2O_5, Cr_2O_3, MoO_3, and WO_3) on weight basis. Activity data were collected at TOS = 2 h. [c]Numbers in the subscript represent V loading on weight basis.

the WO_x addition only preserves VO_x dispersion rather than mediating active sites. Sandupatla et al. have carried out comparative studies among Cr_2O_3-, MoO_3-, and WO_3-modifed VO_x/Al_2O_3 catalysts under a monolayer VO_x coverage.[30] The catalytic performance of monometallic oxide catalysts decreases in the order of V > Cr > Mo > W (Table 4), and both Mo and W display poor activity. By sharp contrast, the mixed oxide catalysts V_7Mo_5 and V_7W_7 exert synergistic promoting effects on C_3H_8 conversion and C_3H_6 yield, especially for V_7W_7, while that synergy is absent for V_7Cr_4. Characterization results imply that these metal oxides are noninteracting with one another in the mixed oxides, and both VO_x and CrO_x are more readily reduced than MoO_x and WO_x. Another reason for the less synergetic effect on V_7Cr_4 originates from the improved CO_2 adsorption on more reduced V and Cr sites, leading to CO_2 poisoning.[30] To alleviate CO_2 poisoning, a relatively higher but proper CO_2 partial pressure is necessary to ensure more oxidized metal species for the ODHP reaction. Na-promoted SiO_2 supports have also been employed in an attempt to anchor more monovanadate species with the surface Si−O−Na^+.[120] Characterization results confirm the improved surface V density, but along with the formation of inactive Na metavanadate species that selectively produce CO instead of C_3H_6 (Table 4).

3.2. Nonredox-Type Catalysts: Gallium (Ga).

3.2.1. Identification of Active Ga_2O_3 Polymorphs. To establish the correlation between activity and Ga_2O_3 polymorphs, Zheng et al. have evaluated the activity performance of α-, β-, γ-, and δ-Ga_2O_3 polymorphs for CO_2−ODHP.[121] β- and γ-Ga_2O_3 outperform the rest in C_3H_8 conversion and C_3H_6 selectivity (Table 5). Surface titration experiments reveal that the surface acidity density decreases in the order of $\beta > \gamma > \delta > \alpha$, so does the surface basicity. The initial activity is dependent on the surface acid density and maximizes on β-Ga_2O_3. Both β- and γ-Ga_2O_3 contain tetrahedral Ga cations in the structure, on which the Lewis acid sites are coordinatively unsaturated Ga^{3+} sites. α- and δ-Ga_2O_3 are constituted by octahedral Ga^{3+}, which are more coordinated with weaker acidity; the reconstruction from octahedral to tetrahedral Ga cations might occur, generating surface Lewis acid sites. Such differences in Lewis acidity explain the activity trend. On the other hand, surface basic sites are too few for CO_2 adsorption and activation, thereby leading to lower CO_2 conversion than C_3H_8. Nevertheless, the surface base site density shows the correlation with initial activity, demonstrating its promotional effect in the initial period of reaction. Combined with the weak reducibility of Ga_2O_3 (1−5 mol % of the fresh Ga_2O_3) and the presence of Ga^+ and Ga^{3+} in catalysts (XPS), one can postulate that the reduction of Ga cations takes place and benefits DHP but only at the initial stage of the reaction. At the steady state, reaction is proposed to proceed via heterolytic dissociation on Ga oxide without the redox cycle, which is discussed in section 3.2.3.

3.2.2. Mixed Ga-Containing Oxide Catalysts. Ga_2O_3−Al_2O_3 solid solutions are characteristic of unique surface acid properties and have shown promising reactivity in selective catalytic reduction (SCR) of NO_x with hydrocarbons.[122−124] Chen et al. have prepared mixed $Ga_xAl_{10-x}O_{15}$ (i.e., x = 2, 5, and 8) oxides with high surface areas (e.g., 119−147 m^2 g^{-1}).[53] These solid solution catalysts enable the changes of Ga ions between tetrahedral Ga(IV) and octahedral Ga(VI) sites by tuning the Ga/Al ratios. The proportion of Ga(IV) sites correlates to weak acid sites, as shown in Figure 9A, implying the essential role of tetrahedral

https://dx.doi.org/10.1021/acscatal.0c03999
ACS Catal. 2021, 11, 2182−2234

Table 5. Summarized Activity Performance of Ga_2O_3-Based Catalysts and Reference Catalysts for CO_2−ODHP

catalyst	temp (°C)	C_3H_8/CO_2 ratio	conversion (%)		yield (%)	selectivity (%)				ref
			C_3H_8	CO_2	C_3H_6	C_3H_6	C_2H_6	C_2H_4	CH_4	
$(Fe_2O_3)_5/SiO_2$[a]	600	1: 5	2.6		1.9	71.5		19.7	8.8	52
$(Fe_2O_3)_5/Al_2O_3$[a]	600	1: 5	3.8		2.9	76.9		12.2	10.9	52
$(Cr_2O_3)_5/SiO_2$[a]	600	1: 5	6.9		5.8	84.0		9.0	6.7	52
$(Cr_2O_3)_{0.97}/SiO_2$-A[a]	600	1: 5	16.2		14.8	91.3		4.5	4.2	52
$(Cr_2O_3)_5/Al_2O_3$[a]	600	1: 5	12.7		10.7	84.4		5.9	9.8	52
$(Ga_2O_3)_5/SiO_2$[a]	600	1: 5	1.3		1.0	77.5		15.2	7.3	52
$(Ga_2O_3)_5/Al_2O_3$[a]	600	1: 5	5.4		5.3	90.8		2.5	6.7	52
γ-Ga_2O_3[b]	500	1: 2	41.3		~38.53	93.3				53
$Ga_8Al_2O_{15}$[b]	500	1: 2	51.7		~47.36	91.6				53
$Ga_5Al_5O_{15}$[b]	500	1: 2	38.4		~35.44	92.3				53
$Ga_2Al_8O_{15}$[b]	500	1: 2	22.8		~21.64	94.9				53
α-Ga_2O_3[c]	500	1: 2	16	4.3	~14.24	89	0.0	7.4	3.4	121
β-Ga_2O_3[c]	500	1: 2	23	6.2	~21.62	94	0.3	3.1	2.3	121
γ-Ga_2O_3[c]	500	1: 2	21	4.4	~18.06	86	0.0	7.9	5.4	121
δ-Ga_2O_3[c]	500	1: 2	18	5.3	~16.74	93	0.0	4.0	2.6	121
$(Ga_2O_3)_5/TiO_2$[d]	600	1: 2	32	30	~23.36	73	1.1	16	10	127
$(Ga_2O_3)_5/Al_2O_3$[d]	600	1: 2	26	5.2	~24.44	94	0.4	3.8	2.9	127
$(Ga_2O_3)_5/ZrO_2$[d]	600	1: 2	30	29	~19.50	65	4.2	17	14	127
$(Ga_2O_3)_5/SiO_2$[d]	600	1: 2	6.4	3.1	~5.89	92	0.3	4.8	3.1	127
$(Ga_2O_3)_5/MgO$[d]	600	1: 2	4.3	4.2	~1.25	29	28	33	10	127
$Ga_2O_3-Al_2O_3$−GM[e]	550	1: 3	8.7	1.6	8.3	95.8	0.3	1.8	1.6	137
$Ga_2O_3-Al_2O_3$−CP[e]	550	1: 3	26.2	4.3	24.9	95.2	0.2	2.2	1.9	137
$Ga_2O_3-Al_2O_3$−HS[e]	550	1: 3	35.2	8.4	33.4	95.1	0.2	2.1	2.0	137
ZrO_2[f]	600	1: 2	5.6		4.4	77.8	1.8	10.2	10.2	126
$(Ga_2O_3)_5/ZrO_2$[f]	600	1: 2	27.9		15.2	54.3	1.3	9.9	34.5	126
$(Ga_2O_3)_{10}/ZrO_2$[f]	600	1: 2	32.8		15.7	48.0	1.7	9.0	41.3	126
$(Ga_2O_3)_{15}/ZrO_2$[f]	600	1: 2	38.6		17.5	45.4	3.8	9.2	41.6	126
$(Ga_2O_3)_{20}/ZrO_2$[f]	600	1: 2	41.8		18.0	43.1	4.2	9.3	43.4	126
Ga_2O_3[g]	600	1: 5	32.8		~30.60	93.3		3.5	3.2	23
Ga_2O_3−K1[g]	600	1: 5	18.6		~17.13	92.1		4.0	3.9	23
β-Ga_2O_3[g]	500	1: 2	5		~4.6	92				133
β-Ga_2O_3−S4[g]	500	1: 2	25		~24	96				133
$Ga_2O_3-Al_2O_3(1/4)$[h]	550	1: 5	~7.5		~7.13	~95				136
$Ga_2O_3-Al_2O_3(4/1)$[h]	550	1: 5	~19		~17.29	~91				136
Ga_2O_3-m[h]	550	1: 5	19	2.4	17.40	91.6	0.4	3.5	2.6	136
Ga_2O_3-t[h]	550	1: 5	~22		~19.58	~89				136
$Ga_2O_3-Al_2O_3(1/4)$[i]	550	1: 5	~7		~6.79	~97				136
$Ga_2O_3-Al_2O_3(4/1)$[i]	550	1: 5	~12		~11.52	~96				136
Ga_2O_3-m[j]	550	1: 5	~10		~9.40	~94				136
Ga_2O_3-t[j]	550	1: 5	~1		~0.85	~85				136

[a]Values in the subscript are loading of metal oxides on weight basis. Cr_2O_3/SiO_2-A was prepared by equilibrium adsorption method, while others are prepared by impregnation. [b]Data were collected at TOS = 0.25 h. [c]Data were collected in the initial period. [d]Ga_2O_3 loading was 5 wt. % for all supported catalysts. Activity data were collected at TOS = 10 min. [e]Data were collected at TOS = 1 h. GM: Grinding mixture. CP: Coprecipitation method. HS: Hydrothermal synthesis. [f]Values in the subscript are loading of Ga_2O_3 in the mixed oxide catalysts. Catalysts were prepared by coprecipitation method. [g]Ga_2O_3 was prepared by thermal decomposition of $Ga(NO_3)_3{\cdot}9H_2O$. K was loaded by impregnation, with K/Ga = 0.03 mol mol^{-1}. [h]β-Ga_2O_3 was prepared by thermal decomposition of $Ga(NO_3)_3{\cdot}9H_2O$. The sucrose/Ga_2O_3 molecular ratio of β-Ga_2O_3−S4 was 4. Data were collected at TOS = 8 h. [i]Data were collected at TOS = 0.25 h. [j]Data were collected at TOS = 3.75 h.

surface Ga^{3+} sites in creating the surface acidity. $Ga_8Al_2O_{15}$ oxide exhibits the best catalytic performance among all solid solution catalysts, and far outperforms the benchmark γ-Ga_2O_3 in C_3H_8 conversion (Table 5). Furthermore, a positive correlation of surface area-based weak acid site density with initial C_3H_8 conversion is evident in Figure 9B. Combined with the fact that Brønsted acid sites are absent in these catalysts, these tetrahedral surface Ga^{3+} sites in the form of Al^{3+}−O−Ga^{3+} are weak Lewis acid sites that account for dehydrogenation reactions.[125] The $Ga_2O_3-Al_2O_3$ solid solution catalysts also exhibit better stability than the benchmark γ-Ga_2O_3, which is attributed to the improved desorption of C_3H_6 on Ga−Al catalysts, as evidenced from transient responses of pulsed C_3H_6 adsorption.

Mixed $Ga_2O_3-ZrO_2$ oxides have also been prepared by a coprecipitation method for CO_2−ODHP.[126] The as-prepared catalysts present higher surface areas (e.g., 34−59 m^2 g^{-1}) than the bare ZrO_2 (e.g., 19 m^2 g^{-1}). Characterization results confirm the homogeneous mixing of Ga with Zr in the oxides with strong interactions, as well as the monotonic increase in Lewis acid sites with the increase in Ga content in the oxides. These features can be reflected from enhanced C_3H_8

https://dx.doi.org/10.1021/acscatal.0c03999
ACS Catal. 2021, 11, 2182−2234

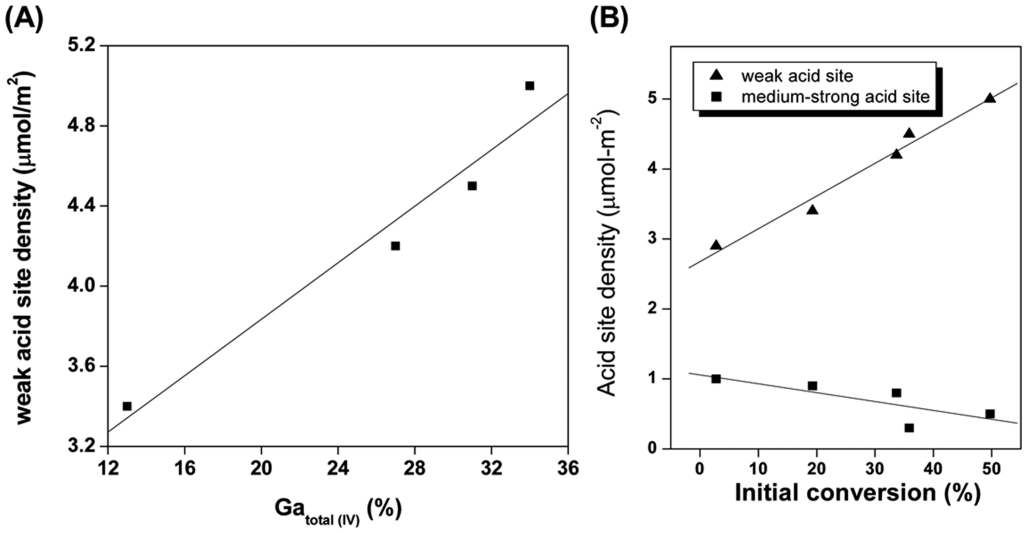

Figure 9. Correlation of weak acid site amount and percentage of Ga(IV) (A) and surface acidic density versus conversion of C_3H_8 at 0.25 h for $Ga_xAl_{10-x}O_{15}$ catalysts for CO_2−ODHP. Weak and medium-strong acid sites are quantified based on the peaks at 120−350 and 400−527 °C, respectively, from NH_3-TPD profiles. Reproduced with the permission from ref 53. Copyright 2008 Elsevier B.V.

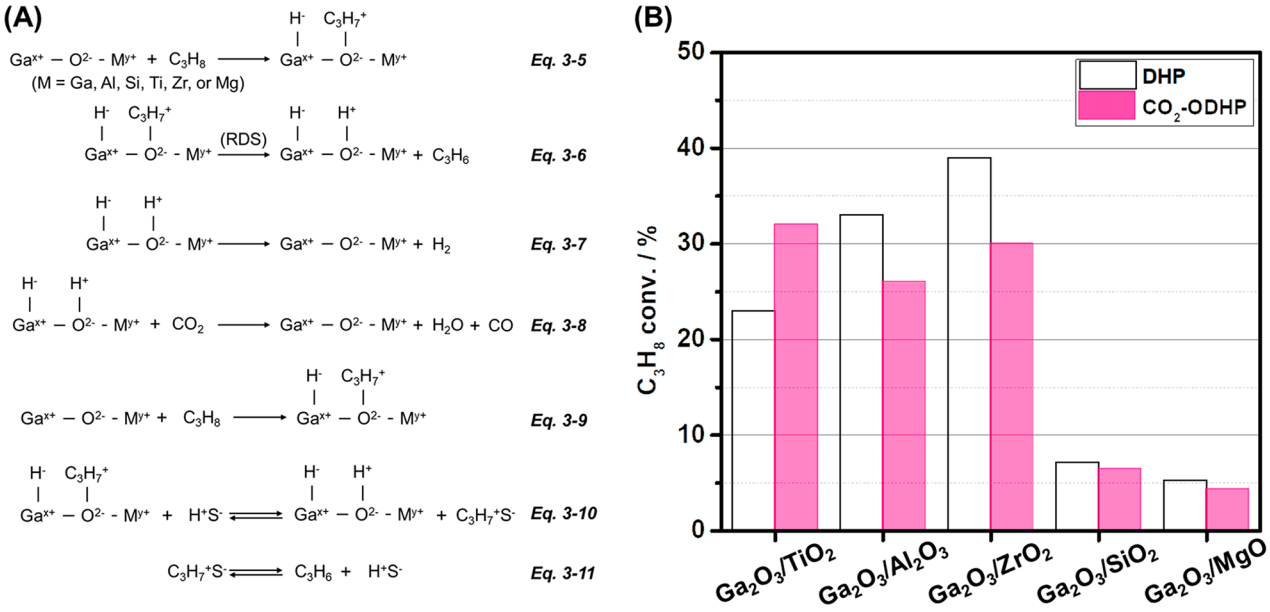

Figure 10. (A) Proposed heterolytic dissociation mechanism on gallium oxide catalysts in CO_2−ODHP and the conjugated effect gallium oxide and proton in promoting DHP activity, wherein S represents the catalyst surface.[127] (B) Comparison of C_3H_8 conversion for DHP and CO_2−ODHP on various supported Ga_2O_3 catalysts. Data in panel B were adapted from ref 127.

conversion and C_3H_6 yield (Table 5). However, the C_3H_6 selectivity is not comparable to Ga_2O_3−Al_2O_3 solid solution catalysts under isoconversional conditions (Table 5).

3.2.3. Effects of Support. The nature of the support and its interaction with gallium oxide are crucial to manipulate the reactivity, and can be reflected in the differences in H_2 adsorption capacities and acid−base properties.[127] Early efforts have been put forth to modify the acid−base properties of Ga_2O_3 catalysts by introducing alkali metal oxides such as K.[23] However, the incorporated K covers the acid sites on Ga_2O_3, exerting a negative impact on both conversion and selectivity (Table 5)

Xu et al. have systematically investigated the support effect by using TiO_2, Al_2O_3, ZrO_2, SiO_2, and MgO as support materials in DHP and CO_2-DOHP, and studied the aspects of acid−base properties, adsorption properties, and metal−support interactions.[127] TiO_2-, ZrO_2-, and Al_2O_3-supported Ga_2O_3 catalysts display higher activity than MgO- and SiO_2-supported counterparts, again corroborating the crucial role of acid sites on Ga_2O_3 for C_3H_8 dehydrogenation (Table 5). Ga_2O_3/MgO shows the lowest activity and selectivity toward C_3H_6 production due to the strong basicity of MgO, which not only neutralizes the acid sites on Ga_2O_3 but also favors CO_2 adsorption over C_3H_8. A similar negative impact on activity is also evident for the Li-promoted MgO catalyst.[128]

Since these catalysts show no reduction behavior as evidenced from H_2-TPR profiles, the C_3H_6 formation on Ga_2O_3 should not proceed through redox mechanisms but rather by following the heterolytic dissociation pathway. Detailed steps in the absence and presence of CO_2, as well as

https://dx.doi.org/10.1021/acscatal.0c03999
ACS Catal. 2021, 11, 2182−2234

Table 6. Activity Performance of Zeolite-Supported Catalysts for CO_2−ODHP

catalyst	temp (°C)	C_3H_8/CO_2 ratio	conversion (%)		yield (%)	selectivity (%)				ref
			C_3H_8	CO_2	C_3H_6	C_3H_6	C_2H_6	C_2H_4	CH_4	
$Cr_{0.5}$SiBeta	550	1: 5	11.0	0.6	10.1	94.7	1.5	3.6	2.8	22
$Cr_{1.0}$SiBeta	550	1: 5	17.6	1.2	16.0	90.8	1.4	4.5	3.3	22
$Cr_{2.0}$SiBeta	550	1: 5	24.8	4.0	21.6	87.1	2.4	4.2	6.2	22
$Cr_{5.0}$SiBeta	550	1: 5	27.6	5.5	23.3	84.4	2.8	4.0	8.8	22
$Cr_{7.0}$SiBeta	550	1: 5	33.3	7.0	27.2	81.6	3.7	4.0	10.7	22
$Cr_{2.0}$AlBeta	550	1: 5	4.5	0.8	2.0	45.1	8.0	25	21.9	22
5% Ga_2O_3/HZSM-5 (700)[a]	600	1: 2	42	∼3	∼22.5	∼54				141
5% Ga_2O_3/HZSM-5[b]	600	1: 2	8.7		6.3	72.3	13.4	10.5	3.8	144
Ga_2O_3/P-HZSM-5(0.5)[b]	600	1: 2	13.0		7.0	55.6	8.3	9.6	3.4	144
Ga_2O_3/P-HZSM-5(1.0)[b]	600	1: 2	17.6		10.1	57.3	6.2	11.8	4.3	144
Ga_2O_3/P-HZSM-5(1.5)[b]	600	1: 2	22.3		12.0	56.4	5.3	13.9	5.2	144
Ga_2O_3/P-HZSM-5(2.0)[b]	600	1: 2	18.4		9.4	51.3	0.1	14.0	5.5	144
3% CrO_x/silicate-1[c]	600	1: 1	3.5		3.2	92	6	0	2	147
CrO_x/H[B]MFI[c]	600	1: 1	22.1		20.1	91	2	5	2	147
CrO_x/H[B]MFI-st[c]	600	1: 1	15.7		14.6	93	1	5	1	147
5% ZnO/HZSM-5(60)[d]	600	1: 2	27.2		16.9	62.3	0.3	10.7	5.7	143
ZnO/HZSM-5(120)[d]	600	1: 2	37.0		20.5	55.4	0.4	12.0	6.3	143
ZnO/HZSM-5(160)[d]	600	1: 2	41.5		25.8	62.1	0.3	7.6	4.7	143
ZnO/HZSM-5(201)[d]	600	1: 2	29.2		18.0	61.8	0.2	9.5	5.0	143
ZnO/HZSM-5(242)[d]	600	1: 2	17.9		11.3	63.0	0.2	13.0	6.3	143
5% ZnO/HZSM-5[e]	600	1: 2	7.1		2.4	33.7	16.5	8.8	3.4	142
ZnO/HZSM-5(600)[e]	600	1: 2	25.6		19.0	74.3	0.1	8.3	4.5	142
ZnO/HZSM-5(650)[e]	600	1: 2	30.9		20.3	65.6	0.2	7.8	4.3	142
ZnO/HZSM-5(700)[e]	600	1: 2	19.8		14.8	74.7	0.1	8.1	4.3	142
5% Ga_2O_3/HZSM-48(130)[f]	600	1: 2	48.2		22.0	45.6	0.2	10.5	2.8	149
5% Ga_2O_3/HZSM-48(160)[f]	600	1: 2	34.3		19.3	56.4	0.2	9.3	2.8	149
5% Ga_2O_3/HZSM-48(220)[f]	600	1: 2	9.1		7.9	87.0	0.0	8.8	4.3	149
5% Ga_2O_3/HZSM-5(150)[f]	600	1: 2	55.3		20.1	36.5	0.3	10.8	3.0	149
5% Ga_2O_3/HZSM-5(200)[f]	600	1: 2	45.7		21.6	47.1	0.3	11.5	3.0	149

[a]Data was read from figures with TOS = ∼40 h. [b]Data was collected at TOS = 50 h. The value in the parentheses represents the weight percentage of P. [c]Data was collected at TOS = 3 h. [d]Data was collected at TOS = 30 h. The value in the parentheses is Si/Al molar ratio. [e]Data was collected at TOS = 30 h. The value in the parentheses represents the temperature in steaming treatment. [f]Data was collected at TOS = 10 h. The value in the parentheses is Si/Al molar ratio.

the conjugated effect of gallium oxide and the proton on DHP, are illustrated in Figure 10A.[129] For C_3H_8 heterolytic dissociation (eqs 3-6 and 3-7 in Figure 10) in DHP, eq 3-6 (Figure 10) proceeds slowly and is, therefore, proposed as the RDS. The presence of acid sites can facilitate eqs 3-10 and 3-11 (Figure 10), providing an alternative to promote C_3H_6 formation by bypassing eq 3-6 (Figure 10). Such a reaction path likely occurs in the cases of TiO_2-, ZrO_2-, and Al_2O_3-supported Ga_2O_3 catalysts with abundant acid sites. For CO_2−ODHP, dissociative chemisorbed H_2 from eqs 3-6 and 3-10 (Figure 10) can be removed through eq 3-8 (i.e., RWGS), as well as eq 3-7(Figure 10). On Ga_2O_3/TiO_2, eq 3-8 is faster than eq 3-7 (Figure 10). More produced H_2 is consumed through RWGS, therefore, significantly boosting C_3H_6 formation by shifting the equilibrium because of the weak adsorption of H_2. Eq 3-7 (Figure 10) is fast and still a dominant reaction for the cases of Al_2O_3-, ZrO_2-, and MgO-supported catalysts. Therefore, the CO_2-promoting effect on these catalysts is absent (Figure 10B). The promoting effect is not evident on Ga_2O_3/SiO_2 either, resulting from its poor activity in RWGS (Figure 10B). The absence of the CO_2-promoting effect is also reported for Ga_2O_3−Al_2O_3 solid solution catalysts.[53] Another drawback of Ga_2O_3/TiO_2 is that the presence of abundant reduced $Ga^{\delta+}$ on the surface is detrimental to C_3H_6 selectivity (Table 5), as it is known with high aromatization efficiency.[130]

3.2.4. Explorations to Prepare Ga_2O_3 with High Surface Area. β-Ga_2O_3 is the most active among all Ga_2O_3 polymorphs, yet its surface area (e.g., 30 m^2 g^{-1}) limits its overall activity. For the DHP reaction, various methods have been developed to tune the textural properties of Ga_2O_3, such as the nanocasting technique using mesoporous carbon as a hard template[131] and the urea-based hydrothermal method using polyethylene glycol as a soft template agent.[132] The former method enables a significant increase in surface area up to 307 m^2 g^{-1}, but it is tedious and time-consuming; the latter one exerts limited accessible area (∼29 m^2 g^{-1}).

Wu et al. have demonstrated a method to synthesize mesoporous Ga_2O_3 with high surface area using a water-soluble, ecofriendly sucrose as a nonsurfactant template.[133] By increasing the sucrose/Ga_2O_3 molar ratio, the surface area of as-prepared β-Ga_2O_3 can be varied in the range of 65−98 m^2 g^{-1}. Among the catalysts, β-Ga_2O_3−S4 (sucrose/Ga_2O_3 molar ratio = 4) exhibits the highest catalytic performance, and outperforms the thermal decomposition-prepared β-Ga_2O_3 (Table 5). Furthermore, nearly 90% initial activity can be recovered after regeneration, which surpasses the value (∼74%) reported by Zheng et al.[121]

https://dx.doi.org/10.1021/acscatal.0c03999
ACS Catal. 2021, 11, 2182−2234

To prepare Ga_2O_3 with high surface area and mesophase, other soft templating approaches have been undertaken.[134,135] However, these are rather challenging because the yielded surfactant−Ga_2O_3 mesophase often collapses during thermal treatment, resulting in poorly ordered mesoporous Ga_2O_3 with low surface area. A nanocasting technique using a hard template, on the other hand, provides avenues to improve the heat tolerance, which uses a well-ordered, mesoporous structured matrix as a hard template, such as siliceous (e.g., SBA-15, KIT-6) or carbonaceous (e.g., CMK-3) materials. Michorczyk et al. have used SBA-15 as a hard template to prepare mesoporous Ga_2O_3-m and mixed Ga_2O_3−Al_2O_3 oxides (Ga/Al = 4/1 and 1/4) by the nanocasting method.[136] The as-prepared catalysts feature (i) high surface area, ranging from 231 to 322 m^2 g^{-1}, wherein the mixed oxide catalysts even show higher surface area than Ga_2O_3-m, (ii) uniform mesopores in the range of 3−14 nm, and (iii) characteristic pore architectures analogous to SBA-15 (hexagonal structure). As listed in Table 5, Ga_2O_3-m and Ga_2O_3−Al_2O_3(4/1) show comparable initial C_3H_8 conversion and C_3H_6 selectivity as the benchmark Ga_2O_3-t, which is produced by thermal decomposition of precursors. Notably, the nanocasting technique-prepared catalysts exert better stability, and all surpass the benchmark Ga_2O_3-t at TOS = ∼3.75 h, particularly for Ga_2O_3−Al_2O_3(1/4). A short regeneration in air can help Ga_2O_3-m almost completely recover its activity.

Alternatively, Xiao et al. have prepared Ga_2O_3−Al_2O_3 (GA) catalysts with high surface area (i.e., 234 and 220 m^2 g^{-1}, respectively) by hydrothermal synthesis (HS) and coprecipitation method (CP).[137] GA-HS exhibits the highest C_3H_8 conversion and C_3H_6 selectivity (Table 5). In addition to high surface area, the HS-prepared catalyst also features large pore sizes and more tetrahedral Ga ions as Lewis acid sites, all of which give rise to the improved catalytic performance.

3.3. Zeolite-Supported Catalysts. As discussed in section 3.1.1.3, the nature of the support has a crucial role in affecting metal dispersion and preserving redox Cr species; therefore, it strongly influences catalytic performance in CO_2−ODHP. In addition to the aforementioned mesoporous silica and various metal oxides, zeolites are also promising support materials because of their microporosity with large surface area, tunable acidity, and excellent thermostability.[138−140] To selectively activate C−H bond rather than C−C bond, the modification of acid sites is critical, especially the strong acid sites.[22] Dealumination is widely used to eliminate the surface acidity, and approaches include acid treatment[22] and steaming treatments at temperatures.[141,142] Weakening acidity is an alternative to control the surface acidity and can be achieved by tuning the Al amount[143] and incorporating another element into the framework of zeolite to displace the original strong Brønsted acid sites.[144] Zeolites that have been introduced as a support include Beta zeolite,[22] HZSM-5[141] and phosphorus-modified HZSM-5,[144] HZSM-48,[145,146] and boron-containing MFI.[147]

3.3.1. Dealumination. 3.3.1.1. Acid Treatment. Michorczyk et al. have prepared Cr-loaded Beta zeolite catalysts by wet impregnation for CO_2−ODHP.[22] Acid sites of the tetraethylammonium Beta (TEABeta) support are eliminated by dealumination with a nitric acid solution, resulting in SiBeta zeolite with Si/Al at 1000. For comparison, AlBeta is prepared by simple calcination of TEABeta with a lower Si/Al ratio of 17. As listed in Table 6, C_3H_8 and CO_2 conversion and C_3H_6 selectivity show an increase with an increase in Cr loading on Cr-SiBeta catalysts under the same reaction conditions, and are all higher than those on Cr-AlBeta. This demonstrates that a high concentration of strong acid prefers C_3H_8 cracking, thus significantly promoting the formation of C_2H_6, C_2H_4, and CH_4.

3.3.1.2. Steaming Treatment. Ga-loaded HZSM-5 catalysts become a potential candidate for CO_2−ODHP because of their reported high activity in aromatization of light paraffins.[148] The reaction is proposed to follow a bifunctional mechanism, in which Ga_2O_3 accounts for catalyzing propane dehydrogenation to light alkenes, while Brønsted acid sites are responsible for subsequent oligomerization of light alkenes and the cyclization of C_6−C_9 alkenes.[148] To transfer this catalyst into CO_2−ODHP, treatments are necessary to eliminate the acid sites or weaken their strength on HZSM-5 by dealumination. Xu et al. have carried out dealumination on HZSM-5 zeolite (Si/Al = 60) by steaming treatments at temperatures (i.e., 600−800 °C), followed by loading Ga_2O_3 via IWI.[141] NH_3−TPD results indicate that the number of acid sites monotonically decreases with the rise of steaming temperature. The dealumination not only enables the reduction of the acid sites on HZSM-5, but it also weakens the interaction between Ga_2O_3 and HZSM-5, resulting in an additional decease in the number of acid sites. As proposed in Figure 10A, CO_2−ODHP proceeds through a heterolytic dissociation reaction pathway on the gallium oxide catalysts. The presence of strong acid sites on HZSM-5 can facilitate the conjugated effect of protons and gallium oxide, resulting in promoted activity (eq 3-10 in Figure 10A). However, excess acid sites on HZSM-5 can promote coke formation via oligomerization and cyclization, causing deactivation. Therefore, a balance of such a trade-off can optimize the catalytic performance on Ga_2O_3/HZSM-5 treated at 700 °C (Table 6).

Zhu et al. eliminate the acid sites on boron-containing MFI zeolite-supported CrO_x catalysts by steaming treatment.[147] Cr/H[B]MFI exhibits higher C_3H_8 conversion and C_3H_6 selectivity than the benchmark Cr/silicate-1 (Table 6). The steaming-treated catalyst, namely Cr/H[B]MFI-st, has comparable C_3H_6 selectivity, yet lower C_3H_8 conversion. Characterization results demonstrate that the steaming treatment results in the autoreduction of some Cr^{6+} to Cr^{3+} which is located at the ion-exchange sites in the vicinity of boron sites. As known in the literature, Cr^{3+} polychromate is less active for CO_2−ODHP than Cr^{6+} monochromate, though it still can catalyze the reaction.[80] This explains the lower conversion observed on Cr/H[B]MFI-st. Noteworthily, Cr/H[B]MFI-st presents higher C_3H_8 conversion after TOS = ∼40 h, indicating its better stability than Cr/H[B]MFI.

3.3.2. Surface Acidity Weakening. Increasing Si/Al ratios is an option to weaken the acidity. HZSM-48 is also a candidate of support material because of its medium pore size and high Si/Al molar ratio, accompanied by weaker acidity compared to HZSM-5.[145,146] Ren et al. have prepared a Ga_2O_3/HZSM-48 catalysts with the Si/Al ratios from 130 to 220, and performed comparative studies with Ga_2O_3/HZSM-5 for CO_2−ODHP.[149] HZSM-48 supported catalysts exhibit higher C_3H_6 selectivity than the HZSM-5 supported counterpart and comparable C_3H_6 yield, but lower C_3H_8 conversion (Table 6). Despite high selectivity, Ga_2O_3/HZSM-48 has worse stability than the HZSM-5-supported counterpart. This can be ascribed to weak-acid-induced side reactions, through which the formed coke clogs the 2D channels. This is

https://dx.doi.org/10.1021/acscatal.0c03999
ACS Catal. 2021, 11, 2182−2234

Table 7. Summarized Activity Performance of Other Transition Metal Catalysts for CO_2−ODHP

catalyst	temp (°C)	C_3H_8/CO_2 ratio	conversion (%)		yield (%)	selectivity (%)				ref
			C_3H_8	CO_2	C_3H_6	C_3H_6	C_2H_6	C_2H_4	CH_4	
Fe_2O_3[a]	600	1: 5	8.2		7.6	92.5		3.8	3.7	154
$(Fe_2O_3)_{7.1}/\gamma\text{-}Al_2O_3$[a]	600	1: 5	2.3		1.9	83.6		8.3	8.1	154
$(Fe_2O_3)_{5.0}/AC$[a]	600	1: 5	29.7		25.6	86.2		5.7	6.1	154
Fe_2O_3−MgO-10[a]	600	1: 5	3.0		2.2	73.7		15.2	11.2	154
Fe_2O_3−MgO-30[a]	600	1: 5	3.0		2.5	83.2		9.9	6.9	154
Mo_2C/SiO_2[b]	500	∼1: 1	∼1.1		∼1	∼92		∼3.5	∼2	159
	670	∼1: 1	∼20.0		∼11	∼55		∼25	∼16	159
Pd_1[c]	550	1: 1	0.4	3.2	0.18	44.4		27.4 (C_1−C_2)		155
Pt_1[c]	550	1: 1	1.6	4.2	0.4	21.2	0.9	0	0.8	12
Ni_1[c]	550	1: 1	3	9.3	0.4	12.3	0.24	0	0.6	12
Ni_3[c]	550	1: 1	9.6	32.8	0.3	2.9	0.05	0.06	2.11	12
Fe_3[c]	550	1: 1	0.45	0.10	0.2	∼44.4				12
Fe_3Pd_1[c]	550	1: 1	0.4	0.1	0.22	57.6		36.8 (C_1−C_2)		155
Co_3Pd_1[c]	550	1: 1	2.8	8.4	0.71	25.2		8.1 (C_1−C_2)		155
Ni_3Pd_1[c]	550	1: 1	5.3	17.6	0.59	11.2		0.8 (C_1−C_2)		155
Fe_3Pt_1[c]	550	1: 1	1.1	2.6	0.3	32	0	1.6	1.3	12
Co_3Pt_1[c]	550	1: 1	5.6	20.3	0.6	10.1		1.1 (C_1−C_2)		155
Ni_3Pt_1[c]	550	1: 1	11.6	39.4	0.3	2.8	0.1	0	0.83	12
Ni_3Pt_1*[c]	550	1: 1	2.2	7.8	0.2	11	0	0.3	0.9	12
Fe_1Co_3[c]	550	1: 1	0.9	1.5	0.39	43.8		14.0 (C_1−C_2)		155
Fe_3Co_1[c]	550	1: 1	0.27	0.23	0.15	57.1		17.3 (C_1−C_2)		155
Fe_3Ni_1[c]	550	1: 1	2.7	4	1.6	58.2	0	0.8	0.8	12
Fe_1Ni_3[c]	550	1: 1	7.4	26.9	0.22	2.9		0.7 (C_1−C_2)		155
Fe_3Ni_3[c]	550	1: 1	5.0	16.1	1.0	20.4		2.7 (C_1−C_2)		155
Fe_9Ni_3[c]	550	1: 1	3.4	10.9	0.83	22.5		4.1 (C_1−C_2)		155
Co_1Ni_3[c]	550	1: 1	7.8	27.8	0.2	2.6		1.8 (C_1−C_2)		155
Co_3Ni_1[c]	550	1: 1	7.6	27.1	0.2	2.1		0.5 (C_1−C_2)		155
Co_3Ni_3[c]	550	1: 1	8.5	29.8	0.2	2.4		2.1 (C_1−C_2)		155
CeO_2[d]	550	1: 1	∼2.5	∼<1	∼1	40				29
Fe_2O_3[d]	550	1: 1	∼5	∼<1	∼1.1	∼22.5				29
Fe_2O_3/CeO_2-phy[d]	550	1: 1	∼7	∼7	∼2.5	∼36				29
Fe_1CeO_2[d]	550	1: 1	∼7	∼7	∼2.2	∼31				29
$Fe_{2.5}CeO_2$[d]	550	1: 1	∼7.5	∼7.5	∼2.6	∼35				29
Fe_5CeO_2[d]	550	1: 1	∼10	∼11	∼3.9	∼39				29
$Fe_{10}CeO_2$[d]	550	1: 1	∼17.5	∼24	∼8.2	∼47				29
$Fe_{15}CeO_2$[d]	550	1: 1	∼22	∼28	∼9.9	∼45				29
$CeZrAlO_x$[e]	500	1: 1	3		2.5	82				171
Pd_5/Al_2O_3[e]	500	1: 1	8.7		5.6	64				171
$Pd_5/ZrAlO_x$[e]	500	1: 1	3.3		2.5	76				171
$Pd_5/CeZrO_x$[e]	500	1: 1	10.1		9.3	92				171
Pd_5/CeO_2[e]	500	1: 1	8		6.7	84				171
$Pd_5/CeZrAlO_x$[e]	500	1: 1	9.5		8.8	93				171

[a] Fe_2O_3 loadings of $Fe_2O_3/\gamma\text{-}Al_2O_3$ and Fe_2O_3/AC are 7.1 and 5.0 wt. %, respectively; those of Fe_2O_3−MgO-10 and Fe_2O_3−MgO-30 are 10 and 30 wt. %, respectively. [b] Mo_2C/SiO_2 catalyst is formed from the original prepared MoO_3/SiO_2 catalyst (2 wt. % of MoO_3) via carburation upon contact with C_3H_8. [c] All catalysts are supported on commercial CeO_2 (35−42 $m^2\ g^{-1}$, Sigma-Aldrich). Catalysts are synthesized by atomic ratios corresponding to a 1.67 wt. % Pt_1 basis; thus, the weight percent values of Pd_1, Fe_1, Fe_3, Co_1, Co_3, Ni_1, and Ni_3 are 0.91%, 0.48%, 1.43%, 0.5%, 1.5%, 0.5%, 1.5%, respectively. The nomenclature assigned by subscripts, such as the Fe_3Ni, means that there are three atoms of Fe for every atom of Ni. Catalysts marked with an asterisk indicate that the sample was diluted to achieve comparable C_3H_8 reactant conversion to Fe_3Ni. [d] Fe_2O_3/Ce_2O_3-phy represents a physical mixture with Fe_2O_3/CeO_2 = 1/20 molar ratio. Other Fe−Ce solid solution catalysts are prepared by coprecipitation; values in the subscript indicate the molar percentage of Fe over Ce atoms. [e] Pd loading is 5 wt. % for all catalysts. The composition of $CeZrO_x$ is $Ce_{0.25}Zr_{0.25}Al_{0.5}O_x$. Data were collected at TOS = 1 h.

reflected from the more serious degradation of pores on HZSM-48 after reaction than on HZSM-5.

Differently, Ren et al. tune the Si/Al molar ratio (i.e., 60−242) of ZnO/HZSM-5 by varying the amount of Al source, namely, $NaAlO_2$, during preparation.[143] As proposed, the reaction proceeds through dissociative adsorption of C_3H_8 on Zn oxide sites and a subsequent one-step elimination to produce H_2 and C_3H_6. This requires that both $[Zn-C_3H_7]^+$ and the framework attached H^+ ions are in proximity. Therefore, the presence of protons from the zeolite framework can facilitate the recovery of active sites, resulting in enhanced activity. However, excess acid sites are detrimental to the activity and stability because of the catalyzed reactions to form coke. Therefore, an optimal Si/Al ratio is obtained at 160 with the highest C_3H_6 yield (Table 6). At TOS = 10 h, the C_3H_8 conversion drops from 68.3% to 50.2%. Regeneration in O_2

https://dx.doi.org/10.1021/acscatal.0c03999
ACS Catal. 2021, 11, 2182−2234

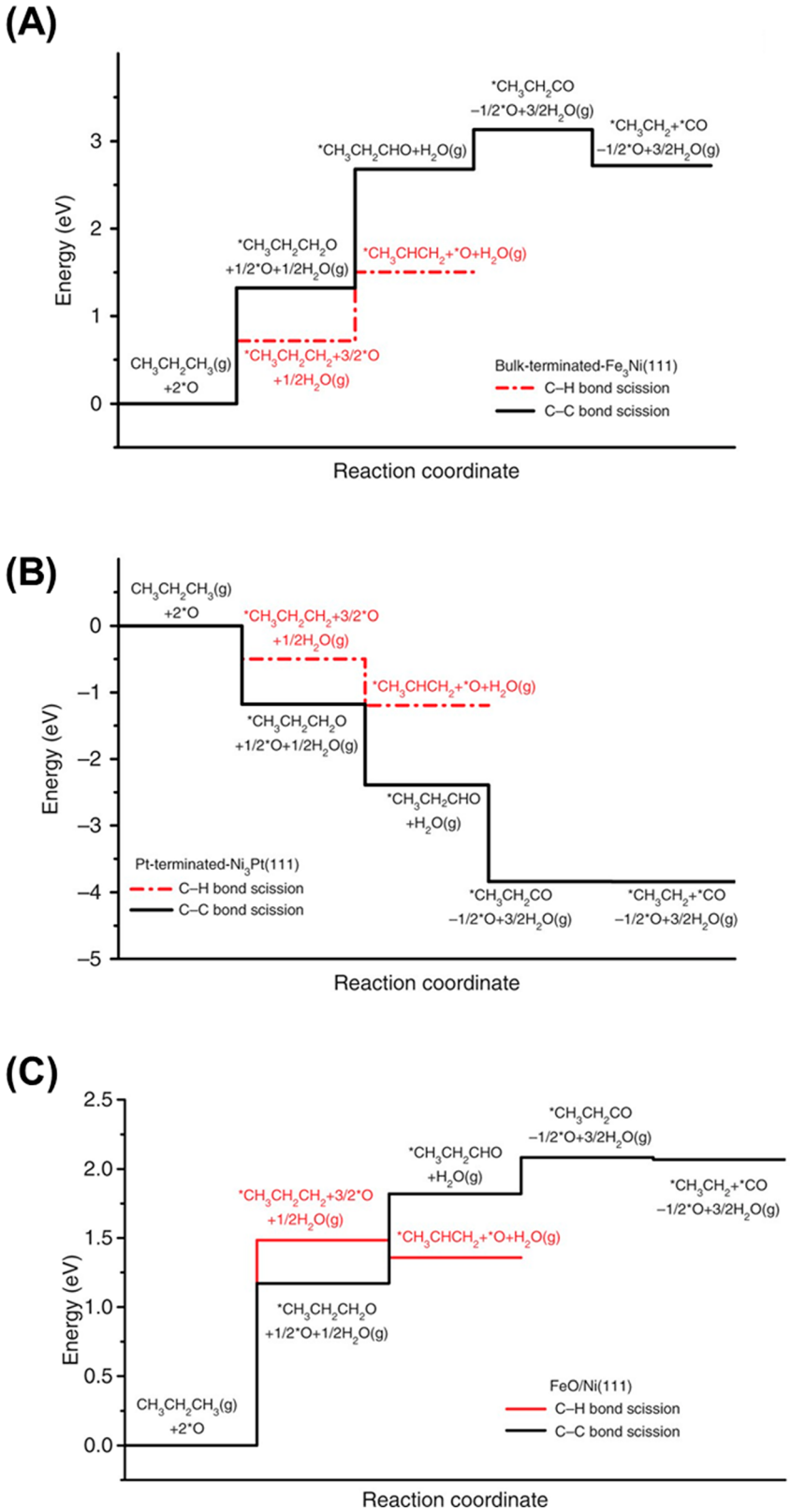

Figure 11. DFT calculated energy profiles for the oxidative C−H and C−C bond scission pathways. (A) Bulk Fe-terminated $Fe_3Ni(111)$ surface, (B) Pt-terminated $Ni_3Pt(111)$ surface, and (C) FeO/Ni(111) interface. Reproduced with the permission from ref 12. Copyright 2018 Springer Nature.

twice can help to completely recover the C_3H_8 conversion. Alternatively, dealumination of the ZnO/HZSM-5 catalysts has also been examined by a steaming treatment, and the 650 °C-treated catalyst exhibits the highest C_3H_6 yield and C_3H_8 conversion (Table 6).[142]

https://dx.doi.org/10.1021/acscatal.0c03999
ACS Catal. 2021, 11, 2182−2234

Introducing phosphorus into HZSM-5 is another option to displace the original strong Brønsted acid sites by newly created weakened Brønsted acid sites, as well as to improve hydrothermal stability.[144] Compared to the benchmark Ga_2O_3/HZSM-5, the enhanced activity and yield are evident (Table 6); yet the Ga_2O_3/P-HZSM-5 catalysts fail to show comparable C_3H_8 conversion or C_3H_6 yield to the steaming-treated, P-free catalyst Ga_2O_3/HZSM-5(700). The created weak acid sites barely show any promotional effect on C_3H_6 formation, while mainly on side reactions, thus leading to deactivation. Clearly, reducing the number of acid sites on HZSM-5 is a more effective approach to boost C_3H_8 dehydrogenation to C_3H_6 than weakening the acidity.

3.4. Other Transition Metal Catalysts. *3.4.1. Fe-Based Catalysts. 3.4.1.1. Fe_2O_3 Catalysts.* Fe oxide-based catalysts are potential candidates for CO_2−ODHP as they have been known to catalyze oxidative dehydrogenation of hydrocarbons, such as ethylbenzene and isobutane.[150−153] Michorczyk et al. have conducted screening tests on bare Fe_2O_3, supported Fe_2O_3 (active carbon (AC) and γ-Al_2O_3) catalysts, and hydrotalcite-derived Mg−Fe oxides.[154] Among them, Fe_2O_3/AC outperforms the rest in both C_3H_8 conversion and C_3H_6 yield, along with comparable C_3H_6 selectivity to the bare Fe_2O_3 (Table 7). H_2-TPR results demonstrate that Fe_2O_3/AC exhibits improved reducibility, and its reduction proceeds through $Fe_2O_3 \rightarrow Fe_3O_4 \rightarrow FeO \rightarrow Fe$. However, the reducibility of Fe_2O_3/γ-Al_2O_3 and hydrotalcite-derived Fe−Mg catalysts is retarded due to the strong interaction between Fe oxide with support. For example, loading Fe_2O_3 on γ-Al_2O_3 leads to the formation of a spinel phase $FeAl_2O_3$ which is hardly reduced; Fe^{3+} cations are reduced to Fe^{2+} ions which are strongly stabilized in the MgO matrix. Clearly, the improved reducibility of Fe_2O_3 on AC accounts for the obtained high catalytic performance among the catalysts tested, and the redox cycle of Fe oxide likely plays a crucial role in CO_2−ODHP. Noteworthily, the absence of H_2 from the reaction excludes the occurrence of RWGS. Combined with these observations, it is postulated that the reaction proceeds through (i) C_3H_8 oxidation to C_3H_6 on lattice oxygen from Fe_2O_3 or Fe_3O_4 and (ii) reoxidation of reduced Fe oxide by the CO_2 soft oxidant.

3.4.1.2. Fe−Ni Bimetallic Catalysts. To prepare cost-effective, selective, and coke-resistant catalysts for CO_2−ODHP, Gomez et al. have conducted screening tests of monometallic and bimetallic transition metals and attempted to establish a library to determine the inherent activity toward either ODHP or DRP.[155] Transition metals that are active in ODHP and dry reforming, as well as efficient in coke resistance, were chosen, such as Fe, Ni/Co, and Pt/Pd. The Fe_xNi_y catalysts favor the CO_2−ODHP path, and selectivity can be manipulated by varying the Ni content; others are active and selective for the DRP path (Table 7). The same group has continued to examine the competitive paths between CO_2−ODHP and DRP at industrial operational conditions over these catalysts.[12] Monometallic catalysts exhibit low activity and selectivity toward C_3H_6 production (Table 7). The combination of Fe and Ni substantially improves both activity and selectivity, while combining Ni and Pt favors dry reforming products with much higher conversion of both reactants (Table 7). Clearly, there is a synergistic effect on Fe_3Ni_1 (i.e., C_3H_6 yield = 1.6%) in comparison to the simple sum of yields on the monometallic counterpart (e.g., 0.4% and 0.2% for Ni_1 and Fe_3, respectively). In situ X-ray absorption spectroscopy measurements (XANES and EXAFS) demonstrate that the Ni_3Pt catalyst consists of metallic Pt and Ni with the formation of Pt−Ni bimetallic bonds, while the metallic Ni and oxidized Fe species present an inserted oxygen through Fe−O−Fe, as well as Fe−O bonds. Combined with DFT calculations, C−H bond scission is shown to be more thermodynamically favorable and kinetically feasible than C−C bond scission on the bulk-terminated $Fe_3Ni(111)$ surface (Figure 11A), while Pt-terminated $Ni_3Pt(111)$ favors C−C bond scission (Figure 11B). Other identified interfacial active sites Fe−O−Ni show competitiveness in the first step of C−H and C−C bond scissions, whereas the following step of C−H scission is downhill in energy, while that of C−C scission is uphill in energy (Figure 11C). These results corroborate the crucial roles of oxidized Fe and metallic Ni in C_3H_6 production.

3.4.1.3. Fe−Ce Solid Solution Catalysts. Inspired by the well-recognized characteristics of CeO_2 in improving oxygen mobility and oxygen storage capacity, Wang et al. report Fe-doped CeO_2 solid solution catalysts for CO_2−ODHP.[29] Among the catalysts with Fe/Ce ratios from 1 to 15%, both activity (C_3H_8 conversion and C_3H_6 yield) and C_3H_6 selectivity are optimized at higher Fe/Ce ratios (Table 7). Deactivation as a consequence of coking occurs at low Fe/Ce ratios (i.e., <5%), while the $FeCeO_2$ catalysts with higher Fe/Ce ratios (i.e., >5%) suffer from CeO_2 crystal sintering and Fe migration to form nanosized crystals. Therefore, Fe_5CeO_2 has the optimal activity at Fe/Ce = 5 and exerts stable performance for more than 20 h on stream.

3.4.2. Mo-Based Catalysts: Mo_2C. Supported Mo_2C is reported to be active for methane conversion to benzene, in which Mo_2C is crucial in activating the C−H bond of methane and subsequently forming CH_x fragments on the surface.[156,157] Also, it is established as an effective catalyst for oxidative dehydrogenation of ethane with CO_2.[158] On the basis of these findings, Solymosi et al. have prepared SiO_2-supported Mo_2C catalysts and evaluated their catalytic performance in CO_2−ODHP.[159] At low temperatures (i.e., ≤ 500 °C), CO_2 adsorption is too weak to dissociate on Mo_2C, leading to poor activity at 500 °C, though a high C_3H_6 selectivity is attained (Table 7). At high temperatures (i.e., 670 °C), CO_2 can oxidize Mo_2C, resulting in enhanced activity, yet C_3H_6 selectivity is compromised because of the thermo-induced cracking to C_2H_4 (Table 7). Oxidation of Mo_2C with CO_2 is proposed as the initial step to activate the Mo_2C surface, through which the Mo oxycarbide is formed with active oxygen to activate the methylene C−H bond in C_3H_8 molecules.[160]

3.4.3. Precious Metal Catalysts (Rh, Ru, Pt, and Pd). An early work, led by Solymosi et al., shows that Al_2O_3-, SiO_2-, TiO_2-, and MgO-supported Rh catalysts have relatively low C_3H_6 selectivity (i.e., 50−60%) in the DHP reaction at 550−650 °C, along with the C_3H_8 conversion varying from ∼1 to 6%.[161] In the presence of CO_2, the reaction pathway shifts from DHP to dry reforming of propylene on the Rh catalyst, resulting in the dominance of CO and H_2 with decreased C_3H_6 selectivity. Similar results are also evident on the Pt/Al_2O_3 catalyst[162] and supported Au catalysts.[163] CO and H_2 become the major products in the case of Ru/CeO_2 and Ru/ZrO_2, regardless of the reducibility of these support materials.[164] Precious and noble metals are active in C−C cleavage and the dry reforming reaction, which make them less suitable for catalyzing CO_2−ODHP as a single active

https://dx.doi.org/10.1021/acscatal.0c03999
ACS Catal. 2021, 11, 2182−2234

component. An option to use precious metals is to make them an assistant component responsible for the regeneration of active sites.

Ceria proves to be an effective catalyst for CO_2-assisted oxidative dehydrogenation of ethylbenzene to styrene, and the high activity is linked with its oxygen storage/release capacity (OSC) in terms of creation and replenishment of oxygen vacancies.[165−168] Adding ZrO_2 into CeO_2 endows the formed bimetallic oxides with more stabilized oxygen vacancies; moreover, CO_2 dissociation can occur on $CeZrO_x$ and lead to a highly oxidized state of Ce.[169] To improve the durability of such oxide combination, Al_2O_3 is used as the underlying support.[170] Inspired by the functionalities of these components in mixed oxide catalysts, Nowicka et al. have prepared Pd catalysts supported on $CeZrAlO_x$ mixed oxides with various compositions and evaluated their activity in CO_2−ODHP.[171] Screening tests clarify that the optimal composition and Pd loading are obtained on $Ce_{0.25}Zr_{0.25}Al_{0.5}O_x$-supported Pd catalyst (Table 7); Pd/$Ce_{0.25}Zr_{0.25}Al_{0.5}O_x$ also displays long-term stability of C_3H_8 conversion from 40 to 140 h on stream, along with a slight rise of C_3H_6 selectivity from ∼94% to 98%. As proposed in Figure 12, reactions on

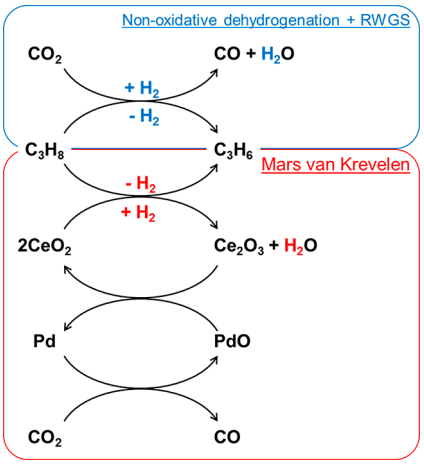

Figure 12. Schematic illustration of reaction involved in the overall CO_2−ODHP over Pd/$CeZrAlO_x$ catalysts. Reproduced with the permission from ref 171. Copyright 2018 American Chemical Society.

$Ce_{0.25}Zr_{0.25}Al_{0.5}O_x$ proceed through a combined Mars van Krevelen (MvK) and RWGS mechanism linked by a common step. The lattice oxygen ions abstract H from C_3H_8 to form C_3H_6 and H_2O. CO_2 takes part in the replenishment of the consumed O species in both $Ce_{0.25}Zr_{0.25}Al_{0.5}O_x$ and Pd sites, releasing CO as a byproduct. Of note, Pd only promotes the oxidation activity of the redox sites $Ce^{3+} \leftrightarrow Ce^{4+}$ in the catalyst rather than the secondary reaction, such as dry reforming of propylene. Therefore, its presence boosts overall C_3H_8 conversion without sacrificing C_3H_6 selectivity.

3.5. Roles of CO_2 in CO_2−ODHP. Early work has considered co-fed CO_2 merely as a diluent and heating medium, yet continuing studies unravel its other important roles.[57] Liu et al. have conducted DFT studies of CO_2−ODHP over Ga_2O_3(100) surface and suggested that C_3H_6 forms via DHP in CO_2−ODHP.[172] Positive roles of CO_2 include (i) reoxidizing the reduced catalyst surface, (ii) shifting the reaction equilibrium to the product side of CO_2−ODHP by consuming the produced H_2 via RWGS, and (iii) removing surface deposited carbon via reverse Boudouard reaction. These positive effects are generally applicable to all catalysts that have been developed but vary depending on the redox properties of the active metal oxides and the nature of the support. Negative impacts also exist, which are mainly reflected in the competitive CO_2 adsorption against C_3H_8.

3.5.1. Oxidation State and Redox Cycle. Redox-active metal oxides can be reduced upon the contact with C_3H_8. In comparison to the direct DHP reaction, a donation of oxygen species in CO_2 can help to maintain Cr at high oxidation states.[173,174] Despite the weak oxidizing potential, CO_2 can take part in the reoxidation of CrO_x to complete the redox cycle, benefiting C_3H_8 dehydrogenation to C_3H_6. This positive role in the case of CrO_x has already been discussed in section 3.1. Similarly, adding CO_2 can change the redox properties of the V-based catalysts, such as the oxidation states. Takahara et al. report that using CO_2 as an oxidant results in the presence of V^{5+} rather than V^{4+}/V^{3+} in the direct DHP reaction.[175] In DHP, the V−OH sites adjacent to V^{4+}/V^{3+} are proposed as acid sites on VO_x, which are detrimental to C_3H_6 yield by boosting the reaction of propylene to aromatics.[176] CO_2 addition reduces the number of acid sites by changing the oxidation state to V^{5+}, leading to a higher propylene yield by inhibiting aromatization.

3.5.2. CO_2-Promoting Effects in Shifting Reaction Equilibrium of CO_2−ODHP. Isotope-labeling experiments have been conducted by introducing D_2 in the feed with C_3H_8 and CO_2, and revealed only 45% of the formed water contains D_2O.[28] This observation confirms the existence of parallel-consecutive reaction networks consisting of ODHP, DHP, and RWGS. Figure 13 shows changes in the C_3H_6 formation rate during switch-operation mode between DHP and CO_2−ODHP on CrSiBeta and CrAlBeta catalysts.[22] Clearly, the CO_2-promoting effect on C_3H_6 formation is only evident on the CrSiBeta catalyst, as evidenced from the alternatingly highest C_3H_6 and H_2 formation rates in CO_2−ODHP (Figure 13A). This indicates that the H_2 formed through the DHP is consumed by reacting with CO_2, which shifts the reaction equilibrium of the ODHP to the product side with a higher C_3H_6 formation rate. This CO_2-promoting effect is also valid on other catalysts, such as Cr/HZSM-5[141,143] and Cr-SBA-1,[66] and Ga_2O_3 catalysts,[121,129] regardless of redox properties.

It is noteworthy that the CO_2-promoting effect is not universal and is affected by the nature of the support, such as CrAlBeta in Figure 13B. Combined with the low Si/Al ratio in this catalyst, the stronger acidity might interfere in the CO_2-promoting effect by shifting the reaction pathways.[22] Among Al_2O_3-, activated carbon (AC)-, and SiO_2-supported Cr_2O_3 catalysts for CO_2−ODHP, Takahara et al. observe that the CO_2-promoting effect is only evident on Cr_2O_3/SiO_2.[74,75] The correlation between CO/H_2 ratio and C_3H_6 yield demonstrates that DHP and RWGS occur in the case of Cr_2O_3/Al_2O_3, while the combination of DHP and DRP occurs on Cr_2O_3/SiO_2.

3.5.3. Agent for Coke Removal. The reverse Boudouard reaction is an endothermic reaction, which likely happens in the temperature range that has been explored (i.e., 500−650 °C) for CO_2−ODHP. Pulse experiments have confirmed that little coke forms in the presence of CO_2 on bulk Ga_2O_3 catalysts, and CO_2 can serve as an agent to remove deposited carbon through the reverse Boudouard reaction.[23] A similar effect on coke removal has also been observed on other

https://dx.doi.org/10.1021/acscatal.0c03999
ACS Catal. 2021, 11, 2182−2234

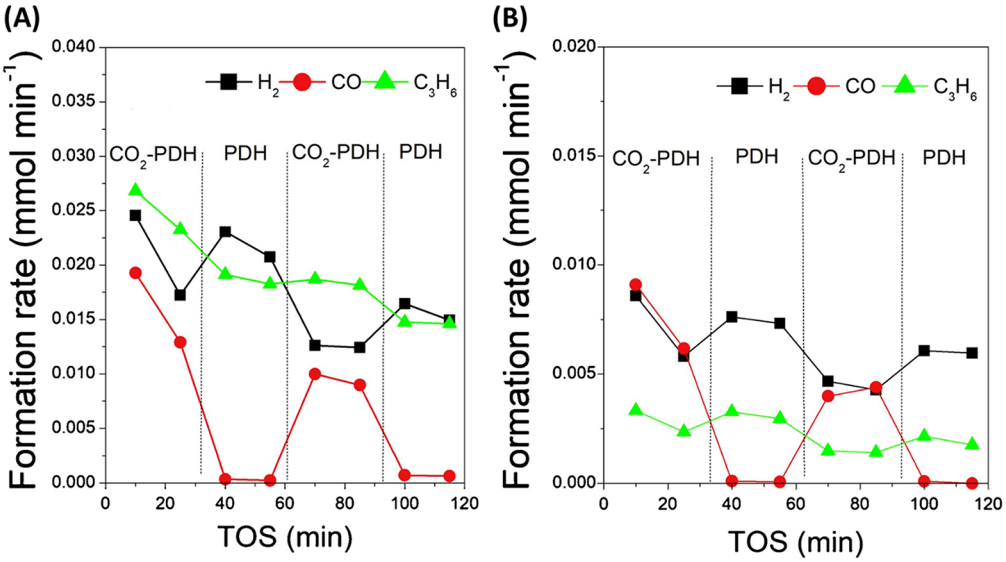

Figure 13. Rate of C_3H_6 formation, H_2, and CO in C_3H_8 dehydrogenation in the presence (CO_2−PDH) and absence (PDH) of CO_2 at 550 °C over $Cr_{2.0}$SiBeta (A) and $Cr_{2.0}$AlBeta catalysts (B). Reproduced with the permission from ref 22. Copyright 2020 Elsevier B.V.

catalyst systems, including Cr_2O_3/SiO_2,[74,75] Cr/HZSM-5,[141,143] and Cr-MCM-41.[173,174] Of note, CO_2 cannot completely prevent deactivation or completely eliminate coke, but it can help to alleviate coke formation.

CO_x-derived coke may form through two conditions on Cr sites: (i) CO_2 fixation caused by reduced Cr species with abundant H species at the surface and (ii) carbon chain growth and aromatization reaction triggered at high temperatures (i.e., >300 °C).[73] The presence of CO_2 consumes the surface atomic H species, the concentration of which becomes too low to deoxygenate C−O species to form hydrocarbon species through C−C coupling chain growth or aromatization. Clearly, not only can CO_2 contribute to the coke removal, but it can also inhibit coking, benefiting the overall stability of Cr catalysts for CO_2−ODHP.

3.5.4. Competitive Adsorption between CO_2, C_3H_8, and C_3H_6. A negative role of CO_2 has also been reported on redox CrO_x catalysts, in which the presence of CO_2 in the feed gas hampers the adsorption of C_3H_8.[24] On the other hand, it prevents the adsorption of C_3H_6 and its subsequent conversion into coke.[24] Therefore, an overall CO_2-promoting effect still predominates in the case of CrO_x. On HZSM-5-supported Ga_2O_3 catalysts with a non-redox property, the reaction proceeds through a heterolytic dissociation mechanism, in which C_3H_8 dissociates on acid−base pairs in the forms of H^- and $C_3H_7^+$, respectively (Figure 10A).[127] As a more acidic molecule than C_3H_8, CO_2 adsorption on basic sites will negatively impact C_3H_8 adsorption on Ga_2O_3, causing drop in activity. In particular, the negative impact prevails at higher CO_2 partial pressures. Hence, a proper C_3H_8/CO_2 ratio is of importance for high dehydrogenation activity in CO_2−ODHP. This is the area where more efforts are needed in future studies.

4. OXIDATIVE DEHYDROGENATION OF PROPANE WITH NITROUS OXIDE

Another milder oxidant that is favored to reduce formation of unwanted overoxidation is nitrous oxide (N_2O). Using N_2O as an oxidant may be an effective way to utilize N_2O, which is an acidic, strong greenhouse gas. Using N_2O as an oxidant instead of oxygen results in a significant increase in propylene selectivity for many different catalysts, including iron-containing zeolites and vanadium-based catalysts.[20,177−181] While iron-based materials, such as Fe-ZSM-5, are found to be the catalysts that give the highest C_3H_6 yield for ODHP using N_2O, other catalysts, including redox metal catalysts, such as vanadium and molybdenum, have been studied as well.[179,182−185] However, despite the improved propylene selectivity, most of N_2O−ODHP catalysts reported to date deactivate quickly, mainly because of coke formation, making N_2O a currently less feasible oxidant than other soft oxidants, such as CO_2.[180−184,186,187] While an in depth study regarding the rate of deactivation or deactivation mechanism has not been reported for molybdenum oxide catalysts, both vanadium- and iron-based catalysts are reported to deactivate within several hours on stream. Therefore, improvement in catalyst stability and clear understanding of deactivation mechanisms remain challenges that need further study in the dehydrogenation of propane using N_2O.

4.1. Metal Oxide Catalysts. *4.1.1. Vanadium Oxides.* In general, for vanadium catalysts, using N_2O instead of O_2 in ODHP results in increased selectivity of C_3H_6.[20,177,186−189] For example, Baerns et al. show that a significant increase in C_3H_6 selectivity from ∼55% to 75% can be obtained by using N_2O instead of O_2 as an oxidant for 0.5% VO_x/γ-Al_2O_3.[188] Also, Dingerdissen et al. show that C_3H_6 selectivity of up to ∼90% can be obtained with a V_2O_5 catalyst when using N_2O as an oxidant, while the highest selectivity obtained using O_2 as the oxidant is ∼78%.[186] Furthermore, while selectivity tends to decrease as C_3H_8 conversion increases, this effect is much less pronounced when N_2O is used as the oxidant.[179,186,189] As reported by Kondratenko et al., when O_2 is used for ODHP, a decrease in C_3H_6 selectivity from ∼75% to ∼50% is observed as C_3H_8 conversion increases from ∼2% to ∼10% using a 2.8% VO_x/SiO_2 catalyst.[186] In contrast, when N_2O is used, a less significant decrease in selectivity is observed, falling from ∼93% to 81%, for a similar change in C_3H_8 conversion.

Such improved C_3H_6 selectivity using N_2O is attributed to the lesser ability of N_2O to oxidize reduced VO_x species. It is

https://dx.doi.org/10.1021/acscatal.0c03999
ACS Catal. 2021, 11, 2182−2234

observed in numerous reports that VO_x species tend to be in a more oxidized state when exposed to O_2 than N_2O.[20,186,188,189] UV−vis measurements of a 9.5% VO_x/γ-Al_2O_3 catalyst in different gas mixtures, as shown in Figure 14,

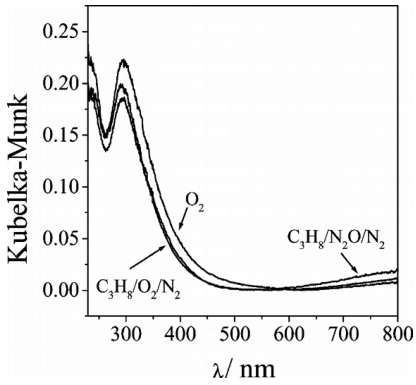

Figure 14. UV−vis−DRS spectra of VO_x (9.5 wt. %)/γ-Al_2O_3 after pretreatment in an O_2/N_2 = 20/80 mixture at 500 °C and under reaction conditions at the same temperature: $C_3H_8/O_2/N_2$ = 30/15/55 and $C_3H_8/N_2O/N_2$ = 30/30/40. Reproduced with the permission from ref 188. Copyright 2001 Elsevier B.V.

are one example that supports such a notion.[188] The intensity of the two bands at 230 and 300 nm, indicating the presence of V^{5+} species, decreases substantially when C_3H_8 oxidation is performed with N_2O rather than O_2. This indicates that more V^{5+} cations are reduced when C_3H_8 oxidation is performed with N_2O than O_2. Similarly, as shown in Table 8, XPS

Table 8. Near Surface Composition Derived from Ex Situ XPS Analysis of Different Vanadium Oxides in Fresh State, as Well as after ODHP with O_2 and N_2O at T= 500 °C ($X(C_3H_8)$ < 5%, $X(O_2)$ < 10%, $X(N_2O)$ < 10%)

	near surface vanadium concentration from ex situ XPS			
		after O_2−ODHP		after N_2O−ODHP
catalyst	fresh	$C_3H_8/O_2/Ne$ = 40/20/40	$C_3H_8/O_2/Ne$ = 40/10/50	$C_3H_8/N_2O/Ne$ = 40/40/20
V_2O_5	V^{5+} (100%)	V^{5+} (100%)	V^{5+} (66%), V^{4+} (26%), V^{3+} (8%)	V^{5+} (58%), V^{4+} (32%), V^{3+} (10%)
VO_2	V^{5+} (90%), V^{4+} (10%)	V^{5+} (100%)		V^{5+} (47%), V^{4+} (37%), V^{3+} (16%)
V_2O_3	V^{5+} (83%), V^{4+} (17%)	V^{5+} (100%)		V^{5+} (47%), V^{4+} (44%), V^{3+} (9%)

Reproduced with the permission from ref 186.Copyright 2007 Elsevier B.V

analysis of V_2O_5, VO_2, and V_2O_3 catalysts after O_2−ODHP also indicates that VO_x species are much more reduced in N_2O than in O_2.[186] Interestingly, as shown in Table 9, C_3H_6 selectivity tends to be higher as the VO_x species are more reduced. From such observations, it is proposed that C_3H_6 selectivity is affected by surface reduction: the higher the surface reduction, the higher the selectivity.

Regarding the vanadium oxide species that are formed in ODHP using O_2 and N_2O, Sauer et al. propose that the formation of peroxovanadate species can be responsible for the decreased selectivity to C_3H_6 when using O_2.[177] In their DFT analysis, it was reported that formation of peroxovanadate species is much more favored in O_2, while the formation of vanadyl oxygen species is more favored under N_2O. On the basis of this observation, Sauer et al. assert that the peroxovanadate site leads to consecutive C_3H_6 oxidation, while such a phenomena is more limited on the vanadyl oxygen site, leading to higher selectivity of C_3H_6 during ODHP.[177] More detailed discussion regarding progress in theoretical studies is covered in section 6.2. In the analysis of ODHP on a VO_x/MCM-41 catalyst using electron paramagnetic resonance (EPR), Bruckner et al. state that higher activity and lower selectivity toward C_3H_8 with O_2 than N_2O are attributed to the formation of highly reactive electrophilic O^- species under O_2, while nucleophilic, less active O^{2-} ions serve as reactants under N_2O.[20] Their results indicate that electrophilic $V^{n+}\cdots O^{\cdot-}$ (n = 4 or 5) species form when the catalyst is pretreated with O_2, likely through the dissociation of adsorbed oxygen species. However, such species are not observed after treatment with N_2O, likely due to rapid formation of O^{2-} oxide ions, which are not EPR-active. Combining previous DFT results with their observation from EPR, Kondratenko et al. propose that high activity and low selectivity of C_3H_6 in ODHP using O_2 is likely due to electrophilic $V^{n+}\cdots O^-$ site formation, which is formed as a result of decomposition of peroxovanadate sites, $O_xV^{5+}\cdots O_2^{2-}$, as summarized in Figure 15. For O_xV^{4+} species, it is suggested that $O_xV^{5+}\cdots O_2^{\cdot-}$ forms upon the reoxidation to further react with another O_xV^{4+} or O_xV^{3+} to yield a $V^{n+}\cdots O^{\cdot-}$ site. Meanwhile for ODHP using N_2O, only less active O^{2-} ions are formed through decomposition of N_2O on O_xV^{3+} sites.

Table 9. Initial C_3H_6 Selectivity ($S(C_3H_6)_{initial}$) for V_2O_5, VO_2, and V_2O_3 Catalysts (T = 500 °C, $C_3H_8/O_2/Ne$ = 40/20/40, $C_3H_8/O_2/Ne$ = 40/10/50, $C_3H_8/N_2O/Ne$ = 40/40/20)

	initial C_3H_6 selectivity (%)		($S(C_3H_6)_{initial}$)
catalysts	20% O_2	10% O_2	40% N_2O
V_2O_5	81	88	89
VO_2	81		88
V_2O_3	75	89	92

Reproduced with the permission from ref 186. Copyright 2007 Elsevier B.V.

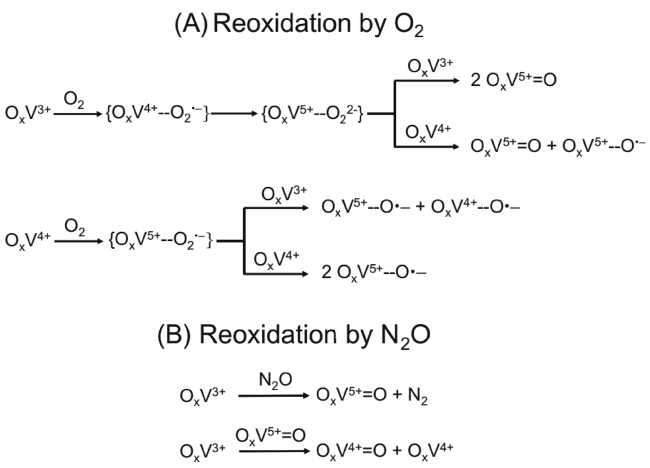

Figure 15. Proposed pathways for reoxidation of O_xV^{3+} and O_xV^{4+} by O_2 (A) and N_2O (B). Reproduced with the permission from ref 20. Copyright 2010 Elsevier B.V.

https://dx.doi.org/10.1021/acscatal.0c03999
ACS Catal. 2021, 11, 2182−2234

DFT results have showed that the reoxidation of O_xV^{4+} species is not favored under N_2O, so it is assumed only O_xV^{3+} species can be reoxidized.

Lastly, type of support and loading of vanadium oxide have been reported as additional factors to affect catalytic activity and C_3H_6 selectivity.[179,189,190] Baerns et al. report that silica-supported VO_x catalysts show higher C_3H_6 selectivity than alumina-supported catalysts, whether O_2 or N_2O is used as oxidant (Figure 16). It is also noted that the C_3H_6 selectivity increases as the loading of VO_x increases, up to a certain loading on the alumina, while it barely shows any change in selectivity for the silica-supported counterpart. On the basis of such observations, it was hypothesized that C_3H_6 adsorption is more likely to occur on the exposed surface of the acidic γ-Al_2O_3 support. The adsorbed C_3H_6 might further transform to CO_x, thereby decreasing C_3H_6 selectivity.[190] For weakly acidic supports, like silica, adsorption of C_3H_6 does not occur well, so very small change in selectivity despite change in the exposed support surface area. Apart from the exposed surface area of the support, the dispersion of VO_x species is another factor that has a crucial impact on the C_3H_6 selectivity.[179,188,189] It has been observed in multiple reports that regardless of the oxidant and support type used, above a certain VO_x loading, the selectivity toward C_3H_6 tends to decrease. On the basis of these observations, it is reported that isolated VO_x sites tend to be more selective toward C_3H_6, while more polymerized VO_x species lead to drop in selectivity.

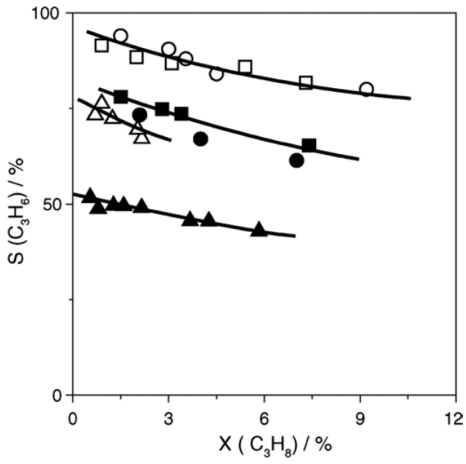

Figure 16. Relationship between selectivity and C_3H_8 conversion over V(2.7)/MCM-41 (squares) and V(2.9)/SiO_2 (circles) at 475 °C (748 K) and V(1)/g-Al_2O_3 (triangles) at 450 °C (723 K): open symbols for N_2O-containing mixtures and solid symbols for O_2^--containing mixtures. Reproduced with the permission from ref 190. Copyright 2006 Elsevier B.V.

4.1.2. Molybdenum Oxides. Molybdenum catalysts also show decreased C_3H_8 conversion and increased C_3H_6 selectivity upon addition of N_2O during C_3H_8 dehydrogenation.[184,185,191−193] For example, in their work on ODHP using a $NiMoO_4$ catalyst, Ruiz et al. report an increase in C_3H_6 selectivity from 18.3% to 24.2%, along with a decrease in CO_2 selectivity from 23.2% to 21.4%, occurs with a decrease in C_3H_8 conversion from 14.6% to 12.4% with 300 ppm of N_2O in the feed gas.[184] Similar results are also evident using a mixture of $NiMoO_4$ and α-Sb_2O_4 catalyst.[191] In the presence of 300 ppm of N_2O, an increase in C_3H_6 selectivity from 34.6% to 37.5% and decrease in C_3H_8 conversion from 9.3% to 8.1% is observed. A decrease in CO_2 selectivity from 24.2% to 22.0% is evident as well. It should be noted that 300 ppm of N_2O has been co-fed with 10% O_2 in all these reports.

In an effort to observe the surface species present after performing ODHP with different concentrations of N_2O as a co-feed, XPS analysis has been performed on the catalysts, with the results shown in Table 10.[184] From these studies, while no Mo^{5+} species are present in the absence of N_2O, Mo^{5+} species emerge after the N_2O dopant is used in the ODHP reaction. On the basis of this result, it was hypothesized that the reduction of molybdenum is induced by propane due to the weaker oxidation capability of N_2O. Surface sites of the $NiMoO_4$ material are further studied by in situ DRIFT spectroscopy. DRIFTS is conducted under 1% N_2O, 10% N_2O, and synthetic air over the $NiMoO_4$ catalyst. As shown in Figure 17, the intensity of the band at 1000 cm^{-1}, assigned as a MoO_3 vibration band ν(Mo═O), decreases in the order of synthetic air >10% N_2O > 1% N_2O. These results corroborate the prior observations from XPS.

Combining the observations made from XPS and DRIFTS, Ruiz et al. assert that while both oxygen and N_2O are able to interact with the surface hydroxyl groups on the catalyst surface, N_2O stabilizes molybdenum in a more reduced state on nickel molybdate compared to molecular oxygen.[184,185] Furthermore, it was hypothesized that N_2O limits the oxidation rate of the catalyst by adsorbing on the same vacancy that O_2 would adsorb, thereby inhibiting adsorption of O_2 on the surface of the catalyst. Consequently, the

Table 10. XPS Analyses of Pure $NiMoO_4$ Catalysts[a]

	fresh	test TR	test with 300 ppm of N_2O	test TXN_2O (1%, 5%, and 10% N_2O)
C	18.3 (284.8)	19.5 (284.8)	20.3 (284.9)	28.0 (285.0)
O	53.7 (530.4)	52.1 (530.4)	52.7 (530.6)	54.3 (530.1)
Mo	12 (232.4)	11.7 (232.6)	12.8 (232.7)	8.3 (232.5)
with Mo^{6+}	12	11.7	12.5	7.9
with Mo^{5+}	0.0	0.0	0.3	0.4
Ni	16.0 (855.6)	16.7 (855.7)	14.3 (855.8)	9.4 (855.7)
C/Mo	1.5	1.7	1.6	3.4
O/Mo	4.5	4.5	4.1	6.5
Ni/Mo	1.3	1.4	1.1	1.1

Reproduced with the permission from ref 184. Copyright 2003 Elsevier B.V. [a]Results before and after TR and TN_2O tests: atomic ratio. Binding energies (in eV) are indicated in parentheses. TR represents the sample after 1 h under 10% O_2 and 10% C_3H_8. TXN_2O represents the sample after 2 h under 1%, 2 h under 5%, and 2 h under 10% N_2O, along with 10% C_3H_8. Reaction temperature was 400 °C (673 K) in both cases.

https://dx.doi.org/10.1021/acscatal.0c03999
ACS Catal. 2021, 11, 2182−2234

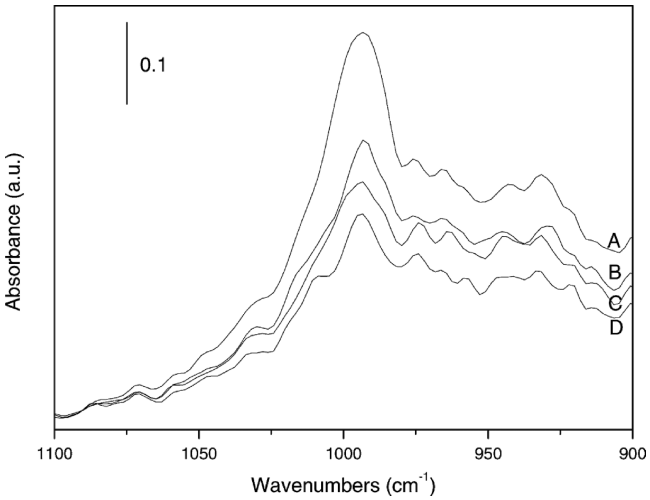

Figure 17. Different DRIFTS spectra of nickel molybdate catalysts at 455 °C (728 K) under different atmospheres, against the initial spectrum under helium: (A) synthetic air, (B) 10% N_2O, (C) 1% N_2O, and (D) helium flow. Reproduced with the permission from ref 184. Copyright 2003 Elsevier B.V.

formation of electrophilic O^- or O_2^- species would be limited, resulting in the decrease in the secondary oxidation of C_3H_6 and higher C_3H_6 selectivity in return. The adsorbed N_2O would further dissociate to O^{2-} species (eq 4-1 and eq 4-2), which can be responsible for the improved C_3H_6 selectivity observed upon addition of N_2O during the ODHP reaction, as O^- is known to lead to overoxidation products, while O^{2-} leads to selective oxidation products.[194]

$$N_2O + e^- \rightarrow N_2 + O^- \quad (4\text{-}1)$$

$$O^- + e^- \rightarrow O^{2-} \quad (4\text{-}2)$$

Of note, there is an optimum amount of N_2O that is beneficial for elevating the C_3H_6 selectivity. It has been observed that, when the concentration of N_2O is too high, a decrease in C_3H_6 selectivity is observed. On the basis of these observations, it was hypothesized that there is an optimum oxidation state for Mo^{n+} species that allows for maximum selectivity; if the extent of reduction is too high, CO_x products are favored, leading to decreased C_3H_6 selectivity. Catalytic performances of reported metal oxide catalysts are summarized in Table 11.

4.2. Zeolite-Based Catalysts. *4.2.1. Metal-Modified Zeolites.* Different metal-containing zeolites, such as MFI[19,35,36,178,180−183,195−199] or BEA,[18,182,200,201] have been widely studied for the N_2O-assisted ODHP reaction. In particular, iron-containing ZSM-5 has been reported as one of the most effective catalysts.[36,182,183,199,202,203] An early work reported that iron-containing ZSM-5, synthesized by steam treatment of an isomorphously substituted zeolite framework, shows C_3H_8 conversion of 48%, N_2O conversion of 96%, and C_3H_6 selectivity of 45% at 450 °C.[180−183] Further studies show that Fe-ZSM-5 synthesized through solid-state ion exchange or liquid exchange methods also deliver good catalytic performance, showing C_3H_8 conversion between 20% and 60%, C_3H_6 selectivity between 25% and 70%, and C_3H_6 yield between 14% and 30% in the temperature range of 377 to 527 °C.[19,35,36,198,199,204]

The high-temperature steam pretreatment of iron-containing zeolites has a positive effect on the C_3H_6 yield and selectivity, as this synthetic method produces extra-framework iron species that are more active than framework iron species for N_2O−ODHP.[178,181,182] This pretreatment also enables

Table 11. Summarized Activity Performance of Various Vanadium and Molybdenum Oxides Catalysts[a]

catalyst	temp (°C)	C_3H_8/N_2O ratio	conversion (%) C_3H_8	yield (%) C_3H_6	selectivity (%) C_3H_6	ref
0.5 wt % VO_x/γ-Al_2O_3	450	1	1		70	188
4.6 wt % VO_x/γ-Al_2O_3	450	1	1		92	188
2.7 wt % VO_x/MCM-41	500	1	2		93	189
2.7 wt % VO_x/MCM-41	500	1	11		81	189
3.4 wt % VO_x/MCM-48	500	1	2.5		90	189
3.4 wt % VO_x/MCM-48	500	1	13		75	189
2.8 wt % VO_x/SiO_2	500	1	2		93	189
2.8 wt % VO_x/SiO_2	500	1	8		83	189
11.2 wt % VO_x/MCM-41	500	1	2.5		87	189
11.2 wt % VO_x/MCM-41	500	1	6		70	189
VO_2	500	1	3		80	186
VO_2	500	1	8		60	186
V_2O_3	500	1	1		90	186
V_2O_3	500	1	7		65	186
V_2O_5	500	1	1		87	186
V_2O_5	500	1	4		70	186
$NiMoO_4$	450	333	12.4	3.0	24.2	184
$NiMoO_4$	450	10	13.5	2.6	19.2	184
$NiMoO_4$	450	2	13.3	3.0	22.8	184
$NiMoO_4$	450	1	12.7	3.2	25.2	184
$NiMoO_4$ and α-Sb_2O_4	450	333	8.1	3.1	37.5	191
$NiMoO_4$/[Si,V]-MCM-41	480	10	8.7	3.9	44.8	193
$NiMoO_4$/[Si,V]-MCM-41	480	2	9.4	3.6	38.2	193

[a]It should be noted that for molybdenum oxides catalysts, N_2O was co-fed with 10% O_2.

https://dx.doi.org/10.1021/acscatal.0c03999
ACS Catal. 2021, 11, 2182−2234

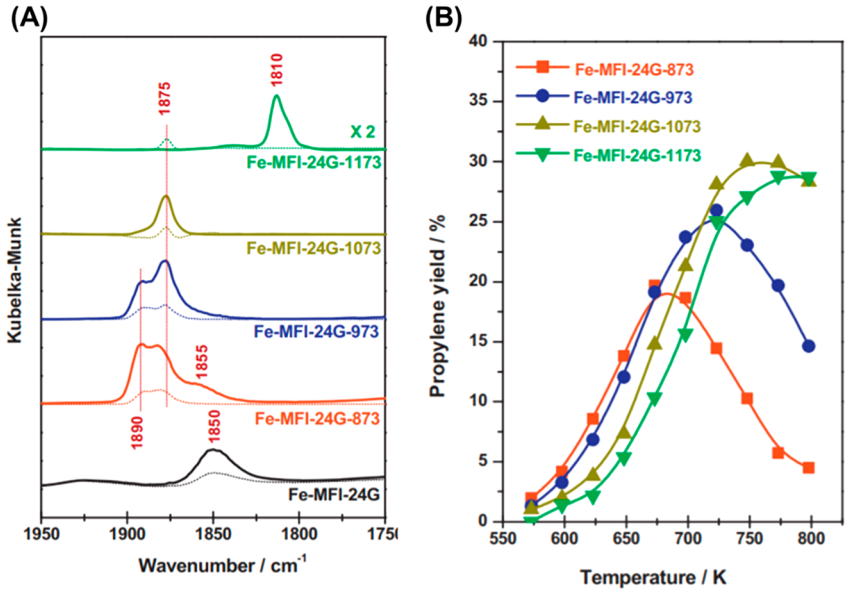

Figure 18. (A) FT-IR spectra of NO adsorption on Fe-MFI-24G samples calcined at different temperatures. (Numbers at the end show calcination temperatures in Kelvin.) Dotted line: Initial adsorption of NO. Solid line: Saturated adsorption of NO temperatures. (B) Propylene yield in N_2O-mediated ODHP catalyzed by Fe-MFI-24G samples calcined at different temperatures. Reaction conditions: 7.5% C_3H_8, 15% N_2O, and He balance; GHSV= 15 000 mL h^{-1} g^{-1}. Reproduced with the permission from ref 36. Copyright 2013 Elsevier B.V.

reduction in surface acidity, resulting in higher C_3H_6 selectivity. Combined with characterization techniques, such as NH_3−TPD and XRD, studies report a significant decrease in the acid site concentration after high-temperature steam pretreatment of Fe-ZSM-5, likely because of extensive dealumination of the zeolite and concomitant decrease in the density of Brønsted acid sites.[205−207] Such pretreated samples present a clear decrease in selectivity toward CO_2, along with increased C_3H_6 selectivity.

On iron containing ZSM-5, studies report that Fe−O−Al species are likely active sites for N_2O-mediated ODHP.[19,35,36] Grunert et al. have used FT-IR analysis paired with NO adsorption to characterize the abundant Fe species (Figure 18A) and catalytic evaluation of Fe-ZSM-5 (Figure 18) to support such hypothesis.[36] Of note, FT-IR spectroscopy, along with NO adsorption, is commonly used to characterize active sites for Fe-containing catalysts. For samples without calcination (Fe-MFI-24G), NO adsorption results in a broad band at 1850 cm^{-1}, indicating mononitrosyl on ferrous ions in the straight channels of ZSM-5. When samples are calcined at high temperatures, two strong bands at 1875 and 1890 cm^{-1} are observed in the IR spectra. The band at 1875 cm^{-1} corresponds to the mononitrosyl species on extra-framework Fe^{2+}−O−Al sites; the other band at 1890 cm^{-1} is assigned to the mononitrosyl species on isolated ferrous ions located on γ sites of the ZSM-5 structure. The band observed at 1810 cm^{-1} is assigned to poly nitrosyl species on ferrous ion sites. As initial adsorption of NO on Fe-MFI-1173 results in the emergence of a band at 1875 cm^{-1}, it is hypothesized that both bands at 1810 and 1875 cm^{-1} come from the same ferrous species, namely isolated extra-framework Fe^{2+}−O−Al species. Clearly, calcining Fe-MFI-24G samples leads to the transformation of iron sites from isolated ions to isolated extra-framework Fe−O−Al species. Figure 18B shows the C_3H_6 yield during N_2O-mediated ODHP for samples calcined at different temperatures. An increase in C_3H_6 yield is observed as the calcination temperature rises from 600 °C (Fe-MFI-24G-873) to 800 °C (Fe-MFI-24G-1073), while the samples calcined at 800 (Fe-MFI-24G-1073) and 900 °C (Fe-MFI-24G-1173) show similar highest C_3H_6 yields between 27% and 30%. On the basis of this correlation between exposed active iron sites and the observed catalytic performance, it is proposed that the isolated Fe−O−Al site is the active center responsible for N_2O-mediated ODHP reaction.[19,35,36]

Further analyses with in situ DRIFTS and TPD reveal that reoxidation of the Fe^{2+}−O−Al site with N_2O forms an O^- species, which is thermally stable and highly selective in the target reaction.[19,35,36] On the basis of such observations, the following mechanism is proposed:

$$Fe^{2+} + N_2O \rightarrow N_2 + Fe^{2+}\text{—}O \quad (4\text{-}3)$$

$$Fe^{2+}\text{—}O \rightarrow Fe^{3+}\text{—}O^- \quad (4\text{-}4)$$

$$Fe^{3+}\text{—}O^- + N_2O \rightarrow Fe^{2+}\text{—}O_2 + N_2 \quad (4\text{-}5)$$

$$Fe^{2+}\text{—}O_2 \rightarrow Fe^{2+} + O_2 \quad (4\text{-}6)$$

$$Fe^{3+}\text{—}O^- + C_3H_8 \rightarrow Fe^{2+} + C_3H_6 + H_2O \quad (4\text{-}7)$$

$$Fe^{3+}\text{—}O^- + C_3H_6 \rightarrow Fe^{2+} + CO_x + H_2O \quad (4\text{-}8)$$

In the proposed mechanism, the Fe^{3+}−Fe^{2+} cycle operates on the highly isolated extra-framework Fe−O−Al site to decompose N_2O to N_2 and O_2 (eq 4-3-eq 4-6) and forms Fe^{3+}−O^- species.[208−210] Since the direct reaction of C_3H_8 and gaseous O_2 produces CO_x as the main products, it is hypothesized that C_3H_8 reacts with the deposited O^- species to produce C_3H_6 with a high selectivity (eq 4-7). The C_3H_6 may further react with adsorbed O^- to form undesired CO_x species, as depicted in eq 4-8.

Despite its high initial catalytic performance, a major drawback of iron-containing zeolites is deactivation by coke, which causes a rapid decrease in C_3H_6 yield.[180−183] A tapered element oscillating microbalance (TEOM) coupled with GC

https://dx.doi.org/10.1021/acscatal.0c03999
ACS Catal. 2021, 11, 2182−2234

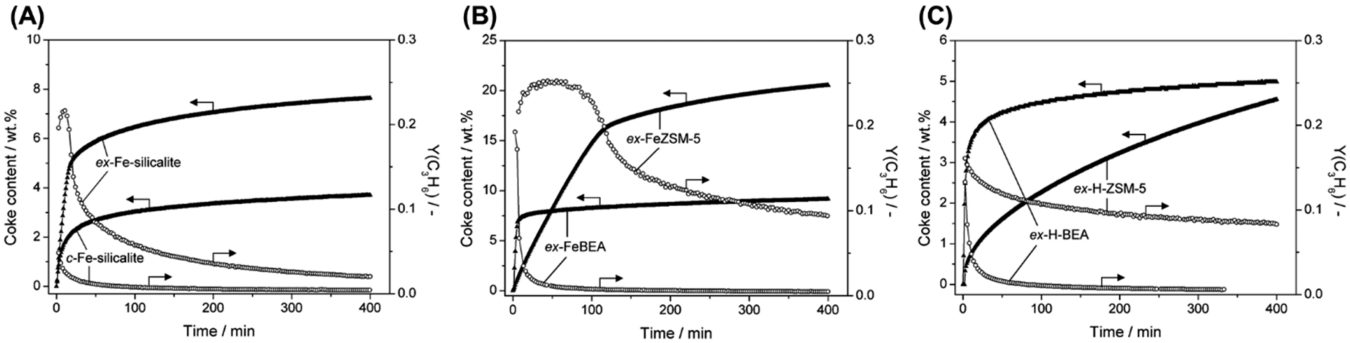

Figure 19. Coke content (black triangle) and C_3H_6 yield (open circle) versus time over ex- and c-Fe-silicate (A), ex-FeZSM-5 and ex-FeBEA (B), and ex-H-ZSM-5 and ex-H-BEA (C). Conditions: 100 mbar C_3H_8 and 100 mbar N_2O in He, T = 450 °C, WSHV = 400 000 mL h^{-1} g^{-1}, and P = 2 bar. Reproduced with the permission from ref 182. Copyright 2004 Elsevier B.V.

Table 12. Summarized Activity Performance of Various Framework Zeolites for N_2O−ODHP

catalyst	temp (°C)	C_3H_8/N_2O ratio	conversion (%)		yield (%)	selectivity (%)	ref
			C_3H_8	N_2O	C_3H_6	C_3H_6	
Fe-ZSM-5 (steam-activated)	450	1	48	96		45	182
Fe-ZSM-5 (solid-state ion exchange)	500	0.5	29		20	69	199
Co-BEA	400	0.5	2	3	2	90	200
Fe-BEA	400	1	30	55	8		201
CrSiBEA (0.2 wt % Cr)	400	0.67	0.4			82	18
CrSiBEA (1.0 wt % Cr)	400	0.67	1.8			71	18
CrSiBEA (3.4 wt % Cr)	400	0.67	2.9			63	18
Fe-FAU	475	0.5	25		17	63	36
Fe-BEA	475	0.5	18		7	42	36
Fe-MOR	475	0.5	5		1	18	36
Fe-FER	475	0.5	17		0	0	36
Fe-FAU	400	0.5	14		10	74	204
Fe-BEA	400	0.5	11		8	70	204
Fe-MOR	400	0.5	3		1	37	204
Fe-FER	400	0.5	3		1	23	204
Fe-$AlPO_4$	525	0.5			14	30	212

analysis (Figure 19) performed on MFI, BEA, and silicate catalysts is used to illustrate how zeolite catalysts deactivates over time during ODHP reaction.[182] Of note, *c*- indicates calcined only, and *ex*- indicates steam-activated samples after calcination; As presented in Figure 19, most catalysts show their highest C_3H_6 yields within the first few minutes on stream, and then deactivate rapidly within the first 20 min on stream. An excellent correlation between the increase in coke formation and decrease in C_3H_6 yield is observed, and based on such correlation it is hypothesized that coke formation is responsible for deactivation of the catalysts during the reaction.[182,183] Among the different zeolites tested, steam activated Fe-ZSM-5, with abundant extra-framework iron sites, presents the highest resistance to deactivation, and shows a C_3H_6 yield above 20% up to 75 min on stream. Even after 400 min on stream, it is able to maintain a C_3H_6 yield of 8%, unlike other catalysts that deactivate almost completely. It is hypothesized that this elevated performance likely originates from the absence of large cages in ZSM-5. Since the size of the channel and intersections are similar, coke precursors are not trapped in intersections and are hypothesized to more effectively diffuse out. On the other hand, BEA zeolites have large cavities with relatively small apertures in the framework. Such cavities may trap bulky organics, completely blocking the access to active sites and causing rapid deactivation. While the amount of coke formation and the C_3H_6 yield usually display a nice correlation, for *ex*-Fe-ZSM-5 and *ex*-H-ZSM-5, this is not the case. While the coke content is 4 to 5 times higher for *ex*-Fe-ZSM-5 than *ex*-H-ZSM-5, similar C_3H_6 yields are obtained after 400 min on stream. On the basis of this observation, Gallardo-Llamas and co-workers hypothesize that the location of the coke is another important factor that affects the deactivation process.[182,183] Such a hypothesis is also supported by the work of Pérez-Ramírez et al., in which gallium-containing MFI zeolites exhibit higher coke formation than the corresponding aluminum-containing zeolite, yet still show a higher C_3H_6 yield after 120 min on stream for the ODHP reaction.[196] While such deactivated zeolite catalysts can be regenerated by treatment with air at elevated temperatures, it is reported that regenerated catalysts tend to deactivate much faster than the fresh ones, showing a sharp decrease in catalytic activity within a few minutes on stream.[180,183,196] Better understanding of catalyst deactivation and improvement of catalyst stability still remain as challenge for efficient utilization of N_2O for ODHP reactions.

There have only been a few reports where other metal-containing MFI catalysts such as cobalt or manganese have been tested for N_2O−ODHP.[198,211] While it is reported that both cobalt- and manganese-containing ZSM-5 catalysts are less active in N_2O−ODHP than iron-containing ZSM-5, there are insufficient data to definitively draw assertion. Furthermore, stability or deactivation studies using N_2O−ODHP on

https://dx.doi.org/10.1021/acscatal.0c03999
ACS Catal. 2021, 11, 2182−2234

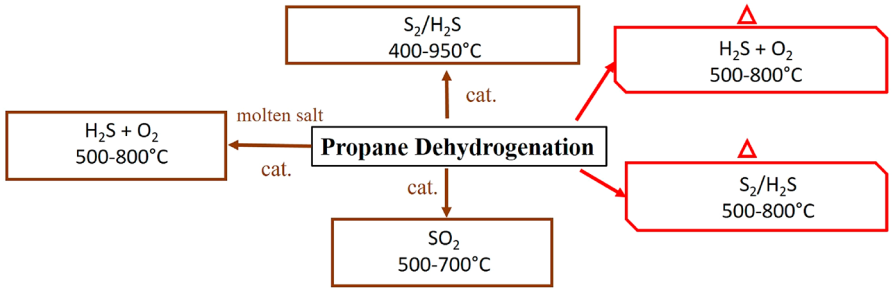

Figure 20. Various routes investigated in the past for propane conversion to propylene, including homogeneous reactions (red box) and catalyst-assisted reactions (brown). Reaction conditions are shown for each route. Typically, reaction studies have been conducted at 1 atm.

such catalysts are still very scarce, thereby making it difficult to evaluate their potential for this reaction at this stage.

4.2.2. Effect of Zeolite Topology. There have been reports deploying other zeolite frameworks for the N_2O−ODHP reaction as well, including MOR, FAU, and BEA.[18,36,182,200,201,204,212] However, the catalytic performance of most of these frameworks is inferior to the MFI zeolites, not only possessing lower C_3H_6 yield but also fast deactivation. FAU and BEA zeolites are the frameworks that show relatively better performance and are close to the MFI-based catalysts, with their highest C_3H_6 yields between 7% and 17%.[36,204] However, the BEA zeolites suffer from rapid deactivation.[182,200] Sobalik and co-workers find that C_3H_6 yield decreases to 25% of its initial yield for iron-containing BEA within 2 h on stream.[201] Pérez-Ramírez et al. also report that a lab-synthesized Fe-BEA deactivates rapidly, showing a decrease by 90% of its initial yield within the first hour of reaction.[182] MOR or FER frameworks are much less active in the N_2O−ODHP reaction, exhibiting very low C_3H_6 yields (i.e., <2%).[36,204] A summary of the catalytic performance of different zeolite catalysts is shown in Table 12. While Fe-ZSM-5 has been extensively studied for this reaction because of its superior performance, studies of other frameworks are still limited. More efforts are needed to explore the effect of other framework topologies on catalytic performance.

5. OXIDATIVE DEHYDROGENATION OF PROPANE WITH SULFUR-/HALOGEN-CONTAINING COMPOUNDS

Alternate oxidants, such as sulfur or halogen-based oxidants, have shown promising results to selectively dehydrogenate propane to propylene. For example, co-feeding sulfur compounds, such as H_2S, S_2, and SO_2, can improve propylene yield. Using SO_2 as an oxidant may be an effective way to utilize SO_2, which is an acidic gas. However, the SO_2−ODHP pathway results in low propylene because of the formation of CO_x products over bulk metal oxide catalysts. Subsequently, the use of a soft oxidant, such as S_2, instead of oxygen can reduce the overoxidation of propane over ZrO_2.[213] Ideally, it would be desirable to kinetically inhibit the formation of byproducts, such as CS_2, which is a major challenge in designing efficient catalysts for S_2−ODHP.[213] In the future, developing a structure−activity relationship will be an important step toward rational catalyst design in this field.

Selective activation of C_3H_8 can also be achieved via halogen-mediated pathways, such as (i) dehydrogenation with molecular halogens (X_2), (ii) oxidative dehydrogenation in the presence of halogen ($X_2 + O_2$), (iii) propane oxyhalogenation via halides ($HX + O_2$), and (iv) molten metal halide salts assisted ODHP ($LiX + O_2$). Specifically, oxychlorination chemistry over CeO_2, EuOX, and metal phosphate-based, such as $CrPO_4$, catalysts have shown good selectivity (up to 95%) and conversion (up to 70% at 500 °C) in comparison to conventional ODHP.[48−50] Still, the olefin selectivity is limited because of the formation of CO_x and polyhalogenation products. Continuous efforts have been put forth to obtain an optimal propane oxyhalogenation catalyst, which should exhibit moderate redox properties so that it enables alkane activation but does not favor alkane overoxidation, combustion, and evolution of Cl_2, while possessing fast dehydrochlorination kinetics.

5.1. Propane Dehydrogenation in the Presence of Sulfur-Based Feed. Thermal (or steam) cracking and fluid catalytic cracking (FCC) of hydrocarbons are the most important processes in the production of olefins, the building blocks of the chemical industry. To improve selectivity (i.e., reduce hydrogenolysis or coke formation), sulfur-based additives, such as dimethyl disulfide (DMDS) and H_2S, are often added as a dilute co-feed during the thermal cracking of hydrocarbons.[214−216] The role of sulfur as a promoter or inhibitor is well studied in the literature for hydrogenation reactions.[217−219] In particular, sulfur has been found to suppress the cracking of organic molecules on metal catalysts. Assuming the ability of sulfur to suppress the cracking reactivity is stronger than its ability to poison the dehydrogenation reactivity of metallic (or metal oxide) catalysts (Fe, Ni, Cu, Co, Zn Mn, Mo), sulfur compounds can be good promoters for enhancing the dehydrogenation performance.[220−222] Typically, the effect of sulfur on the catalytic propane dehydrogenation has been studied in one of the following categories (Figure 20), namely, (i) in situ catalyst sulfidation (in the presence of H_2S) but in the absence of O_2, (ii) mixture of $H_2S + O_2$ or (iii) SO_2, and (iv) S_2.[39,40,44,220−234]

5.1.1. H_2S-Catalyzed DHP/ODHP. Several patents highlight the merits of adding H_2S during the uncatalyzed propane dehydrogenation.[235,236] For example, the addition of H_2S in the reactant stream doubles the C_3H_6 yield to 31% at 815 °C.[235] Further, Resasco et al. demonstrate that the Ni/Al_2O_3, treated with dimethyl sulfoxide (DMSO), exhibits improved selectivity and decreased coke formation during isobutane dehydrogenation.[237] Similarly, the selectivity of C_3H_6 on $Pt/MgAl_2O_4$ is significantly improved from 47% to 95% without changing its activity when H_2S (425 ppm) is co-fed, thus establishing a promoting effect.[238] On the basis of CO-chemisorption and Bader charge analysis, Wang et al. explain that the improved selectivity in the presence of H_2S is due to the electron transfer from adsorbed sulfur species to Pt atoms,

https://dx.doi.org/10.1021/acscatal.0c03999
ACS Catal. 2021, 11, 2182−2234

Table 13. Sulfur Compound Mediated Propane Dehydrogenation

catalyst	temp (°C)	feed composition [residence time in s]	conversion (%)	C_3H_6 selectivity (%)	ref
13 V/Al_2O_3	700	O_2: H_2S: C_3H_8 = 1: 2: 4 [0.005 s]	53.7	56.5	40
20 Fe/Al_2O_3	560	C_3H_8: SO_2: N_2 = 30: 1: 19	25	80	227
Al_2O_3	750	C_3H_8: S_2 = 6: 1	94	87.5	231
Al_2O_3	650	C_3H_8: H_2S: SO_2: He = 1: 0.2: 0.5: 3	76	47	42
Fe/SiO_2	593	C_3H_8: COS = 1: 3	66	95	229
Al_2O_3	550	C_3H_8: S_2 = 1: 1	40	50	230
$Co-Mo/Al_2O_3$	450	C_3H_8: S_2: N_2 = 1: 1.5: 7.5	98	95	232
ZrO_2	550	C_3H_8: S_2 = 1: 3.7	8.1	85.7	213
TiO_2	550	C_3H_8: S_2 = 1: 3.7	7.6	79.6	213
Cr_2O_3	550	C_3H_8: S_2 = 1: 3.7	7.2	68.5	213
Co_3O_4	550	C_3H_8: S_2 = 1: 3.7	4.7	78.0	213
MoS_2	550	C_3H_8: S_2 = 1: 3.7	5.4	53.2	213
PdS	550	C_3H_8: S_2 = 1: 3.7	7.9	38.2	213
$LiCl/KCl/MnCl_2$	705	C_3H_8: H_2S: O_2: He = 1: 2: 1: 10	94	64	39
γ-Al_2O_3	640	C_3H_8 = 10, SO_2 = 10, He = 80 [1 s]	50.6	35.9	242
SiO_2	640	C_3H_8 = 10, SO_2 = 10, He = 80 [10 s]	71.7	56.8	242
Fe_2O_3	640	C_3H_8 = 10, SO_2 = 10, He = 80 [25 s]	23.3	14.3	242
PbO	640	C_3H_8 = 10, SO_2 = 10, He = 80 [20 s]	2.5	12	242
Bi_2O_3	640	C_3H_8 = 10, SO_2 = 10, He = 80 [20 s]	3.0	11.3	242
Ga_2O_3	600	C_3H_8 = 10, SO_2 = 10, He = 80 [5 s]	50.4	69.3	242
$SiO_2-Al_2O_3$	640	C_3H_8 = 10, SO_2 = 10, He = 80 [10 s]	59.6	61.4	244
Pd/Al_2O_3	562	C_3H_8 = 60, SO_2 = 10, N_2 = 30	18.3	22.3	37

thereby resulting in weaker $Pt-C_3H_6$ interactions.[239] Of note, H_2S can inhibit the conversion and adversely affect the selectivity of propylene at higher concentrations (about 850 ppm) over Pt/Al_2O_3 underlining the dual role of H_2S as an inhibitor and promoter depending on H_2S concentration in the feed.[238] Subsequently, Shan et al. show that the exposure of metal oxides to sulfur feed can lead to the formation of corresponding metal sulfides (or surface sulfur species) and reported improved isobutane dehydrogenation yield, suggesting that the sulfur can play a key role in modifying the active phase of the catalyst.[220−222] The authors argued that higher selectivity is due to the preferential activation of C−H bonds over C−C bonds on metal−sulfur ensembles, coupled with facile olefin desorption, thus, effectively reducing the possibility of side reactions and coke generation.[220−222] In summary, the resulting metal sulfides formed due to exposure to H_2S, show improved dehydrogenation performance over their parent metals or metal oxides, presenting a unique opportunity to design new catalysts with enhanced oxidative or nonoxidative dehydrogenation capability with improved selectivity and stability.[220−223]

Sulfur compounds, such as S_2 and H_2S, have been used as cocatalysts to reduce overoxidation of alkanes and olefins during oxidative dehydrogenation reactions (ODH).[40,42,44,240] Clark et al. have investigated the oxidative dehydrogenation of propane using γ-Al_2O_3 and 13% V/Al_2O_3 catalysts in the presence of $H_2S + O_2$ at short residence times (t = 5 ms) and achieved a C_3H_6 yield of ∼30.4% at 700 °C.[40] The C_3H_6 selectivity increases at residence times below 0.5 s, indicating that shorter residence times are required to suppress the cracking reaction.[40] Gasper et al. demonstrate that C_3H_6 yields of up to 60% can be obtained for H_2S-promoted ODH over $LiCl/KCl/MnCl_2$ molten salt at 705 °C.[39] As postulated, sulfur in the diatomic state (active species) may abstract H species from an alkane. Of particular note is that significantly higher C_3H_6 yield (i.e., 60%) is evident in the presence of molten salt for H_2S-assisted ODH than is obtained with the catalyst (i.e., 30%) or in gas-phase reactions (i.e., 20%) at 700 °C.[39,40,44]

The addition of gaseous sulfur, either $S_2/COS/SO_2/H_2S$ or combinations of sulfur compounds over Al_2O_3, (Co, Mo, Fe, W, Ni-mono or bimetallic) metals supported either on Al_2O_3 or SiO_2 demonstrates excellent performance (up to 98% C_3H_8 conversion, C_3H_6 selectivity = 95%, and CS_2 selectivity = 1%) in the temperature range of 400−750 °C, which is summarized in Table 13.[42,229−233] In these studies, the catalyst precursor, which may be metal oxides/metal sulfides/metal oxysulfides, is typically activated in the presence of one or more sulfur-containing compounds, such as S_2, H_2S, SO_2, COS. Recently, oxidative propane dehydrogenation utilizing sulfur vapor (S_2: C_3H_8 = 1: 0.3) as an oxidant has been investigated at 600−950 °C over *bulk* Fe_2O_3, MgO, and Cr_2O_3 catalysts that are activated in a mixture of S_2/H_2S.[234] The study reveals that the C_3H_6 yield and selectivity improve in the presence of S_2; however, the conversion (C_3H_8 conversion = 10% and C_3H_6 selectivity = 73%, at 650 °C) is barely affected by the catalysts, indicating the dominance of gas-phase reactions. DFT calculations on the H_2S-assisted gas-phase ODH reaction reveal that the in situ generated sulfur intermediate (S_2) can abstract the hydrogen from the alkane, leading to the formation of olefin products (see section 6.3 for details).[44] It highlights that the sulfur is participating in the reaction as a catalyst. The formation of sulfur-based byproducts, such as CS_2, 1- and 2-propyl thiol mercaptan, and sulfur (S_8), is also observed in the reactor effluent.[229−234] Recently, Marks and co-workers have evaluated the role of sulfur as a soft oxidant for propane dehydrogenation (S_2−ODHP) over transition metal oxide (ZrO_2, TiO_2, Cr_2O_3) and sulfide (PdS, MoS_2) at milder reaction temperature (T = 470−550 °C).[213] They found that the apparent activation barrier for propylene formation decreases with lower metal−sulfur bond strength, indicating a more active sulfur species. The authors proposed that C−H activation (RDS) proceeds by a surface sulfur species based on first order dependence on

https://dx.doi.org/10.1021/acscatal.0c03999
ACS Catal. 2021, 11, 2182−2234

propane. Consequently, propylene and H_2S formation leads to sulfur vacancy, and gas phase S_2 replenishes these sulfur vacant sites.

5.1.2. Metal Sulfate- and SO_2-Assisted DHP/ODHP. The effect of sulfation has been studied via either synthesizing Me−SO_4 (Me = Co, Fe, Cr, Ni, Cu, and Mn) or the introduction of SO_2 as an oxidant in the co-feed. In the former case, sulfate-promoted FeO_x and Co/Al_2O_3 catalytic systems show excellent activity in C_3H_8 dehydrogenation accompanied by relatively better stability than the nonsulfated catalyst.[225−228] The improved performance of the catalyst is attributed to the electron-withdrawing effect of sulfate species from the metal ion, as illustrated in Figure 21. The strong

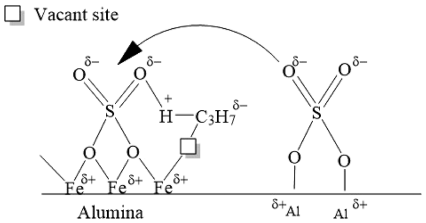

Figure 21. Promoting effect of SO_4^{2-} upon addition on DHP over Fe/Al_2O_3 catalyst. Reproduced with the permission from ref 227. Copyright 2015 Royal Society of Chemistry.

interaction of SO_4^{2-} species with the support and Fe results in C_3H_8 polarization, followed by cleaving of the C−H bond over the $Fe^{\delta+}$ and $O^{\delta-}$ pair. The loss of sulfate groups via in situ generation of SO_2 or FeS_x over prolonged reaction times induces coke formation and results in a loss of activity. The loss in activity with TOS has motivated Sun et al. to introduce SO_2 into the reactant stream over sulfated 20% Fe/Al_2O_3, which results in stable performance for up to 15 h with 20% C_3H_6 yield at 560 °C.[227] Further tests are carried out over 20% Fe anchored on different supports including ZrO_2, SiO_2, and γ-Al_2O_3. Among them, γ-Al_2O_3 has the best performance, which is probably due to the formation of stable sulfate species.

Additionally, propane dehydrogenation has been performed with the introduction of SO_2 as an oxidant.[37,38,241−245] Ashmawy has investigated the reaction of propane with SO_2 over a 0.5% Pd−Al_2O_3 catalyst.[37,38] The addition of SO_2 (i.e., C_3H_8: SO_2 of 6: 1) to the co-feed increases the C_3H_8 conversion; however, the selectivity decreases markedly (i.e., 93.1% to ∼20%) with increasing SO_2 partial pressure in the co-feed. As suggested, SO_2 can abstract a H atom from C_3H_8, and the low selectivity may be caused by oxidation of C_3H_8 or C_3H_6 to form water and CO_x species. Adams et al. further investigate C_3H_8 oxidation with SO_2 using a calcium−nickel phosphate catalyst and reported 14% selectivity toward C_3H_6, along with 31% C_3H_8 conversion at 550 °C and GHSV = 90 h^{-1}.[241] To investigate the factors behind the low C_3H_6 selectivity, the same group has conducted additional experiments in which ammonia is added to the C_3H_8 and SO_2 mixture. It was hypothesized that, in the presence of ammonia, the calcium−nickel phosphate catalyst would scavenge the C_3H_6 molecule formed under reaction conditions via the formation of isothiazole and prevents its oxidation to CO_x compounds. However, the selectivity barely changes with ammonia addition, indicating that the initial reaction of SO_2 with C_3H_8 can be related to the formation of undesired combustion products (CO_x) rather than C_3H_6.

Sokolovskii et al. have investigated the role of activated carbon in selective catalytic oxidation of propane in the presence of SO_2.[242] Improved C_3H_6 formation can be obtained over γ-Al_2O_3, SiO_2, and Ga_2O_3 because of the in situ generation of oxidative condensation products (OCP) or activated coke.[243] In contrast, Fe_2O_3, Bi_2O_3, and PbO-based bulk catalysts undergo sulfidation, which leads to decreases in the C_3H_6 yield under similar reaction conditions (Table 13). Danilova and Ivanova have investigated the effect of pore size (textural properties) on the catalytic performance of SO_2-assisted ODHP over SiO_2−Al_2O_3 catalysts at 640 °C with an SO_2 co-feed of 10 mol %.[244] Pores that are smaller than 10 nm lead to oxidation or coke products, whereas pores between 10 and 100 nm are optimal for C_3H_6 formation. Similar to Sokolovskii's observation, the accrual of OCP over silica is accompanied by the improved C_3H_6 yield from 3.4 to 46 mol % at 640 °C with a C_3H_8: SO_2: He ratio of 10: 10: 80 mol %. It is important to note that, because of the formation of OCP, the carbon balance is reported to vary between 60% and 100%. Danilova et al. have studied the effect of OCP accumulation (0−40 wt %) on catalytic performance over SiO_2 via various ex situ techniques.[245] DRIFTS spectra reveal that the OCP system is composed of a polycyclic aromatic structures consisting of C, O, H, and S atoms with the spectral signature of carbonyl, carboxylic acid, and lactone groups. However, the exact nature of the active sites remain elusive because of the lack of structure−activity relationship and characterization studies using state-of-the-art, in situ/*operando* techniques.[242−245]

5.2. Halogen-Assisted Dehydrogenation. A selective activation of C_3H_8 can be achieved via halogen-mediated pathways under relatively mild temperatures between 300 and 700 °C. To obtain C_3H_6 from C_3H_8, different approaches can be used (Figure 22), such as the dehydrogenation with molecular halogens (X_2), oxidative dehydrogenation in the

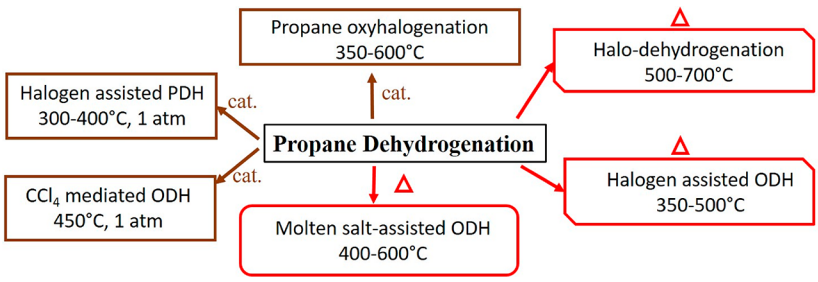

Figure 22. Various routes investigated in past decades for propane conversion to propylene, homogeneous reaction (red box), and catalyst-assisted reaction (brown). Reaction conditions are mentioned for each route.

https://dx.doi.org/10.1021/acscatal.0c03999
ACS Catal. 2021, 11, 2182−2234

Table 14. Summarized Catalytic Performance of Various Catalysts for Oxyhalogenation of C_3H_8

catalyst	temp (°C)	F_T/W ($cm^3\ h^{-1}\ g_{cat}^{-1}$)	feed composition (%)			C_3H_8 conv. (%)	C_3H_6 selec. (%)	C_3H_6 yield (%)	ref
			C_3H_8	O_2	HCl				
CeO_2 rod	500	28 800	18	18	25	38	62	23.5	49
8% NiO−CeO_2	500	28 800	18	18	25	69	80	55.2	49
CeO_2 particle	500	28 800	18	18	25	29	61	18	49
RuO_2	500	28 800	18	18	25	25	2.4	0.6	49
Fe_2O_3	500	28 800	18	18	25	8.1	94	7.6	49
CuO	500	28 800	18	18	25	4.4	84	3.7	49
NiO	500	28 800	18	18	25	2.2	74	1.6	49
$VOPO_4$	500	28 800	18	18	25	16	57	9.1	49
La_2O_3	500	28 800	18	18	25	3.1	72	2.3	49
Eu_2O_3	500	28 800	18	18	25	10	75	7.5	49
CeO_2 rod	500	28 800	18	18	25	38	55	21	49
8% NiO−CeO_2[a]	500	28 800	18	18	25	52	72	37	49
8% V_2O_5−CeO_2[a]	500	28 800	18	18	25	34	68	23	49
8% MoO_3−CeO_2[a]	500	28 800	18	18	25	25	80	20	49
8% MgO−CeO_2[a]	500	28 800	18	18	25	49	62	30	49
8% MnO−CeO_2[a]	500	28 800	18	18	25	55	61	34	49
8% Fe_2O_3−CeO_2[a]	500	28 800	18	18	25	44	51	22	49
8% Co_3O_4−CeO_2[a]	500	28 800	18	18	25	33	62	20	49
8% CuO-CeO_2[a]	500	28 800	18	18	25	40	56	22	49
8% ZnO−CeO_2[a]	500	28 800	18	18	25	43	58	25	49
β-$CrPO_4$[b]	450	6000	6	3	6	7.3	95	6.9	50
β-$CrPO_4$[b]	500	6000	6	3	6	52	95	49.5	50
$FePO_4$[b]	450	6000	6	3	6	5.5	98	5.4	50
$Mn_3(PO_4)_2$[b]	450	6000	6	3	6	1.75	67	1.2	50
$Ti_2P_2O_7$[b]	450	6000	6	3	6	1	65	0.6	50
α-$Ni_2P_2O_7$[b]	450	6000	6	3	6	1.4	65	0.9	50
$Co_3(PO_4)_2$[b]	450	6000	6	3	6	13	62	8.06	50
β-$Cu_2P_2O_7$[b]	450	6000	6	3	6	23	45	10.4	50
$(VO)_2P_2O_7$[b]	450	6000	6	3	6	16.5	30	5	50
EuOCl	400	6000	6	3	6	4.5	95	4.3	48
TiO_2	400	6000	6	3	6	5.9	57	3.4	48
CeO_2	400	6000	6	3	6	16.3	32	5.2	48
$FePO_4$[b]	400	6000	6	3	6	4.0	95	3.8	48
$(VO)_2P_2O_7$[b]	400	6000	6	3	6	13.5	30	4	48
EuOCl	500	6000	6	3	6	20	95	19	45
EuOBr	500	6000	6	3	6	45	22	10	45
$VOPO_4$[b]	420	6000	4.5	1.5	3 (HBr)	35.4	23.8	8.4	251
LaOCl	400		10	10	10	51	40	20.4	253

[a]All catalysts are supported on CeO_2 nanorod (42 $m^2\ g^{-1}$). Catalysts are modified by 8 wt % of metal oxide modifiers. The data is collected at TOS after 3 h. [b]The catalysts nomenclature indicates the major phase determined by X-ray diffraction.

presence of halogen (X_2 + O_2), propane oxyhalogenation via halides (HX + O_2), and molten metal halide salts assisted ODHP (LiX + O_2). It is important to note that the catalytic transformation of C_3H_8 in these routes is quite different from other alkanes such as methane and ethane because of the differences in reactivity of the respective alkanes.[45,46]

5.2.1. Propane Oxyhalogenation. The propane oxyhalogenation reaction proceeds via oxidation of hydrogen halide with O_2, producing alkyl halide, alkene, and water (eqs 2-24−2-29). Theoretically, 100% halogen atom efficiency can be achieved in the presence of O_2, whereas efficiency is limited to 50% for halo-dehydrogenation (eqs 2-18, 2-20, and 2-22) due to the formation of HX.[46] C_3H_6 selectivity during the C_3H_8 oxidative dehydrogenation is generally lower than that of C_2H_4 from C_2H_6 because of the presence of reactive allylic hydrogen atoms in the case of C_3H_6, which can lead to successive oxidation of C_3H_6.[246] It is important to note that during oxyhalogenation reactions, the alkane conversion can be enhanced due to the gas-phase reactions. The highly reactive radical species are liberated from the catalyst surface and allow the formation of desired and undesired products in the gas phase. To date, research has mainly focused on the propane oxychlorination (POC), including reports of a wide range of catalytic materials, such as metal oxides (i.e., CeO_2), metal phosphates, and metal oxyhalides. On the other hand, propane oxybromination (POB) leads to much lower yields because of polyhalogenation and overoxidation.

5.2.1.1. CeO_2-Based Catalyst. CeO_2-based catalysts have been studied extensively because of their high activity toward hydrogen halide oxidation, alkane, and alkene oxyhalogenation.[247] Xie et al. have investigated bulk transition metal oxide catalysts (i.e., RuO_2, Fe_2O_3, CuO, NiO) and rare earth metal oxides (i.e., CeO_2, La_2O_3, Eu_2O_3) for POC.[49] Among transition metal oxides, Fe_2O_3, CuO, and NiO are unstable during the reaction, whereas RuO_2 leads to the formation of CO_x as major products, indicating high reactivity of oxygen

https://dx.doi.org/10.1021/acscatal.0c03999
ACS Catal. 2021, 11, 2182−2234

species on the RuO_2 surface. Bulk CeO_2 shows the highest C_3H_8 conversion (i.e., 29%) and a good C_3H_6 selectivity of 61% at 500 °C (Table 14). The POC is demonstrated to be structure-sensitive over various facets and morphology of CeO_2. CeO_2 nanorods (110 + 100 facet) are the most active for POC.[49] To improve activity and selectivity and suppress the overoxidation potential during POC, a solid solution of transition metal oxides with CeO_2 has been investigated (Table 14).[49] In particular, 8% NiO−CeO_2 demonstrates an excellent single pass yield up to 55% with 80% C_3H_6 selectivity, outperforming other catalysts with different compositions. Raman results demonstrate that the catalyst activity is correlated with surface oxygen vacancies. The band at 831 cm^{-1} due to O_2^{2-} surface species is the strongest for 8% Ni−CeO_2 followed by CeO_2 nanorods and CeO_2 nanocubes, while the bands for CeO_2 nano-octahedra and CeO_2 particles are too weak to be registered. Similarly, surface chloride coverage is determined to be crucial for controlling olefin selectivity, as evidenced by XPS results.[49]

The presence of HCl not only suppresses the reactivity toward oxidation products over CeO_2 but also induces new active site pairs for selective C_3H_6 production. DFT calculations reveal that the reaction is initiated by the formation of peroxide species over oxygen vacancies, which can oxidize Cl^- into $Cl^\bullet$, and the surface-bound $Cl^\bullet$ radical is responsible for C−H activation.[49] DFT calculations combined with detailed kinetic analysis provide insights into the reaction mechanisms, in which the reaction proceeds via propyl chloride generation and subsequent dehydrochlorination into C_3H_6 over the catalyst surface, as illustrated in Figure 23.[49]

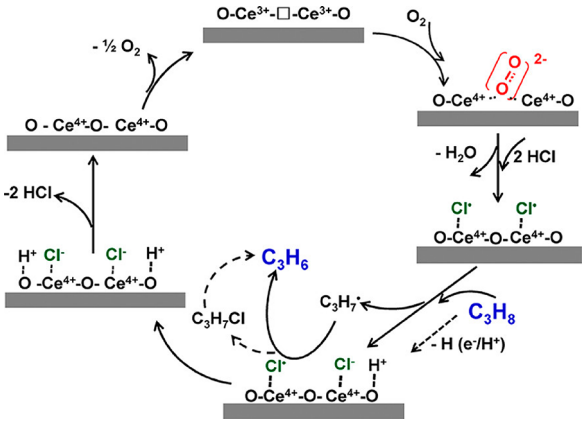

Figure 23. Proposed reaction mechanism for propane oxychlorination to propylene over CeO_2-based catalyst. Reproduced with the permission from ref 49. Copyright 2018 American Chemical Society.

The energy barrier of C−H activation on Ce^{4+}−O^{2-} (1.8 eV) is higher than that on $Cl^\bullet$ adjacent to O^{2-} (0.9 eV), indicating that the latter pair is responsible for C_3H_8 activation.[248] It is generally agreed that the formation of propyl chloride inhibits the overoxidation.[49,248] The formation of Cl_2 is found to be negligible in the presence of C_3H_8, suggesting gas-phase conversion is unlikely.

5.2.1.2. Metal Oxyhalide. While CeO_2 exhibits the highest activity (Table 14), europium oxychloride (EuOCl) leads to better C_3H_6 selectivity (i.e., >95% with C_3H_8 conversion of 20%) during POC.[48,249] The excellent performance in the case of EuOCl can be rationalized by the unique balance of its mild redox nature that enables alkane activation, minimizes gas-phase reaction by inhibiting the evolution of Cl_2 (Figure 24), and suppresses alkane overoxidation. Europium is predominantly found in Eu^{3+} with minor contributions from Eu^{2+} via XPS analysis. As suggested, the presence of a redox couple (Eu^{3+}/Eu^{2+}) is responsible for propane activation.[45] LaOCl is less selective toward C_3H_6 (i.e., 40% with C_3H_8 conversion of 51%) at 400 °C, in contrast to EuOCl (Table 14).

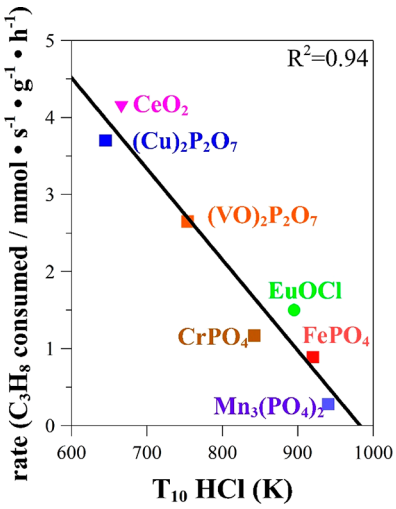

Figure 24. Rate of propane consumption in oxychlorination reaction (POC) as a function of the ability of the catalyst to evolve Cl_2 during oxychlorination (T_{10}(HCl)). T_{10}(HCl) corresponds to the temperature at which 10% HCl is converted into Cl_2. Adapted from refs 48 and 50.

In the case of EuOBr, the POB reaction favors the formation of alkyl bromides (C_3H_7Br), resulting in poor C_3H_6 selectivity (i.e., 22% with C_3H_8 conversion of 45%) at 500 °C.[45] It is postulated that the C_3H_8 activation during POB occurs in the gas phase by the in situ generated Br_2, leading to polyhalogenation, cracking, and combustion (Figure 25).[45]

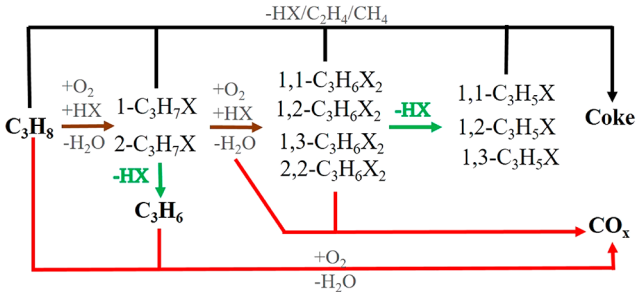

Figure 25. Schematic illustration of reaction network for propane oxyhalogenation, involving consecutive halogenation (brown), dehydrohalogenation (green), oxidation (red), and decomposition reaction (black). Reproduced with permission from ref 246. Copyright 2020 American Chemical Society.

Characterization of the spent EuOBr catalyst reveals the presence of the $EuBr_2$ and EuBr phases after POB reaction, indicating bromination of the catalyst; whereas the EuOBr phase is stable during HBr oxidation and methane oxybromination in contrast to POC.[250] The bromination of the catalyst is formed due to the reduction of the catalyst surface by the C_3H_7Br generated in situ during the reaction.

https://dx.doi.org/10.1021/acscatal.0c03999
ACS Catal. 2021, 11, 2182−2234

Table 15. Molten Salt-Mediated Gas-Phase Dehydrogenation of C_3H_8

mediator	temp (°C)	space time (s)	feed ratio	aimed product	C_3H_8 conv. (%)	C_3H_6 selec. (%)	ref
$LiOH{\cdot}H_2O/LiI$	600		air: C_3H_8 = 2: 1	C_3H_6	64	75	264
$LiOH/LiI/I_2$	500	90	I_2: O_2: C_3H_8 = 0.5: 0.5: 1	C_3H_6	78	81	263
LiI	450			C_3H_6	60−79	88−96	261

5.1.1.3. Metal Phosphates. Transition metal phosphates such as V, Ti, Mn, Cr, Fe, Co, Ni, and Cu have been investigated for the oxyhalogenation reaction of alkanes (Table 14).[50,249] The product distribution is strongly dependent on the nature of catalyst and the type of halogen. Among the metal phosphates, $CrPO_4$ and $FePO_4$ have shown excellent C_3H_6 selectivity (i.e., > 95%) during C_3H_8 oxychlorination. In contrast, Mn-, Ni-, Co-, and Ti-based phosphates result in cracking, V-phosphate only yields oxidation products, and Cu-phosphate favors the formation of chlorinated hydrocarbons. $CrPO_4$ exhibits the maximum C_3H_6 yield ∼50% with selectivity of ∼95%.[50] Similar to EuOBr, vanadium-phosphate (VPO) shows 35% C_3H_8 conversion and 24% C_3H_6 selectivity during POB, but with a yield as low as 8% (Table 14).[251]

Pérez-Ramírez and co-workers describe several kinetic parameters to explain the differences in activity and selectivity toward different products over different catalysts.[50] In particular, the catalytic ability for the oxidation of HCl to molecular Cl_2 is quantified based on the temperature at which 10% conversion of HCl oxidation (T_{10}(HCL)) can be achieved (Figure 24). Similarly, the trends toward dehydrochlorination of C_3H_7Cl, cracking, and oxidation of propane are investigated for all catalysts. As shown in Figure 24, the rate of propane consumption via POC reaction correlates linearly with catalyst ability to evolve molecular Cl_2 during oxidation of HCl. The high C_3H_6 selectivity over $CrPO_4$ is attributed to the fast dehydrochlorination kinetics in combination with a low propensity to cracking and overoxidation, as well as hindered ability to evolve Cl_2.

Operando photoelectron photoion coincidence (PEPICO) spectroscopy enables the detection of reactants, products, and short-lived intermediates such as radicals under reaction conditions. Recently, PEPICO has been applied in propane oxyhalogenation over the $CrPO_4$ catalyst to shed light on mechanisms, especially in the gas phase.[246] Operando PEPICO reveals that neither $Cl^{\bullet}$ nor Cl_2 are present under POC reaction conditions. This indicates that propane activation occurs primarily on the catalyst surface, namely, a surface-confined mechanism, and proceeds via the formation of C_3H_7Cl, followed by fast dehydrochlorination to yield olefins. This is in line with the kinetic studies and corroborates that propane oxychlorination proceeds via surface-driven reaction pathways.[50,246]

The propane oxybromination chemistry leads to a lower propylene yield due to the formation of coke, cracking, and oxidation products (CO_x), as well as brominated hydrocarbons (such as C_3H_7Br and C_3H_5Br) over $VOPO_4/CrPO_4/EuOBr$.[45,246,251,252] Detailed kinetic analysis, complemented by operando PEPICO, demonstrates that C_3H_8 activation proceeds in the gas phase with in situ generated bromine species ($Br^{\bullet}/Br_2$) via catalytic HBr oxidation over $CrPO_4$. The evolution of reactive intermediates, such as $Br^{\bullet}$, is correlated with C_3H_6 formation via operando PEPICO with increasing temperatures indicates that reaction takes place in gas phase primarily. Similar to POC, POB also proceeds through the formation of propyl halide, which subsequently undergo dehydrohalogenation to yield C_3H_6.[246] Further, this technique sheds light on the coking and cracking reaction pathways observed under oxybromination reaction conditions during POB (Figure 25). The presence of C_3 radicals due to the resonance stabilization prolongs their lifetime in the reactor, leading to coke formation. The coke formation proceeds via consecutive hydrogen abstraction of 2-propyl by $Br^{\bullet}$ to yield allyl and propargyl species which results in the formation of coke precursors such as benzene. Additionally, the cracking of C−C bonds may also form ethyl and methyl radicals. The presence of methyl radicals likely facilitates the formation of C_4−C_6 species through chain growth, thus contributing to the formation of coke precursors from alternative pathways.[246]

In brief, the relationships between propane oxyhalogenation, gas-phase halogenation, C_3H_7X elimination, hydrogen halide oxidation, and propane oxidative dehydrogenation have been elucidated over a wide set of catalysts. Results suggest that the selectivity in the oxyhalogenation reaction depends on (i) the ability of the catalyst to selectively dehydrogenate the propyl halide into propylene, (ii) hindered ability to evolve molecular halogen, and (iii) suppressed overoxidation and combustion tendency. Of note, the high reactivity toward HCl oxidation can give rise to undesired products because of the gas-phase reactions, indicating the need for a balanced redox nature.[48,249,253]

5.2.2. Other Halogen-Assisted Systems. Propane halodehydrogenation by Cl_2 has been studied over a 0.28% Ru/TiO_2 catalyst that achieves ∼50% C_3H_8 conversion and 95% C_3H_6 selectivity at 400 °C.[254] The HCl generated during the reaction requires an oxychlorination reactor to recycle Cl_2 via the Deacon reaction ($4\ HCl + O_2 \rightarrow Cl_2 + 2H_2O$). Alkali metal chloride catalysts also have been probed for oxidative dehydrogenation of C_3H_8, though scarcely.[46,255,256] The C_3H_6 yield obtained over Li−K/Dy_2O_3 is below 20% at 600 °C, along with propylene selectivity lower than 60%.[255]

The effect of organochloride compounds, such as CCl_4, has also been studied for oxidative propane dehydrogenation over CeO_2, Fe_2O_3, and CuO, in which improved C_3H_6 selectivities of up to 80% are evident at P(CCl_4) = 0.17 kPa under oxygen-limiting conditions.[257−259] These studies are conducted under relatively low conversions (i.e., 25% at 450 °C and F_T/W ∼ 4000−6000 $cm^3\ h^{-1}\ g_{cat}{}^{-1}$), which limits the C_3H_8 yield below 20%. Of note, the presence of chlorinated species near the surface region and in the gas phase accounts for the improved performance with the addition of CCl_4.[257,258] Oxychlorination on a Pt−Sn/θ-Al_2O_3 catalyst also shows the restoration of catalytic activity during conventional DHP because of the excellent dispersion of sintered Pt agglomerates.[260]

5.2.3. Molten Salt-Catalyzed Oxidative Dehydrogenation. The oxidative dehydrogenation of various hydrocarbons on metal iodide-based molten salt was first developed by Shell.[261,262] In those approaches, the ODHP reaction can occur between 450 and 600 °C in the presence of metal iodides (i.e., LiI, CdI_2, ZnI_2, and PbI_2), and a C_3H_6 yield up to

https://dx.doi.org/10.1021/acscatal.0c03999
ACS Catal. 2021, 11, 2182−2234

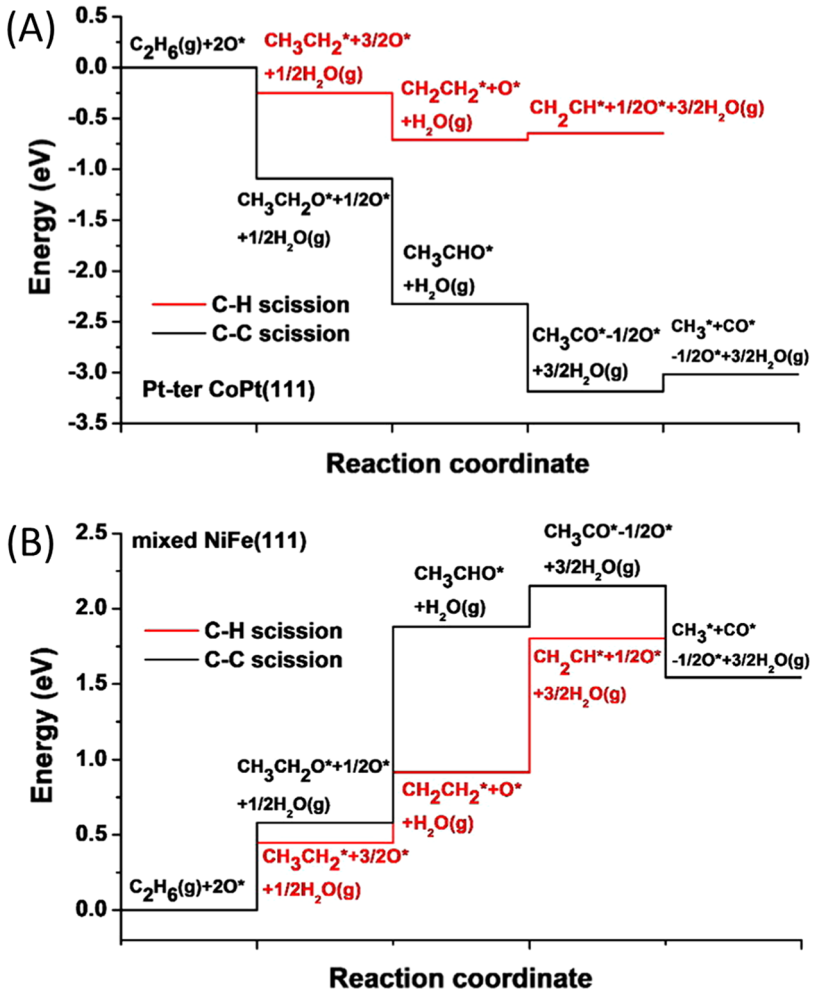

Figure 26. Energy profile of the oxidative dehydrogenation (red) and dry reforming (black) paths for (A) a Pt-terminated CoPt(111) and (B) mixed FeNi(111) surface. Reproduced with the permission from ref 280. Copyright 2016 Elsevier B.V.

70% can be achieved (Table 15). The molten salt catalyzed oxidative dehydrogenation can be considered a special case of halogen-assisted oxidative dehydrogenation, in which a halogen, such as I_2, is generated in situ via the reaction between metal iodide and oxygen. The reaction, however, primarily takes place in the gas phase.

It is generally accepted that the interplay between the metal iodide and metal oxide (LiI/LiOH) plays an important role in the generation of iodine to initiate a radical chain reaction.[263,264] A constant-temperature ab initio molecular dynamics study has been used to investigate the reactions between LiI and gaseous molecules (O_2, H_2O, and I_2).[265] Results demonstrate that the most favorable process is the formation of gaseous I_2, coproduced with LiOH or Li_2O, depending on the availability of water; the reaction most likely occurs in the gas phase. These observations are supported by the fact that a similar product distribution is observed using either LiI/LiOH or I_2 as an iodine source for the dehydrogenation reaction.[263] The high C_3H_6 yield can be achieved if the molten salt meets the following prerequisites: (i) the metal oxide can be converted into the corresponding iodide by exposure to iodide species under the reaction conditions and vice versa and (ii) I_2 (g) can be obtained by oxidation under dehydrogenation conditions.[261] Similarly, an optimal concentration of O_2 is vital for this reaction because (i) it is responsible for generating iodine radicals for chain reactions and (ii) excess oxygen can cause combustion reactions.[263,264] It is important to note that the corrosive nature of the mixture of molten salt, I_2, HI, and alkyl halides, is a serious concern that might impair efforts for its commercial applications.

6. PROGRESS IN THEORETICAL STUDIES OF REACTION MECHANISMS

Regardless of the oxidant or catalyst used in the oxidative dehydrogenation of alkanes, the C−H bond must first be activated. In metal oxides, this commonly occurs homolytically via H abstraction by surface oxygen species, or heterolytically over an acid−base pair.[266−268] In the redox-active oxides, a MvK mechanism is commonly observed where the hydrogen, adsorbed on an oxygen forms a hydroxide, and abstracts a second hydrogen either from a C−H bond or a neighboring hydroxyl group.[269] This forms water, which desorbs and leaves behind an oxygen vacancy that must be filled by an oxidant to regenerate the catalyst.[270−272] In an alternative mechanism, the formation of the vacancy is not required and instead, the catalyst surface brings together the hydrogen and the oxidant, which is reduced directly. This is more commonly observed in redox-inactive oxides, such as MgO and La_2O_3, as reported from theoretical studies.[273−275] In this context, the role of the oxidant is to regenerate the catalyst by either reoxidizing the

https://dx.doi.org/10.1021/acscatal.0c03999
ACS Catal. 2021, 11, 2182−2234

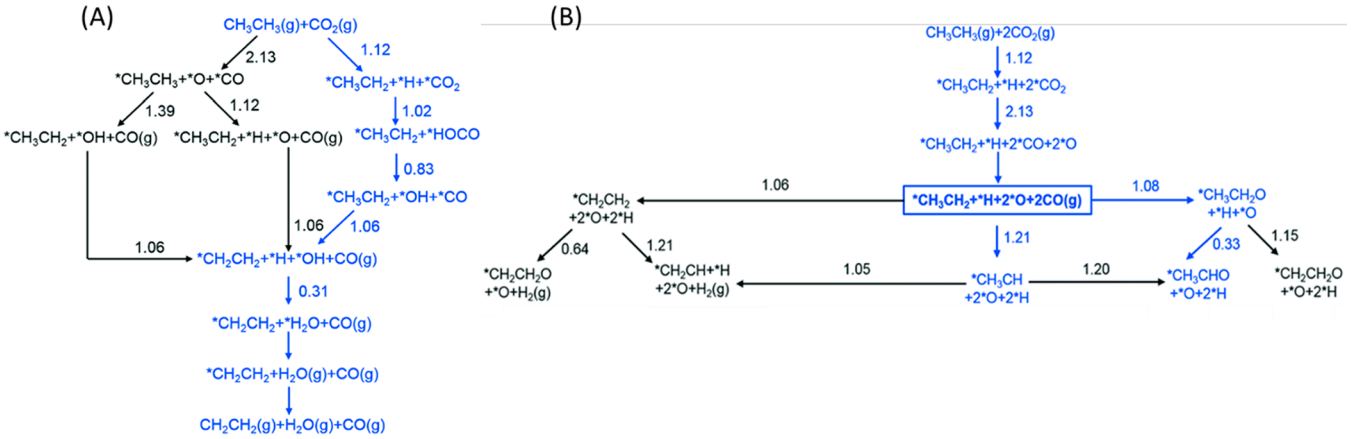

Figure 27. Mechanism for ethane conversion on PtNi(111) following (A) the ODHP pathway and (B) the dry reforming pathway. The dry reforming pathway is shown up to where it branches off from the ODHP one. Reproduced with the permission from ref 283. Copyright 2018 Royal Society of Chemistry.

vacancy site through providing its oxygen, or reacting with adsorbed hydrogen species on the surface.

While ODHP has featured extensively in theoretical studies, examples where soft oxidants are explicitly considered are considerably fewer. In this section, we include examples of ODHP with soft oxidants but also supplement similar examples with other alkanes, such as ethane and methane partial oxidation, which share many similarities in their reaction mechanism. Oxidants discussed in this section include CO_2, N_2O, NO_x, and other soft oxidants, such as sulfides and halides. We discuss both scenarios where the soft oxidant participates in the reaction by regenerating oxygen vacancy sites and where they react with surface hydrogen directly, as well as additional routes such as via forming gas-phase radicals.

6.1. Reactions with CO_2. *6.1.1. CO_2 Dissociation in ODHP.* When CO_2 is used as an oxidant, there are generally two proposed mechanisms for its participation in ODHP. One involves direct CO_2 dissociation to form CO and O, and the other involves the hydrogenation of CO_2 to HOCO or COOH before forming CO. For the CO_2 dissociation route, its high stability can be problematic because it prevents it from being easily activated to oxidize the surface. Therefore, finding a catalyst with a strong affinity for CO_2 and its dissociation is an important criterion for ODHP with CO_2. Fan et al. have explored the feasibility of ethylbenzene dehydrogenation with CO_2 on a V_2O_5 catalyst.[276] They found the barrier for CO_2 to oxidize the V^{III} site is 3.16 eV, with an endothermic reaction energy of 2.21 eV, suggesting an extremely difficult process. The authors therefore have concluded that CO_2 is unable to reoxidize the surfaces following dehydrogenation of ethylbenzene, which leads to a deactivation of the catalyst. Meanwhile, on a VO_x/SiO_2 catalyst, Ascoop et al. find that CO_2 reoxidizes the site with a barrier of 1.76 eV, which is lower than on the pure V_2O_5 surface but still significant in energy.[28] It is concluded that vanadia in the WO_x−VO_x/SiO_2 cannot be fully oxidized to V_2O_5 with CO_2 but instead oxidized to V_2O_4. In contrast, CO_2 dissociation can occur more easily on the CeO_2 (110) surface with a rate-limiting barrier of 1.36 eV on a site containing oxygen vacancies.[277] The ability of the reduced CeO_2 surface to dissociate CO_2 is utilized in a series of studies with bifunctional catalysts containing a CeO_2 support.[12,155,278−280] Transition metals, particularly in the form of subnanometer clusters, have also been found to be highly active for CO_2 dissociation. One study found a low CO_2 dissociation barrier of 0.35 eV could be obtained on Ni_4/MgO which provides active oxygen species for alkane C−H activation.[281]

6.1.2. Factors Controlling Selectivity between ODH and Dry Reforming. CO_2 can often participate in parallel competing reactions from ODHP, such as dry reforming and the RWGS at high temperatures. Selective ODHP catalysts, therefore, need to prevent dry reforming from occurring. In one such study, Myint et al. have examined a number of bifunctional catalysts, containing CoPt, CoMo, and FeNi supported on CeO_2 for ethane ODH with CO_2 from experiments and theory.[280] The authors observe the highest selectivity to the ODH product with $FeNi/CeO_2$. DFT is used to rationalize this behavior by comparing the energy profiles for successive C−H dissociation and C−C dissociation reactions. As shown in Figure 26, these two paths represent the formation of the ODH product ethylene and the dry reforming product, respectively. On the CoPt surface, the intermediates for C−C dissociation are found to be considerably more favorable in energy than the C−H products, whereas the trend is reversed on the FeNi surface. The clear differences in energetics between the two paths in this comparison supports the experimentally observed selectivity trends. Thermodynamic comparisons from DFT have also been used to explain selectivity of ODHP versus dry reforming on a variety of other catalytic systems, such as Pt/CeO_2 and Mo_2C,[282] $FeNi_3$ and $FeO_x/Ni(111)$,[278] and Ni_3Pt and $FeO/Ni(111)$.[12]

Kattel et al. have followed up on this study with a thorough theoretical investigation of the reaction network and kinetics.[283] In the studied reaction network for ethane ODH, CO_2 goes through either a dissociative mechanism or an associative one forming HOCO (Figure 27A). In the dissociative mechanism, CO is formed and desorbs into the gas phase, while the remaining oxygen can assist in the C−H activation or become hydrogenated after unassisted C−H activation. In the associative mechanism, C−H activation first occurs independently of CO_2, which provides hydrogen to form the HOCO intermediate. Once formed, it can dissociate with a barrier of 0.83 eV, significantly lower than the direct dissociation of CO_2 having a barrier of 2.13 eV. In the dry reforming path, ethylene is also formed via the same

https://dx.doi.org/10.1021/acscatal.0c03999
ACS Catal. 2021, 11, 2182−2234

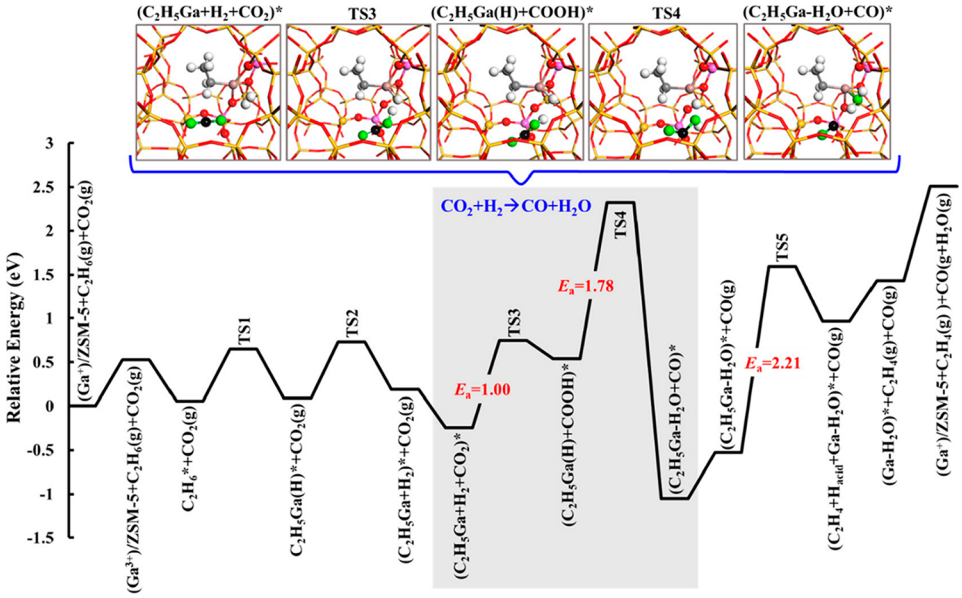

Figure 28. Mechanism of ethane ODH on Ga/ZSM-5 with CO_2. The insets show the geometries for CO_2 hydrogenation and dissociation to form H_2O and CO. Reproduced with the permission from ref 284. Copyright 2019 American Chemical Society.

intermediates (Figure 27B). However, the paths diverge upon further oxidation of ethylene to CH_2CH_2O, CH_2CH, CH_3CH, or CH_2CHO, which eventually leads to C−C scission. Kinetic Monte Carlo calculations find dry reforming to be favored over ODH. Interestingly, it is revealed that the CO_2 dissociation is favored over HOCO formation, despite the higher energy barriers for the former. The calculations also find the dehydrogenation of CH_3CH_2 to CH_2CH_2 to be a key descriptor of ODH selectivity, which should be promoted to improve the selectivity on the catalyst.

6.1.3. CO_2 Hydrogenation in ODHP. In a work by Gomez et al., ethane oxidative dehydrogenation and subsequent aromatization by CO_2 is investigated for P- and Ga-modified ZSM-5 catalysts.[284] The associative pathway for CO_2 is computed with DFT, where CO_2 is hydrogenated by a nearby H_2 that is formed as part of the dehydrogenation of C_2H_6 to C_2H_5 (Figure 28). The reaction of CO_2 follows roughly that of reverse water−gas shift, which forms CO and H_2O. The concerted hydrogenation of CO_2 occurs with the dissociation of H_2 to form COOH with a barrier of 1.00 eV, followed by a second concerted dissociation of the C−OH bond to form CO and H_2O in a single step with a barrier of 1.78 eV. The authors find the primary role of CO_2 for this reaction on Ga/ZSM5 is to consume hydrogen, which promotes portions of the reaction where H_2 formation is kinetically and thermodynamically less favorable. The mechanism is also found to be consistent with $^{13}CO_2$ isotope studies in the same paper, which does not report any carbon from CO_2 in the final hydrocarbon products.

6.1.4. CO_2 Poisoning in ODHP. On catalysts with strong basic sites, such as MgO, CO_2 can interact strongly with surface sites and poisons the catalyst, which is an issue when considering CO_2 as an oxidant. In oxidative coupling and dehydrogenation, it has long been noted in experiments that CO_2 strongly inhibits the reaction from proceeding.[128,285,286] This is consistent with theoretical calculations which find very negative CO_2 adsorption energies of −2 to −3 eV on the MgO and CaO surfaces, particularly at the step sites.[287] On these surfaces CO_2 interacts with the lattice oxygen to form surface bound carbonate species. The same sites which strongly bind CO_2 are also responsible for C−H activation, which remain blocked because of the much weaker interaction between the alkane and the surface. Similarly, on the perovskite $BaZrO_3$, CO_2 is found to bind strongly to form a stable carbonate layer under ambient concentrations, which suggests such a catalyst would also be inactive for ODHP with CO_2.[288] Consequently, poisoning by CO_2 is an important potential factor preventing its use in ODHP and may also apply to the other oxidants as well.

6.2. Reactions with N_2O and NO_x. *6.2.1. Reactions with N_2O.* In an early work, Rozanska et al. have investigated ODHP on vanadia using DFT for a cluster model, and compared the differences between O_2 and N_2O as oxidants.[177] On this catalyst, propane first undergoes homolytic C−H activation on the terminal oxygen of the V^{5+} sites, reducing the site to V^{4+} and forming a hydroxyl. The propyl then undergoes a second C−H activation on the hydroxyl site forming propylene and a water and leaving a further reduced V^{3+} site, which must be regenerated by an oxidant to close the catalytic cycle. From their calculations, they find N_2O to be a weaker oxidant for the catalyst, which can only oxidize the V^{3+} sites, whereas O_2 can oxidize both V^{3+} and V^{4+} sites, as evidenced by the lower energy barriers required for O_2 (Figure 29A). The oxidization of the V^{4+} site by O_2 also leads to the formation of HO_2 radicals, which can either oxidize another V^{4+} site or activate the C−H bonds in a side reaction, with a barrier of 0.67 eV for propane. Finally, when oxidizing the sites, N_2O restores the V^{3+} sites back to V^{5+} by providing its single oxygen, whereas O_2 instead forms a peroxovanadate species. This is found to be possible on both the monomeric and dimeric vanadate. Subsequent investigation found the peroxovanadate to be more active for both propane activation and propylene oxidation than the V^{5+} site, having lower reaction barriers and a more exothermic reaction by comparison (Figure 29B). In particular, propylene activation on peroxovanadate has a low barrier of 0.84 eV and is exothermic by 2.59 eV, whereas activation on V^{5+} has a barrier of 1.43 eV and is endothermic by 1.17 eV. The authors

https://dx.doi.org/10.1021/acscatal.0c03999
ACS Catal. 2021, 11, 2182−2234

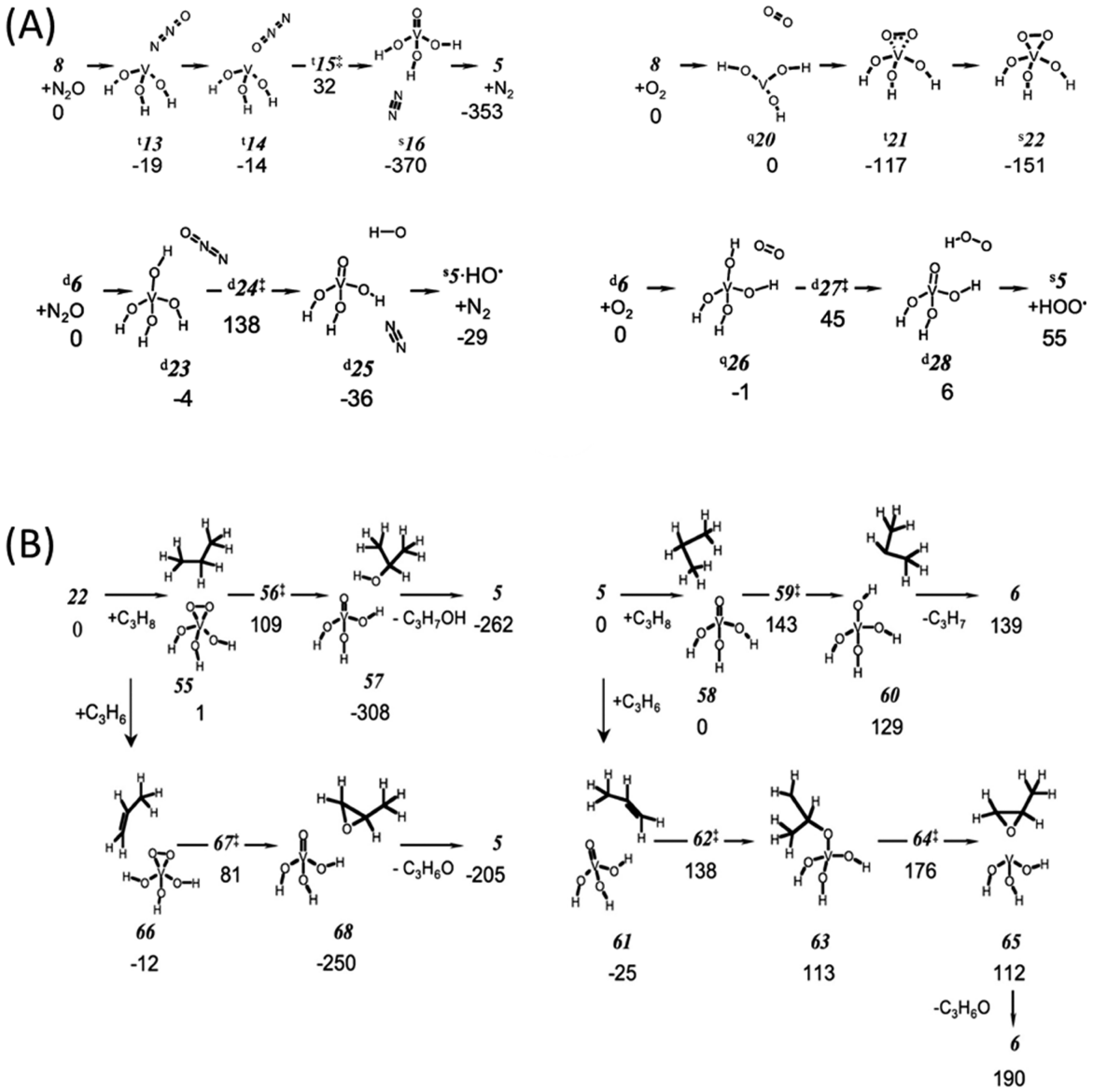

Figure 29. Mechanism of ODHP on vanadia, showing (A) the vacancy regeneration step with either O_2 and N_2O and (B) the differences in propane and propylene activation on the V^V and peroxovanadate sites. Reproduced with the permission from ref 177. Copyright 2008 Elsevier B.V.

estimate the oxidation rate of propylene is one to 2 orders of magnitude greater than propane under the reaction conditions, which could contribute to the overoxidation of propane to undesired CO_x, when O_2 is used as the oxidant. Thus, the authors point toward peroxovanadate formation as a key factor in the lower selectivity to propylene with O_2 as the oxidant over N_2O.

A similar hypothesis regarding differences in active oxygen sites due to the choice of oxidant has been put forward by Dasireddy et al. for butane ODH on the $NiMoO_4$ catalyst.[289] On the basis of the DFT reaction energies for surface oxidation by O_2, N_2O, and CO_2, it is found that the full oxidation of Ni and Mo sites is thermodynamically favorable with O_2, whereas N_2O and CO_2 can only partially oxidize the surface, recovering only the Mo sites. On the fully oxidized surface, C−H activation is facile with a barrier of 0.05 eV, irreversibly forming butan-1-ol in a single, highly exothermic step, which eventually leads to the formation of CO_x. By comparison, on the partially oxidized surface, C−H activation is rate-limiting with a barrier of 1.49 eV, in reasonable agreement with the experimental activation energies in the same paper. Therefore, the higher oxidizing ability of O_2 provides more reactive oxygen species on the surface, leading to the overoxidation of butane.

Using N_2O as an oxidant has also been explored in metal−organic framework (MOF) systems for alkane partial oxidation and ODH. In methane partial oxidation, the terminal oxygen of the metal nodes is commonly proposed to be the active site, which activates the methane C−H bond and forms methanol via a radical-rebound mechanism.[290,291] Upon desorption of the product, N_2O reoxidizes the site. In a more recent combined experimental and theoretical study, Barona et al. propose a similar mechanism for alkane ODH on the Fe_3M nodes of MOF PCN-250 (Figure 30A).[292] Here, the alkane undergoes homolytic C−H activation on the terminal oxygen of the metal node, resulting in a hydroxyl group which is further reduced to form water or an alcohol. The products, then, desorb and leave an open metal site, which is

https://dx.doi.org/10.1021/acscatal.0c03999
ACS Catal. 2021, 11, 2182−2234

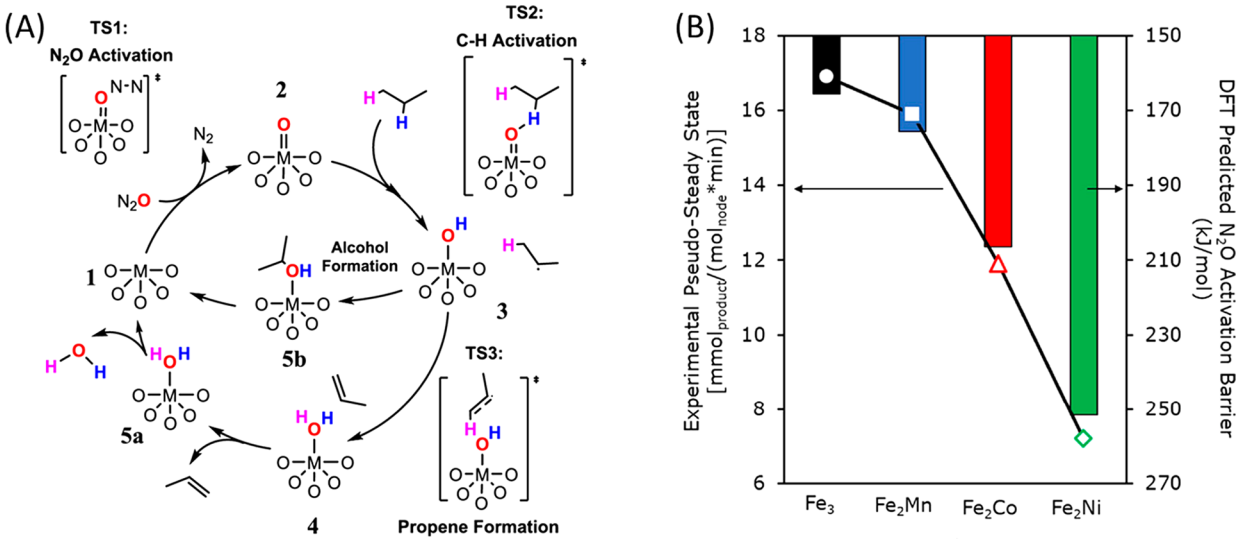

Figure 30. Mechanism of ODHP on MOF PCN-250 with Fe_3M nodes. (A) The proposed catalytic pathway is shown where the terminal O abstracts hydrogen and is consumed, which is regenerated with N_2O. (B) A comparison of the experimental rates and the DFT predicted activation barrier of N_2O for site regeneration. Reproduced with the permission from ref 292. Copyright 2020 American Chemical Society.

subsequently filled by the oxygen from N_2O activation, regenerating the site and closing the catalytic loop. In this work, they find the ability of the site to regenerate the oxygen from N_2O activation and the ability of the oxygen to activate the C−H bond are correlated to a single descriptor, the oxygen binding energy on the metal node. The more negative the oxygen binding energy, the lower the N_2O activation energy and the higher the C−H activation energy, and vice versa. In the regime where N_2O activation is rate-limiting, a direct correlation between the DFT N_2O activation energies and the experimental rates is observed, supporting this mechanism (Figure 30B). The rational design of better MOF catalysts following this mechanism may be realized by tuning the oxygen binding energy of the metal node from changing its elemental composition.

6.2.2. Reactions with NO_x. NO_x is another potential oxidant for alkane oxidation, though few theoretical studies have been conducted in the context of ODHP. However, some hints toward its role and reactivity in ODHP can be found in existing studies of NO_x dissociation and reduction. One DFT study finds that the dissociation of NO_2 can be a moderately facile process on certain metal surfaces, such as Cu(111) with a barrier of 0.61 eV.[293] Another study has looked at NO_2 reduction on V_2O_5, and found that the reduction of NO_2 to HNO_2 over a hydroxyl on the V^{4+} site can occur with little to no barrier.[294] These V^{4+} sites are identical with those formed from C−H activation in ODHP, suggesting that NO_2 can similarly oxidize the V^{4+} site like O_2 as previously described (Figure 29A).[177] For the case of NO, a DFT study on Pt(100) has investigated both dissociation and hydrogenation pathways, finding the dissociation to N and O to be more favorable with a barrier of 0.96 eV.[295] These results provide guidance for catalysts which could effectively use NO_x as an oxidant in the ODHP reaction.

Another perspective for the participation of NO_x in ODHP has been introduced in a recent experimental and theoretical study by Annamalai et al.[296] They find that gas phase NO_x can promote selective ODHP via the formation of OH radicals, which can then activate C−H bonds in ODHP in the absence of a solid catalyst. A reaction mechanism is proposed where OH radicals are formed continuously from the reaction of NO and NO_2 with O_2 and sacrificial H donors, such as the alkyl radicals. The reason behind the high selectivity of OH radicals for ODHP is then explained by the differences in the activation energy of various C−H bonds as a function of the hydrogen abstraction strength of the catalytic site. It is found that sites with low hydrogen abstraction strength have a greater preference for activating weaker C−H bonds (such as propylene) over stronger ones (such as propane), leading to overoxidation and a reduced selectivity to propylene. Meanwhile, the OH radical, having a strong hydrogen abstraction strength (measured by a hydrogen adsorption energy of −5.39 eV from DFT), has no such preference to the weaker C−H bonds, which prevents overoxidation from occurring. Relating this back to heterogeneous catalysis, NO is also found to be generated from boron nitride catalysts under ODHP conditions, which could also participate in this process.[297] Further theoretical studies are needed to elucidate the impact of radical formation by NO_x on the ODHP reaction in the presence of a solid catalyst.

6.3. Reactions with Other Soft Oxidants. *6.3.1. Sulfides.* Zhu et al. have explored the possibility of sulfur as another less active oxidant for alkane conversion, specifically for methane oxidative coupling.[298] The authors note that the thermodynamic well for O_2 oxidation of methane to CO_2 is −13.41 eV, whereas for sulfur oxidation to CS_2, it is considerably higher in energy at −3.45 eV. Therefore, the thermodynamic driving force for overoxidation is much lower for the sulfur oxidant. This approach is realized by carrying out the reaction under gaseous sulfur flow on a selection of transition metal sulfides. Presumably, the gaseous sulfur regenerates vacancies on the surface formed from H_2S desorption during methane coupling. An ethylene selectivity of up to 18% can be achieved on a PdS catalyst at 1050 °C. High temperatures are needed for this process due to both the thermodynamics of the reaction and the relatively high C−H activation barriers on the sulfide catalysts, which are poor hydrogen abstractors compared to metal oxides. These barriers range from 1.91 eV on MoS_2 to 2.68 eV for TiS_2. While the performance of this catalyst is found to be relatively

https://dx.doi.org/10.1021/acscatal.0c03999
ACS Catal. 2021, 11, 2182−2234

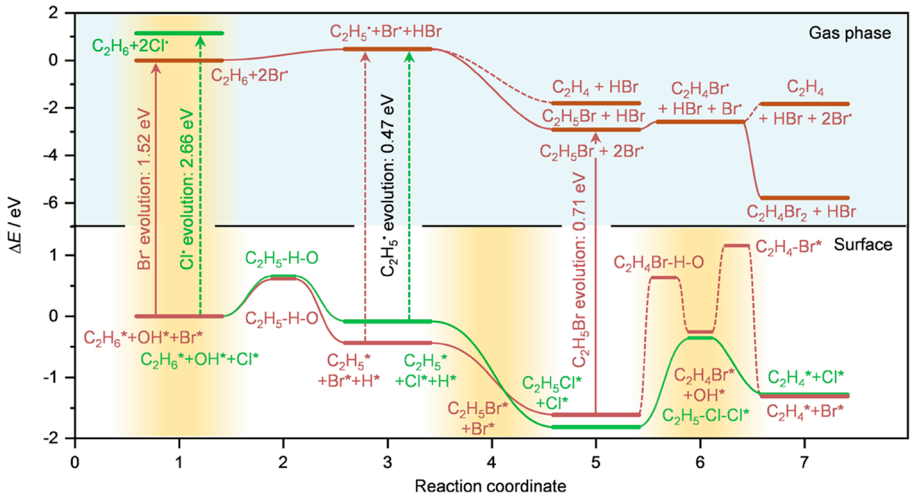

Figure 31. Comparison of oxyhalogenation (green) and oxybromination (brown) energetics for both gas-phase and surface mediated pathways. Reproduced with the permission from ref 252. Copyright 2019 John Wiley and Sons.

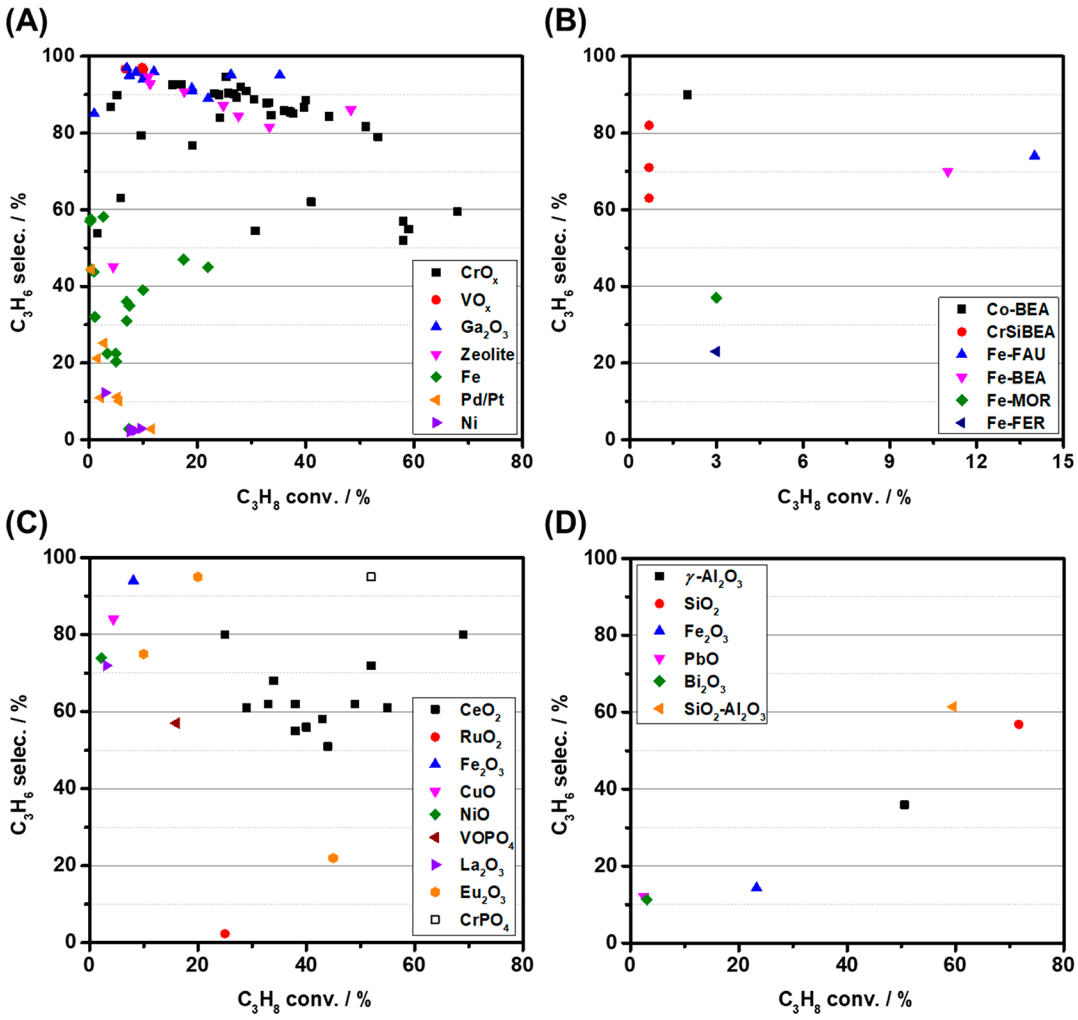

Figure 32. Summarized catalytic performance of developed catalysts for CO_2−ODHP at 550 °C (A), N_2O−ODHP at 400 °C (B), oxyhalogenation at 500 °C (C), and SO_2-mediated dehydrogenation at 640 °C (D).

modest and far from practical consideration, it is conceivable that future studies can identify catalysts with higher conversion rates by descriptor-based theoretical screening. In particular, the authors have observed the M−S bond energy to be a good descriptor for both C−H activation and C−C coupling reaction barriers.

Premji et al. have explored the role of H_2S in ODHP in the gas phase from experimental and theoretical perspectives.[44]

https://dx.doi.org/10.1021/acscatal.0c03999
ACS Catal. 2021, 11, 2182−2234

From theoretical calculations, it was proposed the co-feed of H_2S/O_2 and partial oxidation of H_2S can produce sulfur radical species SH and HS_2 which participate in hydrogen abstraction along with OH and OOH. Subsequently, after C−H activation to form propyl radicals, both O_2 and S_2 can then form adducts with the propyl and undergo further reactions. With the propyl-O_2 adduct, the propylene is the kinetic product, though a side distribution of other products can be formed, such as propanal, methyloxirane, and oxetane, all of which are more thermodynamically stable than propylene. On the other hand, with the propyl-S_2 adduct, propylene is more favored both kinetically and thermodynamically, in part due to the relative instability of the S-containing hydrocarbon products. The more favorable energetics for propylene formation with sulfide species is consistent with experimental observation of higher propylene selectivity observed in the paper.

6.3.2. Halides. There has been recent interests in using halogens, such as Cl_2 and Br_2, as oxidants, particularly in oxyhalogenation reactions, which can be used for alkane to alkene conversion.[249,299] Zichittella et al. have explored the mechanism and factors governing alkene selectivity for oxyhalogenation in a combined theoretical and experimental study of an iron phosphate catalyst.[252] Interestingly, the authors have observed a divergence in the mechanism for ethane oxychlorination and oxybromination, with the former being dominated by surface reactions and the latter being mainly dominated by gas-phase reactions (Figure 31). In the proposed mechanism, ethane oxychlorination follows a surface-mediated C−H activation (with a barrier of 0.61 eV) to form an ethyl intermediate which then reacts with a surface chloride to form ethyl chloride in a barrierless process. Ethyl chloride is subsequently dehydrohalogenated (where a hydrogen and halogen are both removed from the alkyl in a concerted step) to ethylene, the desired product, in another surface reaction. By contrast, when Br_2 is used, a gas-phase reaction is found to be more favorable where bromine desorbs as radicals which dehydrogenate and polybrominate ethane in a process unselective to ethylene. These results highlight the importance of the competition between surface and gas phase reactions that control the selectivity of the alkene and how the different oxidants shift their relative contributions.

7. CONCLUSIONS AND FUTURE DIRECTIONS

Recent advances in oxidative dehydrogenation of propane with soft oxidants over a variety of catalysts are reviewed in this work. Figure 32 summarizes and compares the catalytic performance of key catalysts explored in each reaction route in the form of the correlation between selectivity and conversion. In general, transition metal/metal oxides and metal oxides from the main group elements have been extensively studied for the ODHP reaction with soft oxidants, such as CO_2, N_2O, S-containing compounds, and halogen/halides. For CO_2- and N_2O−ODHP, the explored catalyst systems are analogous. However, differences in inherent properties of reactions and difficulties in dealing with corrosiveness have led to complications in advancing the research, resulting in unique challenges and future research directions for each route. In general, future efforts should be devoted to designing catalysts that can facilitate the activation of the C−H bond in C_3H_8 with good regenerability, as well as to renovating the reaction systems that can reconcile the need for industrial processes with challenges associated with utilizing various acid gases.

In CO_2−ODHP, the major efforts have been devoted toward exploring redox-type and nonredox-type catalysts and developing composition−structure−catalysis relationship. As a representative of redox-type catalysts, CrO_x exhibits higher C_3H_6 selectivity at elevated C_3H_8 conversion among all catalysts at 550 °C, as presented in Figure 32A. The activity is found to depend on the redox cycles, dispersion of Cr species, surface Cr density, and nature of the support. The catalytic performance of other redox-type catalysts, VO_x, has not yet reached high C_3H_8 conversion at 550 °C (i.e., >20%), though high C_3H_6 selectivity (i.e., ∼95%−98%) is achieved at low conversion (Figure 32A). The non-redox-type catalyst, Ga_2O_3, shows comparable selectivity to CrO_x below 40% conversion. Although Ga_2O_3 can be reduced upon contact with C_3H_8 molecules, its oxidation state remains stable during reaction. Instead, the reaction appears to proceed through the proposed heterolytic dissociation mechanism.[127] Combined with these developed redox- and nonredox-type catalysts, the zeolite-supported counterparts are also promising candidates (Figure 32A). Other catalysts that have been explored include Fe, precious metal, Mo_2C, and Ni catalysts. Screening tests and mechanistic studies on these materials shed light on their roles in the selective activation of the C−H bond. For example, the Mo oxycarbide, formed through CO_2-induced oxidation of Mo_2C, favors the activation of methylene C−H bond in C_3H_8 molecules;[160] the presence of Pd can promote the oxidation activity of redox sites such as $Ce^{4+} \leftrightarrow Ce^{3+}$, through which it promotes not only C_3H_8 conversion, but also inhibits Pd-catalyzed DRP reactions to undesired CO and H_2, leading to well-preserved C_3H_6 selectivity.[171]

The presence of CO_2 shows an overall promoting effect on C_3H_6 formation. Major positive roles of CO_2 include: (i) completing redox cycles, though the oxidation potential is weak, (ii) shifting the reaction equilibrium of ODHP to the product side by consuming the produced H_2 via RWGS, and (iii) serving as an agent for coke removal by the reverse Boudouard reaction. Competitive adsorption between C_3H_8 and CO_2 is known for CrO_x[24] and HZSM-5-supported Ga_2O_3.[127] However, the presence of CO_2 also enhances C_3H_6 production on CrO_x as a result of promoted C_3H_6 desorption.[24]

Despite these achievements, there are still elusive points that need to be addressed in future studies:

(i) Identification of redox cycles on redox-type catalysts. In the case of redox-type catalysts, there exist two different redox scenarios, including $Cr^{6+} \leftrightarrow Cr^{3+}/Cr^{2+}$ and $Cr^{3+} \leftrightarrow Cr^{2+}$, which seems to depend on the nature of the support and metal−support interactions. Such divergence necessitates the efforts to develop an in-depth understanding of the correlations.

(ii) Reaction mechanisms. Liu et al. have observed the resemblance of DRIFT spectra between DHP and the reverse reaction C_3H_6 hydrogenation in terms of strong adsorbed surface species.[109] A new intermediate propenyl-vanadium (V−C_3H_5) has been proposed as an alternative key intermediate for CO_2−ODHP by taking the elementary steps of C_3H_6 hydrogenation into consideration, yet still requiring solid evidence. Besides, side reactions are involved in addition to CO_2−ODHP reaction, such as RWGS and reverse Boudouard reaction. Continuous efforts have been put forth to identify the intermediates and plausible reaction paths

https://dx.doi.org/10.1021/acscatal.0c03999
ACS Catal. 2021, 11, 2182−2234

of each reaction by both experimental and computational approaches. However, there is a lack of studies in clarifying the key intermediates and dominating reaction paths by taking the entire reaction network of CO_2−ODHP into consideration. In particular, this requires a sufficient amount of in situ characterization techniques to fill the gap.

(iii) Competitive adsorption between CO_2, C_3H_8, and C_3H_6. There is a competitive adsorption between these molecules, which impacts the C_3H_8 adsorption and C_3H_6 yield. Dopants that enable the balance between C_3H_8 and CO_2 adsorption and inhibition of strong C_3H_6 adsorption are desired.

(iv) Catalyst deactivation and regeneration. For CO_2−ODHP, rapid deactivation occurs as a consequence of reduction of active sites and coke formation. Although catalyst stability and regenerability have been examined, testing of long-term stability is rather scarce, nor have regeneration guidelines been comprehensively covered for different catalyst systems. Therefore, endeavors should be made in developing robust, coke-resistant catalysts that meet the requirement of practical implementation in the mid to long-term.

VO_x and Fe-containing zeolites are reported to be the most superior catalysts for N_2O−ODHP (Figure 32B). Because of the absence of thermodynamic restraints, these Fe-containing zeolite catalysts show activity at a relatively lower temperature of 400 °C. Notwithstanding, potential catalysts that have been tested for N_2O−ODHP are still scarce, and more catalyst screening is needed in future studies. For example, there are only a few works regarding metals other than iron-supported/modified zeolites which have been reported. Also, while there are multiple reports regarding MFI and BEA zeolite topology for N_2O−ODHP, the effects of other zeolite topologies remain unknown.

Similar to CO_2−ODHP, deactivation and regeneration of catalysts in N_2O−ODHP remains a challenge. As discussed in section 3.5.3, CO_2 can serve as an agent for coke removal, thereby enhancing the catalyst stability, while N_2O cannot. Together with the variation in oxidation potential between N_2O and CO_2, these are likely the reasons why similar catalysts show worse stability in N_2O−ODHP. Although a few studies have reported the rapid deactivation of iron-containing zeolite catalysts and vanadia oxide-based catalysts for N_2O−ODHP, deactivation studies regarding molybdenum oxide catalysts have been scarcely touched. Thus, further study of these catalysts is needed to address the challenges of stability of catalysts for N_2O−ODHP route.[180−183,186,187] For iron-containing zeolite catalysts, there have been studies suggesting that the nature and strength of acid sites have significant impacts on the rate of deactivation, implying that catalyst stability can be further improved based on catalyst design.[182,211] Noteworthily, dehydrogenation using N_2O as a soft oxidant has been studied for other alkanes as well, such as ethane, butane, or isobutane, of which isobutane dehydrogenation shows better catalytic performance than propane dehydrogenation using N_2O.[211,289,300−303] Therefore, further study to improve catalyst stability seems to be warranted, as dehydrogenation using N_2O may not only offer additional ways to subvert challenges faced by O_2 oxidant but also may provide a method to utilize N_2O.

The introduction of exogenous mild oxidizers is a potentially selective route for DHP. Catalytic oxyhalogenation is a promising route for single-step C_3H_6 production and yields of up to 55% have been achieved.[49,50] Specifically, oxychlorination chemistry over CeO_2 and metal phosphate-based catalysts show good selectivity (up to 95%) and conversion (up to 70% at 500 °C) in comparison to conventional ODHP (Figure 32C). In contrast, the selective activation of propane in oxybromination chemistry is impractical either because of poor selectivity or insufficient stability of catalysts.[45,251] CeO_2 possesses strong oxidizing characteristics and results in the highest reactivity in oxychlorination reactions. The overoxidation potential of Ce-based catalysts can be improved by heteroatom doping into the CeO_2 structure. The high C_3H_6 yield (i.e., 55%) and selectivity (i.e., 80%) for 8% NiO−CeO_2 are mainly due to a balanced redox ability at 500 °C.[49] On the other hand, metal phosphates such as $CrPO_4$ (yield = 50% at 500 °C) are moderate oxidizers, leading to high selectivity (i.e., ≥95%) but lower activity than CeO_2 under identical conditions.[50] To summarize, an optimal propane oxychlorination catalyst should exhibit moderate redox properties so that it enables alkane activation but does not favor alkane overoxidation, combustion, and evolution of Cl_2, while possessing fast dehydrochlorination kinetics.

The gaseous sulfur compounds, on the other hand, act as effective DHP mediators because of their high affinity for hydrogen abstraction from a hydrocarbon molecule (Figure 32D). C_3H_6 yield rises up to 81% over Al_2O_3 at 750 °C and 93% over Co−Mo/Al_2O_3 at 450 °C, indicating a potential to revolutionize propane dehydrogenation chemistry.[231,232] Interestingly, the highest reported yield for C_3H_6 (either in DHP or ODHP) in various patents are over Al_2O_3 and Co−Mo/Al_2O_3, which are used in industrial Claus or hydrodesulfurization process. However, the exact nature of the active sites is still unclear from the studies to date because of the lack of catalyst characterization and mechanistic studies.[40,222,242−245]

Because of the extremely corrosive nature of sulfur or halogen, operando and in situ techniques are seldom used. The potential scalability of the underlying process and corrosion issues combined with the recovery process of sulfur, halogen, or hydrogen halide products will require suitable materials, reactors, and sophisticated process engineering. Sulfur-mediated dehydrogenation chemistry in particular has shown potential to selectively activate propane by capitalizing on abundant natural gas reserves.[25,26] However, the susceptibility of the material to be attacked by sulfur, halogens, HX, and halogenated products requires testing of materials under actual reaction conditions. To deal with the above-mentioned hurdles, significant endeavors should be devoted to developing a sufficiently active and stable catalyst with an in-depth understanding of the structure−activity relationship, as well as reaction kinetics. This is especially true for various recent industry efforts outlined in a number of patents, where efforts toward developing innovative strategies, such as either using gaseous sulfur or some sulfur compound ($H_2S/S_2/COS$) with O_2 have ensued. However, catalyst characterization, stability tests, structure−activity relationships, and reaction kinetics are nearly nonexistent in the patent literature. The absence of detailed kinetic studies makes it impossible to have information about the reaction network for sulfur-based ODHP. Therefore, this process requires the

https://dx.doi.org/10.1021/acscatal.0c03999
ACS Catal. 2021, 11, 2182−2234

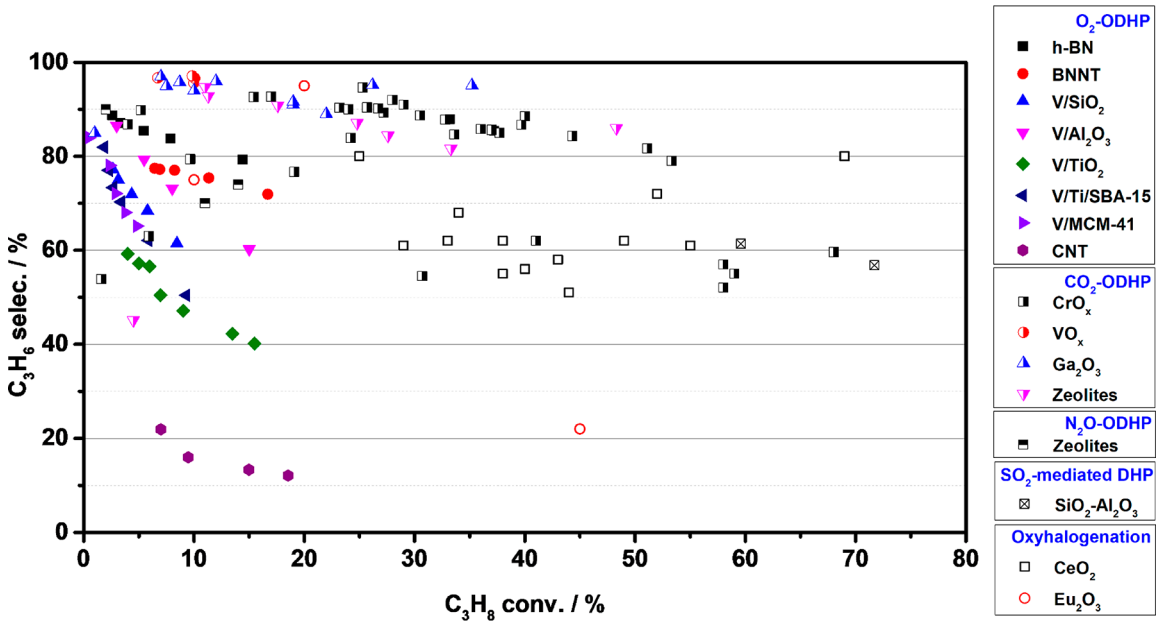

Figure 33. Propylene selectivity plotted against propane conversion for ODHP with different oxidants. Data of O_2−ODHP were adapted from ref 7. h-BN and BNNTs stand for hexagonal boron nitride and boron nitride nanotubes, respectively.

systematic kinetic and operando studies (such as PEPICO) to understand the genesis of sulfur-based byproducts obtained in the process. Furthermore, techno-economic analysis is scarce and should be performed comparing the best catalyst (or processes) with existing technologies, such as DHP and ODHP.

A comparison of catalytic performance is also made between O_2−ODHP and ODHP with soft oxidants in the form of selectivity−conversion correlation over the array of developed catalysts, as presented in Figure 33. In comparison to O_2−ODHP, ODHP with soft oxidants shows comparable C_3H_6 selectivity under the same range of C_3H_8 conversion (i.e., <∼20%). In particular, CO_2−ODHP exhibits higher selectivity among all reaction routes. Moreover, the high selectivity, namely, >∼80%, can be well retained at the C_3H_8 conversion as high as ∼53%. The C_3H_8 conversion of other reaction routes with soft oxidants, such as SO_2-mediated DHP and oxyhalogenation can also reach high values (i.e., 30−70%), yet with lower selectivity (i.e., 50−80%). Noteworthily, this way of comparison is not completely fair, as it overlooks the effects of other critical parameters, such as temperature, feed compositions, GHSV, etc. However, a general trend of activity−selectivity spans of each reaction route has been revealed and provided perspective for further research in the dehydrogenation of propane and other light alkanes.

While there is still significant progress to be made in the development of better ODHP catalysts, theoretical studies in the literature have provided useful insights toward this problem with regards to mechanistic understanding and catalyst design principles. With CO_2 for example, its dissociation, hydrogenation, and poisoning on the surface can all factor prominently toward its catalytic activity. In addition, there are a number of competing reactions that can govern the selectivity to the ODHP product that also should be considered.[304] Modeling these pathways through microkinetics or kinetic Monte Carlo has been shown to be very useful in that regard.[283] On the other hand, descriptors, when available, have also proven to be useful when there is a need to screen across a large number of potential catalysts.[292,298] However, high-throughput screening of catalysts for alkane conversion has remained primarily focused on C−H activation, with far less study on the catalyst reoxidation step.[269] In addition, investigations into the catalyst stability using soft oxidants have yet to feature prominently in modeling efforts, which is relevant for the practical applications. In conclusion, additional theoretical studies in these areas would be highly beneficial to move the field forward and guide experimental efforts, particularly in finding catalysts suitable for corrosive or less-studied oxidants, such as NO_x, SO_x, and halides.

Efforts are also devoted to developing alternative technologies beyond packed catalyst bed, such as chemical looping and membrane reactor. Chemical looping offers opportunities for process intensification and energy loss minimization, which is of significance in future commercialization.[305] Current progress focuses on the feasibility of O_2-assisted dehydrogenation of light alkanes.[306,307] Membrane reactors are emerging as an active research direction in light alkane conversion, such as propane dehydrogenation[308,309] and methane conversion,[310] because it enables the process intensification by integrating oxidant permeability and catalytic activity in one unit.[311] In ODHP, this novel reactor can achieve a uniform distribution of oxidant, thereby resulting in inhibited overoxidation and enhanced C_3H_6 selectivity. Kawi et al. have applied a novel hollow fiber catalytic membrane reactor for O_2−ODHP, in which the membrane reactor was fabricated by integrating $BaBi_{0.05}Ci_{0.8}Nb_{0.15}O_{3-\delta}$ (BBCN) perovskite hollow fiber membrane with silica-supported isolated Co^{2+} catalyst.[311] The fabricated membrane reactor has achieved C_3H_6 yield and selectivity of ∼50% and ∼74%, respectively, at 650 °C with the TOS at 50 h. The key aspect to guarantee a higher C_3H_6 selectivity is to optimize the C_3H_8/O_2 ratio to maintain high C_3H_8 conversion and to avoid overoxidation. Specifically, the C_3H_8 feeding rate should match the oxygen permeation through the membrane. The soft oxidants discussed in this

https://dx.doi.org/10.1021/acscatal.0c03999
ACS Catal. 2021, 11, 2182−2234

review have similar kinetic diameters (i.e., ∼320−360 pm), which are all smaller than the reagent C_3H_8 (i.e., 430 pm) and target product C_3H_6 (i.e., 450 pm), corroborating the feasibility of utilizing membrane reactors for further enhancement in activity and selectivity.

AUTHOR INFORMATION

Corresponding Author

Zili Wu − *Chemical Sciences Division and Center for Nanophase Materials Sciences, Oak Ridge National Laboratory, Oak Ridge, Tennessee 37831, United States;* orcid.org/0000-0002-4468-3240; Email: wuz1@ornl.gov

Authors

Xiao Jiang − *Chemical Sciences Division and Center for Nanophase Materials Sciences, Oak Ridge National Laboratory, Oak Ridge, Tennessee 37831, United States*

Lohit Sharma − *Department of Chemical & Biomolecular Engineering, Lehigh University, Bethlehem, Pennsylvania 18015, United States*

Victor Fung − *Center for Nanophase Materials Sciences, Oak Ridge National Laboratory, Oak Ridge, Tennessee 37831, United States;* orcid.org/0000-0002-3347-6983

Sang Jae Park − *School of Chemical & Biomolecular Engineering, Georgia Institute of Technology, Atlanta, Georgia 30332, United States*

Christopher W. Jones − *School of Chemical & Biomolecular Engineering, Georgia Institute of Technology, Atlanta, Georgia 30332, United States;* orcid.org/0000-0003-3255-5791

Bobby G. Sumpter − *Center for Nanophase Materials Sciences, Oak Ridge National Laboratory, Oak Ridge, Tennessee 37831, United States;* orcid.org/0000-0001-6341-0355

Jonas Baltrusaitis − *Department of Chemical & Biomolecular Engineering, Lehigh University, Bethlehem, Pennsylvania 18015, United States;* orcid.org/0000-0001-5634-955X

Complete contact information is available at: https://pubs.acs.org/10.1021/acscatal.0c03999

Notes

Notice: This manuscript has been authored by UT-Battelle, LLC, under Contract No. DE-AC05-00OR22725 with the U.S. Department of Energy. The United States Government retains and the publisher, by accepting the article for publication, acknowledges that the United States Government retains a non-exclusive, paid-up, irrevocable, world-wide license to publish or reproduce the published form of this manuscript, or allow others to do so, for United States Government purposes. The Department of Energy will provide public access to these results of federally sponsored research in accordance with the DOE Public Access Plan (http://energy.gov/downloads/doe-public-access-plan).
The authors declare no competing financial interest.

ACKNOWLEDGMENTS

This work was supported by the Center for Understanding and Control of Acid Gas-Induced Evolution of Materials for Energy (UNCAGE-ME), an Energy Frontier Research Center funded by U.S. Department of Energy, Office of Science, Basic Energy Sciences.

REFERENCES

(1) Carrero, C. A.; Schloegl, R.; Wachs, I. E.; Schomaecker, R. Critical Literature Review of the Kinetics for the Oxidative Dehydrogenation of Propane over Well-Defined Supported Vanadium Oxide Catalysts. *ACS Catal.* **2014**, *4*, 3357−3380.

(2) Zhao, G. L.; Teng, J. W.; Xie, Z. K.; Yang, W. M.; Chen, Q. L.; Tang, Y. Catalytic Cracking Reactions of C_4-Olefin over Zeolites H-ZSM-5, H-Mordenite and H-SAPO-34. *Stud. Surf. Sci. Catal.* **2007**, *170*, 1307−1312.

(3) Sattler, J. J.; Ruiz-Martinez, J.; Santillan-Jimenez, E.; Weckhuysen, B. M. Catalytic Dehydrogenation of Light Alkanes on Metals and Metal Oxides. *Chem. Rev.* **2014**, *114*, 10613−10653.

(4) Larsson, M.; Hulten, M.; Blekkan, E. A.; Andersson, B. The Effect of Reaction Conditions and Time on Stream on the Coke Formed during Propane Dehydrogenation. *J. Catal.* **1996**, *164*, 44−53.

(5) Atanga, M. A.; Rezaei, F.; Jawad, A.; Fitch, M.; Rownaghi, A. A. Oxidative Dehydrogenation of Propane to Propylene with Carbon Dioxide. *Appl. Catal., B* **2018**, *220*, 429−445.

(6) Cavani, F.; Ballarini, N.; Cericola, A. Oxidative Dehydrogenation of Ethane and Propane: How Far from Commercial Implementation? *Catal. Today* **2007**, *127*, 113−131.

(7) Grant, J. T.; Carrero, C. A.; Goeltl, F.; Venegas, J.; Mueller, P.; Burt, S. P.; Specht, S. E.; McDermott, W. P.; Chieregato, A.; Hermans, I. Selective Oxidation Dehydrogenation of Propane to Propene Using Boron Nitride Catalysts. *Science* **2016**, *354*, 1570−1573.

(8) Lu, W.-D.; Wang, D.; Zhao, Z.; Song, W.; Li, W.-C.; Lu, A.-H. Supported Boron Oxide Catalysts for Selective and Low-Temperature Oxidative Dehydrogenation of Propane. *ACS Catal.* **2019**, *9*, 8263−8270.

(9) Venegas, J. M.; Zhang, Z.; Agbi, T. O.; McDermott, W. P.; Alexandrova, A.; Hermans, I. Why Boron Nitride is such a Selective Catalyst for the Oxidative Dehydrogenation of Propane. *Angew. Chem., Int. Ed.* **2020**, *59*, 16527−16535.

(10) Zhang, X.; You, R.; Wei, Z.; Jiang, X.; Yang, J.; Pan, Y.; Wu, P.; Jia, Q.; Bao, Z.; Bai, L.; Jin, M.; Sumpter, B.; Fung, V.; Huang, W.; Wu, Z. Radical Chemistry and Reaction Mechanisms of Propane Oxidative Dehydrogenation over Hexagonal Boron Nitride Catalysts. *Angew. Chem., Int. Ed.* **2020**, *59*, 8042−8046.

(11) Burri, A.; Hasib, M. A.; Mo, Y.-H.; Reddy, B. M.; Park, S.-E. An Efficient Cr-TUD-1 Catalyst for Oxidative Dehydrogenation of Propane to Propylene with CO_2 as Soft Oxidant. *Catal. Lett.* **2018**, *148*, 576−585.

(12) Gomez, E.; Kattel, S.; Yan, B.; Yao, S.; Liu, P.; Chen, J. G. Combining CO_2 Reduction with Propane Oxidative Dehydrogenation over Bimetallic Catalysts. *Nat. Commun.* **2018**, *9*, 1398.

(13) Bhasin, M. M.; McCain, J. H.; Vora, B. V.; Imai, T.; Pujado, P. R. Dehydrogenation and Oxydehydrogenation of Paraffins to Olefins. *Appl. Catal., A* **2001**, *221*, 397−419.

(14) Ansari, M. B.; Park, S.-E. Carbon Dioxide Utilization as A Soft Oxidant and Promoter in Catalysis. *Energy Environ. Sci.* **2012**, *5*, 9419−9437.

(15) Wang, S.; Zhu, Z. H. Catalytic Conversion of Alkanes to Olefins by Carbon Dioxide Oxidative Dehydrogenation - A Review. *Energy Fuels* **2004**, *18*, 1126−1139.

(16) Krylov, O. V.; Mamedov, A. K.; Mirzabekova, S. R. Catalytic Oxidation of Hydrocarbons and Alcohols by Carbon Dioxide on Oxide Catalysts. *Ind. Eng. Chem. Res.* **1995**, *34*, 474−482.

(17) Arinaga, A. M.; Ziegelski, M. C.; Marks, T. J. Alternative Oxidants for the Catalytic Oxidative Coupling of Methane. *Angew. Chem., Int. Ed.* **2020**, DOI: 10.1002/anie.202012862.

(18) Janas, J.; Gurgul, J.; Socha, R. P.; Kowalska, J.; Nowinska, K.; Shishido, T.; Che, M.; Dzwigaj, S. Influence of the Content and Environment of Chromium in CrSiBEA Zeolites on the Oxidative Dehydrogenation of Propane. *J. Phys. Chem. C* **2009**, *113*, 13273−13281.

(19) Sazama, P.; Sathu, N. K.; Tabor, E.; Wichterlová, B.; Sklenák, Š.; Sobalík, Z. Structure and Critical Function of Fe and Acid Sites in

Fe-ZSM-5 in Propane Oxidative Dehydrogenation with N_2O and N_2O Decomposition. *J. Catal.* **2013**, *299*, 188−203.
(20) Kondratenko, E. V.; Brückner, A. On the Nature and Reactivity of Active Oxygen Species Formed from O_2 and N_2O on VO_x/MCM-41 Used for Oxidative Dehydrogenation of Propane. *J. Catal.* **2010**, *274*, 111−116.
(21) Botavina, M. A.; Agafonov, Y. A.; Gaidai, N. A.; Groppo, E.; Cortés Corberán, V.; Lapidus, A. L.; Martra, G. Towards Efficient Catalysts for the Oxidative Dehydrogenation of Propane in the Presence of CO_2: Cr/SiO_2 Systems Prepared by Direct Hydrothermal Synthesis. *Catal. Sci. Technol.* **2016**, *6*, 840−850.
(22) Michorczyk, P.; Zeńczak-Tomera, K.; Michorczyk, B.; Węgrzyniak, A.; Basta, M.; Millot, Y.; Valentin, L.; Dzwigaj, S. Effect of Dealumination on the Catalytic Performance of Cr-Containing Beta Zeolite in Carbon Dioxide Assisted Propane Dehydrogenation. *J. CO2 Util.* **2020**, *36*, 54−63.
(23) Michorczyk, P.; Ogonowski, J. Dehydrogenation of Propane to Propene over Gallium Oxide in the Presence of CO_2. *Appl. Catal., A* **2003**, *251*, 425−433.
(24) Agafonov, Y. A.; Gaidai, N. A.; Lapidus, A. L. Propane Dehydrogenation on Chromium Oxide and Gallium Oxide Catalysts in the Presence of CO_2. *Kinet. Catal.* **2018**, *59*, 744−753.
(25) Pirzadeh, P.; Lesage, K. L.; Marriott, R. A. Hydraulic Fracturing Additives and the Delayed Onset of Hydrogen Sulfide in Shale Gas. *Energy Fuels* **2014**, *28*, 4993−5001.
(26) Marriott, R. A.; Pirzadeh, P.; Marrugo-Hernandez, J. J.; Raval, S. Hydrogen Sulfide Formation in Oil and Gas. *Can. J. Chem.* **2016**, *94*, 406−413.
(27) Zhu, M.; Li, B.; Jehng, J.-M.; Sharma, L.; Taborda, J.; Zhang, L.; Stach, E.; Wachs, I. E.; Wu, Z.; Baltrusaitis, J. Molecular Structure and Sour Gas Surface Chemistry of Supported $K_2O/WO_3/Al_2O_3$ Catalysts. *Appl. Catal., B* **2018**, *232*, 146−154.
(28) Ascoop, I.; Galvita, V. V.; Alexopoulos, K.; Reyniers, M.-F.; Van Der Voort, P.; Bliznuk, V.; Marin, G. B. The Role of CO_2 in the Dehydrogenation of Propane over WO_x-VO_x/SiO_2. *J. Catal.* **2016**, *335*, 1−10.
(29) Wang, H.; Tsilomelekis, G. Catalytic Performance and Stability of Fe-Doped CeO_2 in Propane Oxidative Dehydrogenation Using Carbon Dioxide as An Oxidant. *Catal. Sci. Technol.* **2020**, *10*, 4362−4372.
(30) Sandupatla, A. S.; Ray, K.; Thaosen, P.; Sivananda, C.; Deo, G. Oxidative Dehydrogenation of Propane over Alumina Supported Vanadia Catalyst - Effect of Carbon Dioxide and Secondary Surface Metal Oxide Additive. *Catal. Today* **2020**, *354*, 176−182.
(31) Du, X.; Yao, B.; Gonzalez-Cortes, S.; Kuznetsov, V. L.; AlMegren, H.; Xiao, T.; Edwards, P. P. Catalytic Dehydrogenation of Propane by Carbon Dioxide: A Medium-Temperature Thermochemical Process for Carbon Dioxide Utilisation. *Faraday Discuss.* **2015**, *183*, 161−76.
(32) Engelen, C. W. R.; Wolthuizen, J. P.; van Hooff, J. H. C. Reactions of Propane over A Bifunctional Pt/H-ZSM-5 Catalyst. *Appl. Catal.* **1985**, *19*, 153−163.
(33) Zhang, S.; Zhou, Y.; Zhang, Y.; Huang, L. Effect of K Addition on Catalytic Performance of PtSn/ZSM-5 Catalyst for Propane Dehydrogenation. *Catal. Lett.* **2010**, *135*, 76−82.
(34) Zangeneh, F. T.; Taeb, A.; Gholivand, K.; Sahebdelfar, S. Thermodynamic Equilibrium Analysis of Propane Dehydrogenation with Carbon Dioxide and Side Reactions. *Chem. Eng. Commun.* **2016**, *203*, 557−565.
(35) Wu, G.; Hao, Y.; Zhang, N.; Guan, N.; Li, L.; Grünert, W. Oxidative Dehydrogenation of Propane with Nitrous Oxide over Fe-O-Al Species Occluded in ZSM-5: Reaction and Deactivation Mechanisms. *Microporous Mesoporous Mater.* **2014**, *198*, 82−91.
(36) Wu, G.; Hei, F.; Zhang, N.; Guan, N.; Li, L.; Grünert, W. Oxidative Dehydrogenation of Propane with Nitrous Oxide over Fe-ZSM-5 Prepared by Grafting: Characterization and Performance. *Appl. Catal., A* **2013**, *468*, 230−239.
(37) Ashmawy, F. M. Catalytic Oxidative Dehydrogenation of Propane to Propylene. *J. Catal.* **1977**, *46*, 424−425.
(38) Ashmawy, F. M. Kinetic Investigations of the Reaction of Propane with Sulphur Dioxide on a Palladium-Alumina Catalyst. *J. Chem. Technol. Biotechnol., Chem. Technol.* **1984**, *34A*, 183−186.
(39) Gaspar, N. J.; Pasternak, I. S.; Vadekar, M. H_2S Promoted Oxidative Dehydrogenation of Hydrocarbons in Molten Media. *Can. J. Chem. Eng.* **1974**, *52*, 793−797.
(40) Clark, P. D.; Dowling, N. I.; Long, X.; Li, Y. Oxidative Dehydrogenation of Propane to Propene in the Presence of H_2S at Short Contact Times. *J. Sulfur Chem.* **2004**, *25*, 381−387.
(41) Shah, M. S.; Tsapatsis, M.; Siepmann, J. I. Hydrogen Sulfide Capture: From Absorption in Polar Liquids to Oxide, Zeolite, and Metal-Organic Framework Adsorbents and Membranes. *Chem. Rev.* **2017**, *117*, 9755−9803.
(42) Vadekar, M.; Pasternak, I. S. Sulfur-Promoted Oxidative Dehydrogenation Process. US 3403192, 1968.
(43) Pasternak, I. S.; Vadekar, M. Sulphur/Halogen Promoted Oxidative Dehydrogenation of Hydrocarbons. *Can. J. Chem. Eng.* **1970**, *48*, 212−215.
(44) Premji, Z. A.; Lo, J. M.; Clark, P. D. Experimental and Ab Initio Investigations of H_2S-Assisted Propane Oxidative Dehydrogenation Reactions. *J. Phys. Chem. A* **2014**, *118*, 1541−1556.
(45) Zichittella, G.; Puértolas, B.; Paunović, V.; Block, T.; Pöttgen, R.; Pérez-Ramírez, J. Halogen Type as A Selectivity Switch in Catalysed Alkane Oxyhalogenation. *Catal. Sci. Technol.* **2018**, *8*, 2231−2243.
(46) Lin, R.; Amrute, A. P.; Perez-Ramirez, J. Halogen-Mediated Conversion of Hydrocarbons to Commodities. *Chem. Rev.* **2017**, *117*, 4182−4247.
(47) Ding, K.; Metiu, H.; Stucky, G. D. Interplay Between Bromine and Iodine in Oxidative Dehydrogenation. *ChemCatChem* **2013**, *5*, 1906−1910.
(48) Zichittella, G.; Lüthi, J.; Paunović, V.; Pérez-Ramírez, J. Alkane Functionalization via Catalytic Oxychlorination: Performance as A Function of the Carbon Number. *Energy Technol.* **2020**, *8*, 1900622.
(49) Xie, Q.; Zhang, H.; Kang, J.; Cheng, J.; Zhang, Q.; Wang, Y. Oxidative Dehydrogenation of Propane to Propylene in the Presence of HCl Catalyzed by CeO_2 and NiO-Modified CeO_2 Nanocrystals. *ACS Catal.* **2018**, *8*, 4902−4916.
(50) Zichittella, G.; Stähelin, S.; Goedicke, F. M.; Pérez-Ramírez, J. Selective Propylene Production via Propane Oxychlorination on Metal Phosphate Catalysts. *ACS Catal.* **2019**, *9*, 5772−5782.
(51) Ge, X.; Zou, H.; Wang, J.; Shen, J. Modification of Cr/SiO_2 for the Dehydrogenation of Propane to Propylene in Carbon Dioxide. *React. Kinet. Catal. Lett.* **2005**, *85*, 253−260.
(52) Michorczyk, P.; Ogonowski, J. Dehydrogenation of Propane in the Presence of Carbon Dioxide over Oxide-Based Catalysts. *React. Kinet. Catal. Lett.* **2003**, *78*, 41−47.
(53) Chen, M.; Xu, J.; Su, F.; Liu, Y.; Cao, Y.; He, H.; Fan, K. Dehydrogenation of Propane over Spinel-Type Gallia-Alumina Solid Solution Catalysts. *J. Catal.* **2008**, *256*, 293−300.
(54) Michorczyk, P.; Ogonowski, J.; Zeńczak, K. Activity of Chromium Oxide Deposited on Different Silica Supports in the Dehydrogenation of Propane with CO_2 - A Comparative Study. *J. Mol. Catal. A: Chem.* **2011**, *349*, 1−12.
(55) Botavina, M. A.; Martra, G.; Agafonov, Y. A.; Gaidai, N. A.; Nekrasov, N. V.; Trushin, D. V.; Coluccia, S.; Lapidus, A. L. Oxidative Dehydrogenation of C_3-C_4 Paraffins in the Presence of CO_2 over CrO_x/SiO_2 Catalysts. *Appl. Catal., A* **2008**, *347*, 126−132.
(56) Yun, D.; Baek, J.; Choi, Y.; Kim, W.; Lee, H. J.; Yi, J. Promotional Effect of Ni on a CrO_x Catalyst Supported on Silica in the Oxidative Dehydrogenation of Propane with CO_2. *ChemCatChem* **2012**, *4*, 1952−1959.
(57) Michorczyk, P.; Ogonowski, J. Role of CO_2 in Dehydrogenation of Propane over CrO_x/SiO_2 Catalyst with Low Cr Content. *React. Kinet. Catal. Lett.* **2007**, *92*, 61−68.
(58) Wang, Y.; Ohishi, Y.; Shishido, T.; Zhang, Q.; Yang, W.; Guo, Q.; Wan, H.; Takehira, K. Characterizations and Catalytic Properties of Cr-MCM-41 Prepared by Direct Hydrothermal Synthesis and Template-Ion Exchange. *J. Catal.* **2003**, *220*, 347−357.

(59) Michorczyk, P.; Pietrzyk, P.; Ogonowski, J. Preparation and Characterization of SBA-1-Supported Chromium Oxide Catalysts for CO_2 Assisted Dehydrogenation of Propane. *Microporous Mesoporous Mater.* **2012**, *161*, 56−66.
(60) Zhang, X.; Yue, Y.; Gao, Z. Chromium Oxide Supported on Mesoporous SBA-15 as Propane Dehydrogenation and Oxidative Dehydrogenation Catalysts. *Catal. Lett.* **2002**, *83*, 19−25.
(61) de Oliveira, J. F. S.; Volanti, D. P.; Bueno, J. M. C.; Ferreira, A. P. Effect of CO_2 in the Oxidative Dehydrogenation Reaction of Propane over Cr/ZrO_2 Catalysts. *Appl. Catal., A* **2018**, *558*, 55−66.
(62) Kocoń, M.; Michorczyk, P.; Ogonowski, J. Effect of Supports on Catalytic Activity of Chromium Oxide-Based Catalysts in the Dehydrogenation of Propane with CO_2. *Catal. Lett.* **2005**, *101*, 53−57.
(63) Michorczyk, P.; Góra-Marek, K.; Ogonowski, J. Dehydrogenation of Propane in the Presence and Absence of CO_2 Over β-Ga_2O_3 Supported Chromium Oxide Catalysts. *Catal. Lett.* **2006**, *109*, 195−198.
(64) Michorczyk, P.; Ogonowski, J.; Kuśtrowski, P.; Chmielarz, L. Chromium Oxide Supported on MCM-41 as A Highly Active and Selective Catalyst for Dehydrogenation of Propane with CO_2. *Appl. Catal., A* **2008**, *349*, 62−69.
(65) Liu, L.; Li, H.; Zhang, Y. Mesoporous Silica-Supported Chromium Catalyst: Characterization and Excellent Performance in Dehydrogenation of Propane to Propylene with Carbon Dioxide. *Catal. Commun.* **2007**, *8*, 565−570.
(66) Michorczyk, P.; Ogonowski, J.; Niemczyk, M. Investigation of Catalytic Activity of CrSBA-1 Materials Obtained by Direct Method in the Dehydrogenation of Propane with CO_2. *Appl. Catal., A* **2010**, *374*, 142−149.
(67) Kuśtrowski, P.; Michorczyk, P.; Chmielarz, L.; Piwowarska, Z.; Dudek, B.; Ogonowski, J.; Dziembaj, R. TG Study on Real Role of Active Carbon Support in Propane Dehydrogenation with CO_2. *Thermochim. Acta* **2008**, *471*, 26−32.
(68) Jin, R.; Easa, J.; Tran, D. T.; O'Brien, C. P. Ru-Promoted CO_2 Activation for Oxidative Dehydrogenation of Propane over Chromium Oxide Catalyst. *Catal. Sci. Technol.* **2020**, *10*, 1769−1777.
(69) Baek, J.; Yun, H. J.; Yun, D.; Choi, Y.; Yi, J. Preparation of Highly Dispersed Chromium Oxide Catalysts Supported on Mesoporous Silica for the Oxidative Dehydrogenation of Propane Using CO_2: Insight into the Nature of Catalytically Active Chromium Sites. *ACS Catal.* **2012**, *2*, 1893−1903.
(70) Botavina, M. A.; Evangelisti, C.; Agafonov, Y. A.; Gaidai, N. A.; Panziera, N.; Lapidus, A. L.; Martra, G. CrO_x/SiO_2 Catalysts Prepared by Metal Vapour Synthesis: Physical-Chemical Characterisation and Functional Testing in Oxidative Dehydrogenation of Propane. *Chem. Eng. J.* **2011**, *166*, 1132−1138.
(71) Wang, H.-M.; Chen, Y.; Yan, X.; Lang, W.-Z.; Guo, Y.-J. Cr Doped Mesoporous Silica Spheres for Propane Dehydrogenation in the Presence of CO_2: Effect of Cr Adding Time in Sol-Gel Process. *Microporous Mesoporous Mater.* **2019**, *284*, 69−77.
(72) Wu, R.; Xie, P.; Cheng, Y.; Yue, Y.; Gu, S.; Yang, W.; Miao, C.; Hua, W.; Gao, Z. Hydrothermally Prepared Cr_2O_3-ZrO_2 as A Novel Efficient Catalyst for Dehydrogenation of Propane with CO_2. *Catal. Commun.* **2013**, *39*, 20−23.
(73) Xie, Z.; Ren, Y.; Li, J.; Zhao, Z.; Fan, X.; Liu, B.; Song, W.; Kong, L.; Xiao, X.; Liu, J.; Jiang, G. Facile In Situ Synthesis of Highly Dispersed Chromium Oxide Incorporated into Mesoporous ZrO_2 for the Dehydrogenation of Propane with CO_2. *J. Catal.* **2019**, *372*, 206−216.
(74) Takahara, I.; Chang, W.-C.; Mimura, N.; Saito, M. Promoting Effects of CO_2 on Dehydrogenation of Propane over a SiO_2-Supported Cr_2O_3 Catalyst. *Stud. Surf. Sci. Catal.* **1998**, *114*, 419−422.
(75) Takahara, I.; Chang, W.-C.; Mimura, N.; Saito, M. Promoting Effects of CO_2 on Dehydrogenation of Propane over a SiO_2-Supported Cr_2O_3 Catalyst. *Catal. Today* **1998**, *45*, 55−59.
(76) Cavani, F.; Koutyrev, M.; Trifirò, F.; Bartolini, A.; Ghisletti, D.; Iezzi, R.; Santucci, A.; Del Piero, G. Chemical and Physical Characterization of Alumina-Supported Chromia-based Catalysts and Their Activity in Dehydrogenation of Isobutane. *J. Catal.* **1996**, *158*, 236−250.
(77) Argyle, M. D.; Chen, K.; Bell, A. T.; Iglesia, E. Effect of Catalyst Structure on Oxidative Dehydrogenation of Ethane and Propane on Alumina-Supported Vanadia. *J. Catal.* **2002**, *208*, 139−149.
(78) Wachs, I. E. Raman and IR Studies of Surface Metal Oxide Species on Oxide Support: Supported Metal Oxide Catalysts. *Catal. Today* **1996**, *27*, 437−455.
(79) Mitra, B.; Wachs, I. E.; Deo, G. Promotion of the Propane ODH Reaction over Supported V_2O_5/Al_2O_3 Catalyst with Secondary Surface Metal Oxide Additives. *J. Catal.* **2006**, *240*, 151−159.
(80) Takehira, K.; Ohishi, Y.; Shishido, T.; Kawabata, T.; Takaki, K.; Zhang, Q.; Wang, Y. Behavior of Active Sites on Cr-MCM-41 Catalysts during the Dehydrogenation of Propane with CO_2. *J. Catal.* **2004**, *224*, 404−416.
(81) Takehira, K.; Oishi, Y.; Shishido, T.; Kawabata, T.; Takaki, K.; Zhang, Q.; Wang, Y. CO_2 Dehydrogenation of Propane over Cr-MCM-41 Catalyst. *Stud. Surf. Sci. Catal.* **2004**, *153*, 323−328.
(82) Shishido, T.; Shimamura, K.; Teramura, K.; Tanaka, T. Role of CO_2 in Dehydrogenation of Propane over Cr-Based Catalysts. *Catal. Today* **2012**, *185*, 151−156.
(83) Michorczyk, P.; Ogonowski, J. Simultaneous Propane Dehydrogenation and CO_2 Hydrogenation over CrO_x/SiO_2 Catalyst. *React. Kinet. Catal. Lett.* **2005**, *87*, 177−183.
(84) Zhang, Q.; Wang, Y.; Ohishi, Y.; Shishido, T.; Takehira, K. Vanadium-Containing MCM-41 for Partial Oxidation of Lower Alkanes. *J. Catal.* **2001**, *202*, 308−318.
(85) Wang, Y.; Zhang, Q.; Shishido, T.; Takehira, K. Characterizations of Iron-Containing MCM-41 and Its Catalytic Properties in Epoxidation of Styrene with Hydrogen Peroxide. *J. Catal.* **2002**, *209*, 186−196.
(86) Zhang, Q.; Wang, Y.; Itsuki, S.; Shishido, T.; Takehira, K. Manganese-Containing MCM-41 for Epoxidation of Styrene and Stilbene. *J. Mol. Catal. A: Chem.* **2002**, *188*, 189−200.
(87) Ohishi, Y.; Kawabata, T.; Shishido, T.; Takaki, K.; Zhang, Q.; Wang, Y.; Takehira, K. Dehydrogenation of Ethylbenzene with CO_2 over Cr-MCM-41 Catalyst. *J. Mol. Catal. A: Chem.* **2005**, *230*, 49−58.
(88) Kim, S.-S.; Pauly, T. R.; Pinnavaia, T. J. Non-Ionic Surfactant Assembly of Wormhole Silica Molecular Sieves from Water Soluble Silicates. *Chem. Commun.* **2000**, 835−836.
(89) Srinivasu, P.; Vinu, A. Three-Dimensional Mesoporous Gallosilicate with *Pm3n* Symmetry and Its Unusual Catalytic Performances. *Chem. - Eur. J.* **2008**, *14*, 3553−61.
(90) Vinu, A.; Murugesan, V.; Hartmann, M. Pore Size Engineering and Mechanical Stability of the Cubic Mesoporous Molecular Sieve SBA-1. *Chem. Mater.* **2003**, *15*, 1385−1393.
(91) Ge, X.; Zhu, M.; Shen, J. Catalytic Performance of Silica-Supported Chromium Oxide Catalysts in Ethane Dehydrogenation with Carbon Dioxide. *React. Kinet. Catal. Lett.* **2002**, *77*, 103−108.
(92) Bansode, A.; Tidona, B.; von Rohr, P. R.; Urakawa, A. Impact of K and Ba Promoters on CO_2 Hydrogenation over Cu/Al_2O_3 Catalysts at High Pressure. *Catal. Sci. Technol.* **2013**, *3*, 767−778.
(93) Lapidus, A. L.; Agafonov, Y. A.; Gaidai, N. A.; Trushin, D. V.; Nekrasov, N. V. Effect of the Introduction of Alkaline Promoters into Chromium Oxide Catalysts for Propane Dehydrogenation in the Presence of CO_2. *Solid Fuel Chem.* **2012**, *46*, 14−22.
(94) Aitbekova, A.; Goodman, E. D.; Wu, L.; Boubnov, A.; Hoffman, A. S.; Genc, A.; Cheng, H.; Casalena, L.; Bare, S. R.; Cargnello, M. Engineering of Ruthenium-Iron Oxide Colloidal Heterostructures: Improved Yields in CO_2 Hydrogenation to Hydrocarbons. *Angew. Chem., Int. Ed.* **2019**, *58*, 17451−17457.
(95) Kim, C.; Hyeon, S.; Lee, J.; Kim, W. D.; Lee, D. C.; Kim, J.; Lee, H. Energy-Efficient CO_2 Hydrogenation with Fast Response Using Photoexcitation of CO_2 Adsorbed on Metal Catalysts. *Nat. Commun.* **2018**, *9*, 3027.

(96) Castro Luna, A. E.; Iriarte, M. E. Carbon Dioxide Reforming of Methane over A Metal Modified Ni-Al_2O_3 Catalyst. *Appl. Catal., A* **2008**, *343*, 10−15.
(97) He, S.; Jing, Q.; Yu, W.; Mo, L.; Lou, H.; Zheng, X. Combination of CO_2 Reforming and Partial Oxidation of Methane to Produce Syngas over Ni/SiO_2 Prepared with Nickel Citrate Precursor. *Catal. Today* **2009**, *148*, 130−133.
(98) Ranjbar, A.; Irankhah, A.; Aghamiri, S. F. Reverse Water Gas Shift Reaction and CO_2 Mitigation: Nanocrystalline MgO as A Support for Nickel based Catalysts. *J. Environ. Chem. Eng.* **2018**, *6*, 4945−4952.
(99) Wu, H. C.; Chang, Y. C.; Wu, J. H.; Lin, J. H.; Lin, I. K.; Chen, C. S. Methanation of CO_2 and Reverse Water Gas Shift Reactions on Ni/SiO_2 Catalysts: The Influence of Particle Size on Selectivity and Reaction Pathway. *Catal. Sci. Technol.* **2015**, *5*, 4154−4163.
(100) Roiaz, M.; Monachino, E.; Dri, C.; Greiner, M.; Knop-Gericke, A.; Schlogl, R.; Comelli, G.; Vesselli, E. Reverse Water-Gas Shift or Sabatier Methanation on Ni(110)? Stable Surface Species at Near-Ambient Pressure. *J. Am. Chem. Soc.* **2016**, *138*, 4146−4154.
(101) Yuan, Q.; Liu, Q.; Song, W.-G.; Feng, W.; Pu, W.-L.; Sun, L.-D.; Zhang, Y.-W.; Yan, C.-H. Ordered Mesoporous $Ce_{1-x}Zr_xO_2$ Solid Solutions with Crystalline Walls. *J. Am. Chem. Soc.* **2007**, *129*, 6698−6699.
(102) Lamanna, W. M. Metal Vapor Synthesis of a Novel Triple-Decker Sandwich Complex: $(\eta^6$-Mesitylene$)_2(\mu$-η^6:η^6-Mesitylene)-Cr_2. *J. Am. Chem. Soc.* **1986**, *108*, 2096−2097.
(103) Aronica, L. A.; Schiavi, E.; Evangelisti, C.; Caporusso, A. M.; Salvadori, P.; Vitulli, G.; Bertinetti, L.; Martra, G. Solvated Gold Atoms in the Preparation of Efficient Supported Catalysts: Correlation between Morphological Features and Catalytic Activity in the Hydrosilylation of 1-Hexyne. *J. Catal.* **2009**, *266*, 250−257.
(104) Vitulli, G.; Evangelisti, C.; Pertici, P.; Caporusso, A. M.; Panziera, N.; Salvadori, P.; Faga, M. G.; Manfredotti, C.; Martra, G.; Coluccia, S.; Balerna, A.; Colonna, S.; Mobilio, S. Supported Rhodium Nanoparticles in Catalysis: The Role of Stabilizers on Catalytic Activity and Structural Features. *J. Organomet. Chem.* **2003**, *681*, 37−50.
(105) Evangelisti, C.; Panziera, N.; Pertici, P.; Vitulli, G.; Salvadori, P.; Battocchio, C.; Polzonetti, G. Palladium Nanoparticles Supported on Polyvinylpyridine: Catalytic Activity in Heck-Type Reactions and XPS Structural Studies. *J. Catal.* **2009**, *262*, 287−293.
(106) Tian, B.; Liu, X.; Tu, B.; Yu, C.; Fan, J.; Wang, L.; Xie, S.; Stucky, G. D.; Zhao, D. Self-Adjusted Synthesis of Ordered Stable Mesoporous Minerals by Acid-base Pairs. *Nat. Mater.* **2003**, *2*, 159−63.
(107) Zhaorigetu, B.; Kieffer, R.; Hindermann, J.-P. Oxidative Dehydrogenation of Propane on Rare Earth Vanadates Influence of the Presence of CO_2 in the Feed. *Stud. Surf. Sci. Catal.* **1996**, *101*, 1049−1058.
(108) Zhaorigetu, B.; Kieffer, R.; Li, W. Investigations on the Promoting Effect of Metal Oxides on La-V-O Catalyst in Propane Oxidative Dehydrogenation. *Catal. Lett.* **2001**, *73*, 133−136.
(109) Liu, G.; Zhao, Z.-J.; Wu, T.; Zeng, L.; Gong, J. Nature of the Active Sites of VO_x/Al_2O_3 Catalysts for Propane Dehydrogenation. *ACS Catal.* **2016**, *6*, 5207−5214.
(110) Rossetti, I.; Fabbrini, L.; Ballarini, N.; Oliva, C.; Cavani, F.; Cericola, A.; Bonelli, B.; Piumetti, M.; Garrone, E.; Dyrbeck, H. V_2O_5-SiO_2 Systems Prepared by Flame Pyrolysis as Catalysts for the Oxidative Dehydrogenation of Propane. *J. Catal.* **2008**, *256*, 45−61.
(111) Alexopoulos, K.; Reyniers, M.-F.; Marin, G. B. Reaction Path Analysis of Propane Selective Oxidation over V_2O_5 and V_2O_5/TiO_2. *J. Catal.* **2012**, *289*, 127−139.
(112) Nakagawa, K.; Kajita, C.; Ikenaga, N.-o.; Nishitani-Gamo, M.; Ando, T.; Suzuki, T. Dehydrogenation of Light Alkanes over Oxidized Diamond-Supported Catalysts in the Presence of Carbon Dioxide. *Catal. Today* **2003**, *84*, 149−157.
(113) Liu, Y.-M.; Cao, Y.; Yi, N.; Feng, W.-L.; Dai, W.-L.; Yan, S.-R.; He, H.-Y.; Fan, K.-N. Vanadium Oxide Supported on Mesoporous SBA-15 as Highly Selective Catalysts in the Oxidative Dehydrogenation of Propane. *J. Catal.* **2004**, *224*, 417−428.
(114) Xue, X. L.; Lang, W. Z.; Yan, X.; Guo, Y. J. Dispersed Vanadium in Three-Dimensional Dendritic Mesoporous Silica Nanospheres: Active and Stable Catalysts for the Oxidative Dehydrogenation of Propane in the Presence of CO_2. *ACS Appl. Mater. Interfaces* **2017**, *9*, 15408−15423.
(115) Ando, T.; Yamamoto, K.; Ishii, M.; Kamo, M.; Sato, Y. Vapour-Phase Oxidation of Diamond Surfaces in O_2 Studied by Diffuse Reflectance Fourier-Transform Infrared and Temperture-Programmed Desorption Spectroscopy. *J. Chem. Soc., Faraday Trans.* **1993**, *89*, 3635−3640.
(116) Raymakers, J.; Haenen, K.; Maes, W. Diamond Surface Functionalization: from Gemstone to Photoelectrochemical Applications. *J. Mater. Chem. C* **2019**, *7*, 10134−10165.
(117) Grant, J. T.; Carrero, C. A.; Love, A. M.; Verel, R.; Hermans, I. Enhanced Two-Dimensional Dispersion of Group V Metal Oxides on Silica. *ACS Catal.* **2015**, *5*, 5787−5793.
(118) Kompio, P. G. W. A.; Brückner, A.; Hipler, F.; Auer, G.; Löffler, E.; Grünert, W. A New View on the Relations between Tungsten and Vanadium in V_2O_5-WO_3/TiO_2 Catalysts for the Selective Reduction of NO with NH_3. *J. Catal.* **2012**, *286*, 237−247.
(119) Vuurman, M. A.; Wachs, I. E.; et al. Structural Determination of Supported V_2O_5-WO_3/TiO_2 Catalysts by In Situ Raman Spectroscopy and X-Ray Photoelectron Spectroscopy. *J. Phys. Chem.* **1991**, *95*, 9928−9937.
(120) Kang, J.; Czaja, A. D.; Guliants, V. V. Carbon Dioxide as Feedstock in Selective Oxidation of Propane. *Eur. J. Inorg. Chem.* **2017**, *2017*, 4757−4762.
(121) Zheng, B.; Hua, W.; Yue, Y.; Gao, Z. Dehydrogenation of Propane to Propene over Different Polymorphs of Gallium Oxide. *J. Catal.* **2005**, *232*, 143−151.
(122) Haneda, M.; Kintaichi, Y.; Hamada, H. Activity Enhancement of SnO_2-Doped Ga_2O_3-Al_2O_3 Catalysts by Coexisting H_2O for the Selective Reduction of NO with Propene. *Appl. Catal., B* **1999**, *20*, 289−300.
(123) Haneda, M.; Kintaichi, Y.; Hamada, H. Effect of SO_2 on the Catalytic Activity of Ga_2O_3-Al_2O_3 for the Selective Reduction of NO with Propene in the Presence of Oxygen. *Appl. Catal., B* **2001**, *31*, 251−261.
(124) Takahashi, M.; Nakatani, T.; Iwamoto, S.; Watanabe, T.; Inoue, M. Performance of Solvothermally Prepared Ga_2O_3-Al_2O_3 Catalysts for SCR of NO with Methane. *Appl. Catal., B* **2007**, *70*, 73−79.
(125) Chen, M.; Xu, J.; Liu, Y.-M.; Cao, Y.; He, H.-Y.; Zhuang, J.-H.; Fan, K.-N. Enhanced Activity of Spinel-type Ga_2O_3-Al_2O_3 Mixed Oxide for the Dehydrogenation of Propane in the Presence of CO_2. *Catal. Lett.* **2008**, *124*, 369−375.
(126) Li, H.; Yue, Y.; Miao, C.; Xie, Z.; Hua, W.; Gao, Z. Dehydrogenation of Ethylbenzene and Propane over GaO_3-ZrO_2 Catalysts in the Presence of CO_2. *Catal. Commun.* **2007**, *8*, 1317−1322.
(127) Xu, B.; Zheng, B.; Hua, W.; Yue, Y.; Gao, Z. Support Effect in Dehydrogenation of Propane in the Presence of CO_2 over Supported Gallium Oxide Catalysts. *J. Catal.* **2006**, *239*, 470−477.
(128) Leveles, L.; Seshan, K.; Lercher, J. A.; Lefferts, L. Oxidative Conversion of Propane over Lithium-Promoted Magnesia Catalyst I. Kinetics and Mechanism. *J. Catal.* **2003**, *218*, 296−306.
(129) Meriaudeau, P.; Naccache, C. The Role of Ga_2O_3 and Proton Acidity on the Dehydrogenation Activity of Ga_2O_3-HZSM-5 Catalysts: Evidence of a Bifunctional Mechanism. *J. Mol. Catal.* **1990**, *59*, L31−L36.
(130) Nowak, I.; Quartararo, J.; Derouane, E. G.; Vedrine, J. C. Effect of H_2-O_2 Pre-Treatments on the State of Gallium in Ga/H-ZSM-5 Propane Aromatisation Catalysts. *Appl. Catal., A* **2003**, *251*, 107−120.
(131) West, C.; Mokaya, R. Nanocasting of High Surface Area Mesoporous Ga_2O_3 and GaN Semiconductor Materials. *Chem. Mater.* **2009**, *21*, 4080−4086.

(132) Zhao, W.; Yang, Y.; Hao, R.; Liu, F.; Wang, Y.; Tan, M.; Tang, J.; Ren, D.; Zhao, D. Synthesis of Mesoporous β-Ga_2O_3 Nanorods Using PEG as Template: Preparation, Characterization and Photocatalytic Properties. *J. Hazard. Mater.* **2011**, *192*, 1548−1554.
(133) Wu, J.-L.; Chen, M.; Liu, Y.-M.; Cao, Y.; He, H.-Y.; Fan, K.-N. Sucrose-Templated Mesoporous β-Ga_2O_3 as A Novel Efficient Catalyst for Dehydrogenation of Propane in the Presence of CO_2. *Catal. Commun.* **2013**, *30*, 61−65.
(134) Yada, M.; Ohya, M.; Machida, M.; Kijima, T. Mesoporous Gallium Oxide Structurally Stabilized by Yttrium Oixde. *Langmuir* **2000**, *16*, 4752−4755.
(135) Deshmane, C. A.; Jasinski, J. B.; Carreon, M. A. Thermally Stable Nanocrystalline Mesoporous Gallium Oxide Phases. *Eur. J. Inorg. Chem.* **2009**, *2009*, 3275−3281.
(136) Michorczyk, P.; Kuśtrowski, P.; Kolak, A.; Zimowska, M. Ordered Mesoporous Ga_2O_3 and Ga_2O_3-Al_2O_3 Prepared by Nanocasting as Effective Catalysts for Propane Dehydrogenation in the Presence of CO_2. *Catal. Commun.* **2013**, *35*, 95−100.
(137) Xiao, H.; Zhang, J.; Wang, P.; Wang, X.; Pang, F.; Zhang, Z.; Tan, Y. Dehydrogenation of Propane over a Hydrothermal-Synthesized Ga_2O_3-Al_2O_3 Catalyst in the Presence of Carbon Dioxide. *Catal. Sci. Technol.* **2016**, *6*, 5183−5195.
(138) Beale, A. M.; Gao, F.; Lezcano-Gonzalez, I.; Peden, C. H.; Szanyi, J. Recent Advances in Automotive Catalysis for NO_x Emission Control by Small-Pore Microporous Materials. *Chem. Soc. Rev.* **2015**, *44*, 7371−7405.
(139) Shi, J.; Wang, Y.; Yang, W.; Tang, Y.; Xie, Z. Recent Advances of Pore System Construction in Zeolite-Catalyzed Chemical Industry Processes. *Chem. Soc. Rev.* **2015**, *44*, 8877−8903.
(140) Dusselier, M.; Davis, M. E. Small-Pore Zeolites: Synthesis and Catalysis. *Chem. Rev.* **2018**, *118*, 5265−5329.
(141) Xu, B. J.; Zheng, B.; Hua, W. M.; Yue, Y. H.; Gao, Z. High Si/Al Ratio HZSM-5 Supported Ga_2O_3: A Highly Stable Catalyst for Dehydrogenation of Propane to Propene in the Presence of CO_2. *Stud. Surf. Sci. Catal.* **2007**, *170*, 1072−1079.
(142) Zhang, F.; Miao, C.; Yue, Y.; Hua, W.; Gao, Z. Dehydrogenation of Propane to Propylene in the Presence of CO_2 over Steaming-Treated HZSM-5 Supported ZnO. *Chin. J. Chem.* **2012**, *30*, 929−934.
(143) Ren, Y.; Zhang, F.; Hua, W.; Yue, Y.; Gao, Z. ZnO Supported on High Silica HZSM-5 as New Catalysts for Dehydrogenation of Propane to Propene in the Presence of CO_2. *Catal. Today* **2009**, *148*, 316−322.
(144) Ren, Y.; Hua, W.; Yue, Y.; Gao, Z. Dehydrogenation of Propane to Propene over Phosphorus-modified HZSM-5 Supported Ga_2O_3. *React. Kinet. Catal. Lett.* **2008**, *95*, 113−122.
(145) Chu, P. (Mobil Oil Corporation, New York)Silico-Crystal Method of Preparing Same and Catalytic Conversion Therewith. U.S. Patent 4,397,827, 1983.
(146) Zhao, G.; Teng, J.; Zhang, Y.; Xie, Z.; Yue, Y.; Chen, Q.; Tang, Y. Synthesis of ZSM-48 Zeolites and Their Catalytic Performance in C_4-Olefin Cracking Reactions. *Appl. Catal., A* **2006**, *299*, 167−174.
(147) Zhu, Q.; Takiguchi, M.; Setoyama, T.; Yokoi, T.; Kondo, J. N.; Tatsumi, T. Oxidative Dehydrogenation of Propane with CO_2 Over Cr/H[B]MFI Catalysts. *Catal. Lett.* **2011**, *141*, 670−677.
(148) Guisnet, M.; Gnep, N. S.; Alario, F. Aromatization of Short Chain Alkanes on Zeolite Catalysts. *Appl. Catal., A* **1992**, *89*, 1−30.
(149) Ren, Y.; Wang, J.; Hua, W.; Yue, Y.; Gao, Z. Ga_2O_3/HZSM-48 for Dehydrogenation of Propane: Effect of Acidity and Pore Geometry of Support. *J. Ind. Eng. Chem.* **2012**, *18*, 731−736.
(150) Shimada, H.; Akazawa, T.; Ikenaga, N.-o.; Suzuki, T. Dehydrogenation of Isobutane to Isobutene with Iron-Loaded Activated Carbon Catalyst. *Appl. Catal., A* **1998**, *168*, 243−250.
(151) Sugino, M.-o.; Shimada, H.; Turuda, T.; Miura, H.; Ikenaga, N.; Suzuki, T. Oxidative Dehydrogenation of Ethylbenzene with Carbon Dioxide. *Appl. Catal., A* **1995**, *121*, 125−137.
(152) Badstube, T.; Papp, H.; Kustrowski, P.; Dziembaj, R. Oxidative Dehydrogenation of Ethylbenzene with Carbon Dioxide on Alkali-Promoted Fe/Active Carbon Catalysts. *Catal. Lett.* **1998**, *55*, 169−172.
(153) Badstube, T.; Papp, H.; Dziembaj, R.; Kustrowski, P. Screening of Catalysts in the Oxidative Dehydrogenation of Ethylbenzene with Carbon Dioxide. *Appl. Catal., A* **2000**, *204*, 153−165.
(154) Michorczyk, P.; Kustrowski, P.; Chmielarz, L.; Ogonowski, J. Influence of Redox Properties on the Activity of Iron Oxide Catalysts in Dehydrogenation of Propane with CO_2. *React. Kinet. Catal. Lett.* **2004**, *82*, 121−130.
(155) Gomez, E.; Xie, Z.; Chen, J. G. The Effects of Bimetallic Interactions for CO_2-Assisted Oxidative Dehydrogenation and Dry Reforming of Propane. *AIChE J.* **2019**, *65*, No. e16670.
(156) Solymosi, F.; Szoke, A.; Cserenyi, J. Conversion of Methane to Benzene over Mo_2C and Mo_2C/ZSM-5 Catalysts. *Catal. Lett.* **1996**, *39*, 157−161.
(157) Solymosi, F.; Cserenyi, J.; Szoke, A.; Bansagi, T.; Oszko, A. Aromatization of Methane over Supported and Unsupported Mo-Based Catalysts. *J. Catal.* **1997**, *165*, 150−161.
(158) Solymosi, F.; Nemeth, R. The Oxidative Dehydrogenation of Ethane with CO_2 over Mo_2C/SiO_2 Catalyst. *Catal. Lett.* **1999**, *62*, 197−200.
(159) Solymosi, F.; Németh, R.; Oszkó, A. The Oxidative Dehydrogenation of Propane with CO_2 over Supported Mo_2C Catalyst. *Stud. Surf. Sci. Catal.* **2001**, *136*, 339−344.
(160) Sullivan, M. M.; Bhan, A. Effects of Oxygen Coverage on Rates and Selectivity of Propane-CO_2 Reactions on Molybdenum Carbide. *J. Catal.* **2018**, *357*, 195−205.
(161) Solymosi, F.; Tolmacsov, P.; Kedves, K. CO_2 Reforming of Propane over Supported Rh. *J. Catal.* **2003**, *216*, 377−385.
(162) Solymosi, F.; Tolmacsov, P. Decomposition of Propane and Its Reaction with CO_2 over Alumina-Supported Pt Metals. *Catal. Lett.* **2002**, *83*, 183−186.
(163) Tóth, A.; Halasi, G.; Bánsági, T.; Solymosi, F. Reactions of Propane with CO_2 over Au Catalysts. *J. Catal.* **2016**, *337*, 57−64.
(164) Pradhan, S.; Upham, D. C.; Metiu, H.; McFarland, E. W. Partial Oxidation of Propane with CO_2 on Ru Doped Catalysts. *Catal. Sci. Technol.* **2016**, *6*, 5483−5493.
(165) Sharma, S.; Hilaire, S.; Vohs, J. M.; Gorte, R. J.; Jen, H. W. Evidence for Oxidation of Ceria by CO_2. *J. Catal.* **2000**, *190*, 199−204.
(166) Valenzuela, R. X.; Bueno, G.; Solbes, A.; Sapiña, F.; Martínez, E.; Cortés Corberán, V. C. Nanostructured Ceria-Based Catalysts for Oxydehydrogenation of Ethane with CO_2. *Top. Catal.* **2001**, *15*, 181−188.
(167) Zhang, L.; Wu, Z.; Nelson, N. C.; Sadow, A. D.; Slowing, I. I.; Overbury, S. H. Role of CO_2 As A Soft Oxidant for Dehydrogenation of Ethylbenzene to Styrene over A High-Surface-Area Ceria Catalyst. *ACS Catal.* **2015**, *5*, 6426−6435.
(168) Kovacevic, M.; Agarwal, S.; Mojet, B. L.; Ommen, J. G. v.; Lefferts, L. The Effects of Morphology of Cerium Oxide Catalysts for Dehydrogenation of Ethylbenzene to Styrene. *Appl. Catal., A* **2015**, *505*, 354−364.
(169) Demoulin, O.; Navez, M.; Mugabo, J. L.; Ruiz, P. The Oxidizing Role of CO_2 at Mild Temperature on Ceria-Based Catalysts. *Appl. Catal., B* **2007**, *70*, 284−293.
(170) Wang, T.; Guan, X.; Lu, H.; Liu, Z.; Ji, M. Nanoflake-Assembled Al_2O_3-Supported CeO_2-ZrO_2 As An Efficient Catalyst for Oxidative Dehydrogenation of Ethylbenzene with CO_2. *Appl. Surf. Sci.* **2017**, *398*, 1−8.
(171) Nowicka, E.; Reece, C.; Althahban, S. M.; Mohammed, K. M. H.; Kondrat, S. A.; Morgan, D. J.; He, Q.; Willock, D. J.; Golunski, S.; Kiely, C. J.; Hutchings, G. J. Elucidating the Role of CO_2 in the Soft Oxidative Dehydrogenation of Propane over Ceria-Based Catalysts. *ACS Catal.* **2018**, *8*, 3454−3468.

(172) Liu, Y.; Li, Z.; Lu, J.; Fan, K.-N. Periodic Density Functional Theory Study of Propane Dehydrogenation over Perfect Ga_2O_3(100) Surface. *J. Phys. Chem. C* **2008**, *112*, 20382−20392.
(173) Nakagawa, K.; Kajita, C.; Ikenaga, N.-o.; Suzuki, T.; Kobayashi, T.; Nishitani-Gamo, M.; Ando, T. The Role of Chemisorbed Oxygen on Diamond Surfaces for the Dehydrogenation of Ethane in the Presence of Carbon Dioxide. *J. Phys. Chem. B* **2003**, *107*, 4048−4056.
(174) Dury, F.; Gaigneaux, E. M.; Ruiz, P. The Active Role of CO_2 at Low Temperature in Oxidation Processes: The Case of the Oxidative Dehydrogenation of Propane on $NiMoO_4$ Catalysts. *Appl. Catal., A* **2003**, *242*, 187−203.
(175) Takahara, I.; Saito, M.; Inaba, M.; Murata, K. Dehydrogenation of Propane over A Silica-Supported Vanadium Oxide Catalyst. *Catal. Lett.* **2005**, *102*, 201−205.
(176) Takahara, I.; Saito, M.; Inaba, M.; Murata, K. Effects of Pre-Treatment of A Silica-Supported Gallium Oxide Catalyst with H_2 on Its Catalytic Performance for Dehydrogenation of Propane. *Catal. Lett.* **2004**, *96*, 29−32.
(177) Rozanska, X.; Kondratenko, E.; Sauer, J. Oxidative Dehydrogenation of Propane: Differences between N_2O and O_2 in the Reoxidation of Reduced Vanadia Sites and Consequences for Selectivity. *J. Catal.* **2008**, *256*, 84−94.
(178) Perez-Ramirez, J.; Gallardo-Llamas, A. Framework Composition Effects on the Performance of Steam-Activated FeMFI Zeolites in the N_2O-Mediated Propane Oxidative Dehydrogenation to Propylene. *J. Phys. Chem. B* **2005**, *109*, 20529−20538.
(179) Kondratenko, E.; Cherian, M.; Baerns, M.; Su, D.; Schlogl, R.; Wang, X.; Wachs, I. Oxidative Dehydrogenation of Propane over V/MCM-41 Catalysts: Comparison of O_2 and N_2O as Oxidants. *J. Catal.* **2005**, *234*, 131−142.
(180) Gallardo-Llamas, A.; Mirodatos, C.; Perez-Ramirez, J. Cyclic Process for Propylene Production via Oxidative Dehydrogenation of Propane with N_2O over FeZSM_5. *Ind. Eng. Chem. Res.* **2005**, *44*, 455−462.
(181) Pérez-Ramírez, J.; Gallardo-Llamas, A. Impact of the Preparation Method and Iron Impurities in Fe-ZSM-5 Zeolites for Propylene Production via Oxidative Dehydrogenation of Propane with N_2O. *Appl. Catal., A* **2005**, *279*, 117−123.
(182) Pérez-Ramírez, J.; Gallardo-Llamas, A. N_2O-Mediated Propane Oxidative Dehydrogenation over Steam-Activated Iron Zeolites. *J. Catal.* **2004**, *223*, 382−388.
(183) Pérez-Ramírez, J.; Gallardo-Llamas, A.; Daniel, C.; Mirodatos, C. N_2O-Mediated Propane Oxidative Dehydrogenation over Fe-Zeolites. TEOM Studies for Continuous Propylene Production in A Cyclically-Operated Reactor. *Chem. Eng. Sci.* **2004**, *59*, 5535−5543.
(184) Dury, F.; Centeno, M. A.; Gaigneaux, E. M.; Ruiz, P. Interaction of N_2O (as Gas Dope) with Nickel Molybdate Catalysts during the Oxidative Dehydrogenation of Propane to Propylene. *Appl. Catal., A* **2003**, *247*, 231−246.
(185) Dury, F.; Centeno, M. A.; Gaigneaux, E. M.; Ruiz, P. An Attempt to Explain the Role of CO_2 and N_2O as Gas Dopes in the Feed in the Oxidative Dehydrogenation of Propane. *Catal. Today* **2003**, *81*, 95−105.
(186) Kondratenko, E. V.; Ovsitser, O.; Radnik, J.; Schneider, M.; Kraehnert, R.; Dingerdissen, U. Influence of Reaction Conditions on Catalyst Composition and Selective/Non-Selective Reaction Pathways of the ODP Reaction over V_2O_3, VO_2 and V_2O_5 with O_2 and N_2O. *Appl. Catal., A* **2007**, *319*, 98−110.
(187) Held, A.; Kowalska-Kuś, J.; Nowińska, K. Propane-to-Propene Oxide Oxidation on Silica-Supported Vanadium Catalysts with N_2O as An Oxidant. *J. Catal.* **2016**, *336*, 23−32.
(188) Kondratenko, E. V.; Baerns, M. Catalytic Oxidative Dehydrogenation of Propane in the Presence of O_2 and N_2O - the Role of Vanadia Distribution and Oxidant Activation. *Appl. Catal., A* **2001**, *222*, 133−143.
(189) Ovsitser, O.; Cherian, M.; Kondratenko, E. V. In-Situ UV/vis and Transient Isotopic Analysis of the Role of Oxidizing Agent in the Oxidative Dehydrogenation of Propane over Silica-Supported Vanadia Catalysts. *J. Phys. Chem. C* **2007**, *111*, 8594−8602.
(190) Kondratenko, E. V.; Cherian, M.; Baerns, M. Oxidative Dehydrogenation of Propane over Differently Structured Vanadia-based Catalysts in the Presence of O_2 and N_2O. *Catal. Today* **2006**, *112*, 60−63.
(191) Demoulin, O.; Dury, F.; Navez, M.; Gaigneaux, E. M.; Ruiz, P. Modification of Active Catalytic Sites with N_2O and CO_2 As Gas Promoters during Oxidation Reactions. *Catal. Today* **2004**, *91−92*, 27−31.
(192) Kaddouri, A. CH Bond Activation in the Presence or Absence of Oxygen or Nitrous Oxide. *React. Kinet. Catal. Lett.* **2004**, *82*, 401−409.
(193) Demoulin, O.; Seunier, I.; Dury, F.; Navez, M.; Rachwalik, R.; Sulikowski, B.; Gonzalez-Carrazan, S. R.; Gaigneaux, E. M.; Ruiz, P. Modulation of Selective Sites by Introduction of N_2O, CO_2 and H_2 as Gaseous Promoters into the Feed during Oxidation Reactions. *Catal. Today* **2005**, *99*, 217−226.
(194) Barbaux, Y.; Elamrani, A.; Bonnelle, J. P. Catalytic Oxidation of Methane on MoO_3-SiO_2: Mechanism of Oxidation with O_2 and N_2O Studied by Surface Potential Measurements. *Catal. Today* **1987**, *1*, 147−156.
(195) Vereshchagin, S. N.; Kirik, N. P.; Shishkina, N. N.; Morozov, S. V.; Shakirov, M. M.; Mamatyuk, V. I.; Anshits, A. G. Hydrocarbon Conversion on ZSM-5 in the Presence of N_2O: Relative Reactivity and Routes of Product Formation Studied by GC-MS and ^{13}C NMR. *J. Mol. Catal. A: Chem.* **2000**, *158*, 377−380.
(196) Sanchezgalofre, O.; Segura, Y.; Perezramirez, J. Deactivation and Regeneration of Iron-Containing MFI Zeolites in Propane Oxidative Dehydrogenation by N_2O. *J. Catal.* **2007**, *249*, 123−133.
(197) Kondratenko, E. V.; Pérez-Ramírez, J. Oxidative Functionalization of Propane over FeMFI Zeolites. *Appl. Catal., A* **2004**, *267*, 181−189.
(198) Nowińska, K.; Wącław, A.; Izbińska, A. Propane Oxydehydrogenation over Transition Metal Modified Zeolite ZSM-5. *Appl. Catal., A* **2003**, *243*, 225−236.
(199) Ates, A.; Hardacre, C.; Goguet, A. Oxidative Dehydrogenation of Propane with N_2O over Fe-ZSM-5 and Fe-SiO_2: Influence of the Iron Species and Acid Sites. *Appl. Catal., A* **2012**, *441−442*, 30−41.
(200) Bulanek, R.; Novoveska, K. Oxidative Dehydrogenation of Propane by Nitrous Oxide and/or Oxygen over Co Beta Zeolite. *React. Kinet. Catal. Lett.* **2003**, *80*, 337−343.
(201) Sathu, N. K.; Sazama, P.; Valtchev, V.; Bernauer, B.; Sobalik, Z. Oxidative Dehydrogenation of Propane over Fe-BEA Catalysts. *Stud. Surf. Sci. Catal.* **2008**, *174*, 1127−1130.
(202) Bulánek, R.; Wichterlová, B.; Novoveská, K.; Kreibich, V. Oxidation of Propane with Oxygen and/or Nitrous Oxide over Fe-ZSM-5 with Low Iron Concentrations. *Appl. Catal., A* **2004**, *264*, 13−22.
(203) Pérez-Ramírez, J.; Kondratenko, E. V. Steam-Activated FeMFI Zeolites as Highly Efficient Catalysts for Propane and N_2O Valorisation via Oxidative Conversions. *Chem. Commun.* **2003**, 2152−3.
(204) Wu, G.; Hei, F.; Guan, N.; Li, L. Oxidative Dehydrogenation of Propane with Nitrous Oxide over Fe-MFI Prepared by Ion-Exchange: Effect of Acid Post-Treatments. *Catal. Sci. Technol.* **2013**, *3*, 1333−1342.
(205) Zhu, Q; Mojet, B.L.; Janssen, R.A.J.; Hensen, E.J.M.; van Grondelle, J.; Magusin, P.C.M.M.; van Santen, R.A. N_2O Decomposition over Fe/ZSM-5: Effect of High-Temperature Calcination and Steaming. *Catal. Lett.* **2002**, *81*, 205−212.
(206) Roy, P.; Prins, R.; Pirngruber, G. The Effect of Pretreatment on the Reactivity of Fe-ZSM-5 Catalysts for N_2O Decomposition: Dehydroxylation vs. Steaming. *Appl. Catal., B* **2008**, *80*, 226−236.
(207) Pérez-Ramírez, J.; Mul, G.; Kapteijn, F.; Moulijn, J. A.; Overweg, A. R.; Doménech, A.; Ribera, A.; Arends, I. W. C. E. Physicochemical Characterization of Isomorphously Substituted FeZSM-5 during Activation. *J. Catal.* **2002**, *207*, 113−126.

(208) Kondratenko, E. V.; Perez-Ramirez, J. Mechanism and Kinetics of Direct N2O Decomposition over Fe-MFI Zeolites with Different Iron Speciation from Temporal Analysis of Products. *J. Phys. Chem. B* **2006**, *110*, 22586−22595.
(209) Pieterse, J. A. Z.; Booneveld, S.; Brink, R. W. v. d. Evaluation of Fe-Zeolite Catalysts Prepared by Different Methods for the Decomposition of N_2O. *Appl. Catal., B* **2004**, *51*, 215−228.
(210) Pérez-Ramírez, J. Active Iron Sites Associated with the Reaction Mechanism of N2O Conversions over Steam-Activated FeMFI Zeolites. *J. Catal.* **2004**, *227*, 512−522.
(211) Kowalska-Kuś, J.; Held, A.; Nowińska, K. Oxydehydrogenation of Ethane and Propane over Alkaline Metal Modified Fe-ZSM-5 Zeolites. *Catal. Lett.* **2010**, *136*, 199−208.
(212) Wei, W.; Moulijn, J. A.; Mul, G. FAPO and Fe-TUD-1: Promising Catalysts for N_2O Mediated Selective Oxidation of Propane? *J. Catal.* **2009**, *262*, 1−8.
(213) Arinaga, A. M.; Liu, S.; Marks, T. J. Oxidative Dehydrogenation of Propane over Transition Metal Sulfides Using Sulfur as An Alternative Oxidant. *Catal. Sci. Technol.* **2020**, *10*, 6840−6848.
(214) Jazayeri, S. M.; Karimzadeh, R. Experimental Investigation of Initial Coke Formation over Stainless Steel, Chromium, and Iron in Thermal Cracking of Ethane with Hydrogen Sulfide as an Additive. *Energy Fuels* **2011**, *25*, 4235−4247.
(215) Reyniers, M.-F. S. G.; Froment, G. F. Influence of Metal Surface and Sulfur Addition on Coke Deposition in the Thermal Cracking of Hydrocarbons. *Ind. Eng. Chem. Res.* **1995**, *34*, 773−785.
(216) Wang, J.; Reyniers, M.-F.; Marin, G. B. Influence of Dimethyl Disulfide on Coke Formation during Steam Cracking of Hydrocarbons. *Ind. Eng. Chem. Res.* **2007**, *46*, 4134−4148.
(217) Farag, H.; Sakanishi, K.; Kouzu, M.; Matsumura, A.; Sugimoto, Y.; Saito, I. Dual Character of H_2S as Promoter and Inhibitor for Hydrodesulfurization of Dibenzothiophene. *Catal. Commun.* **2003**, *4*, 321−326.
(218) Sharma, L.; Upadhyay, R.; Rangarajan, S.; Baltrusaitis, J. Inhibitor, Co-Catalyst, or Co-Reactant? Probing the Different Roles of H_2S during CO_2 Hydrogenation on the MoS_2 Catalyst. *ACS Catal.* **2019**, *9*, 10044−10059.
(219) Brémaud, M.; Vivier, L.; Pérot, G.; Harlé, V.; Bouchy, C. Hydrogenation of Olefins over Hydrotreating Catalysts Promotion Effect on the Activity and on the Involvement of H_2S in the Reaction. *Appl. Catal., A* **2005**, *289*, 44−50.
(220) Wang, G.; Gao, C.; Zhu, X.; Sun, Y.; Li, C.; Shan, H. Isobutane Dehydrogenation over Metal (Fe, Co, and Ni) Oxide and Sulfide Catalysts: Reactivity and Reaction Mechanism. *ChemCatChem* **2014**, *6*, 2305−2314.
(221) Wang, G.; Meng, Z.; Liu, J.; Li, C.; Shan, H. Promoting Effect of Sulfur Addition on the Catalytic Performance of Ni/$MgAl_2O_4$ Catalysts for Isobutane Dehydrogenation. *ACS Catal.* **2013**, *3*, 2992−3001.
(222) Wang, G.; Li, C.; Shan, H. Highly Efficient Metal Sulfide Catalysts for Selective Dehydrogenation of Isobutane to Isobutene. *ACS Catal.* **2014**, *4*, 1139−1143.
(223) Watanabe, R.; Hirata, N.; Miura, K.; Yoda, Y.; Fushimi, Y.; Fukuhara, C. Formation of Active Species for Propane Dehydrogenation with Hydrogen Sulfide Co-Feeding over Transition Metal Catalyst. *Appl. Catal., A* **2019**, *587*, 117238.
(224) Sun, Y.; Wu, Y.; Tao, L.; Shan, H.; Wang, G.; Li, C. Effect of Pre-Reduction on the Performance of Fe_2O_3/Al_2O_3 Catalysts in Dehydrogenation of Propane. *J. Mol. Catal. A: Chem.* **2015**, *397*, 120−126.
(225) Sun, Y.-n.; Tao, L.; You, T.; Li, C.; Shan, H. Effect of Sulfation on the Performance of Fe_2O_3/Al_2O_3 Catalyst in Catalytic Dehydrogenation of Propane to Propylene. *Chem. Eng. J.* **2014**, *244*, 145−151.
(226) Sun, Y.-n.; Gao, Y.-n.; Wu, Y.; Shan, H.; Wang, G.; Li, C. Effect of Sulfate Addition on the Performance of Co/Al_2O_3 Catalysts in Catalytic Dehydrogenation of Propane. *Catal. Commun.* **2015**, *60*, 42−45.
(227) Sun, Y.; Wu, Y.; Shan, H.; Wang, G.; Li, C. Studies on the Promoting Effect of Sulfate Species in Catalytic Dehydrogenation of Propane over Fe_2O_3/Al_2O_3 Catalysts. *Catal. Sci. Technol.* **2015**, *5*, 1290−1298.
(228) Watanabe, R.; Hirata, N.; Fukuhara, C. Active Species of Sulfated Metal Oxide Catalyst for Propane Dehydrogenation. *J. Jpn. Pet. Inst.* **2017**, *60*, 223−231.
(229) Haag, W. O.; Miale, J. N. Oxidative Dehydrogenation of Paraffins. US 3787517, 1974.
(230) Legendre, O. Catalytic Conversion of Alkanes to Alkenes. US 0092784 A1, 2004.
(231) Nikolaevich, K. N.; Nikolaevna, K. O. g.; Mikhajlovna, N. V.; Valentinovna, G. L.; Alekandrovich, L. V. Method of Production of Olefins. RU 2280021 C1. 2005.
(232) Gendre, O. L. Oxidative Catalytic Conversion of Alkanes into Alkenes in the Presence of Sulfur-Containing Compounds. EP 1136467 A1, 2000.
(233) Andre, L.; Lohr, T. L. Dehydrogenation of Aliphatic Hydrocarbons Using Sulfur. FR 1487433 A, 1967.
(234) Marks, T. J. Oxidative Dehydrogenation of Alkanes to Alkenes Using Sulfur as An Oxidant. WO 036923 A1, 2020.
(235) Tischler, L. G.; Wing, M. S. Process for Dehydrogenation of Propane. US 3773850, 1973.
(236) Porchey, D. V.; Royer, D. J. H_2S Modified Dehydrogenation of Lower Alkanes. US 3803260 A, 1974.
(237) Resasco, D. E.; Marcus, B. K.; Huang, C. S.; Durante, V. A. Isobutane Dehydrogenation over Sulfided Nickel Catalysts. *J. Catal.* **1994**, *146*, 40−55.
(238) Rennard, R. J.; Freel, J. The Role of Sulfur in Deactivation of Pt/$MgAl_2O_4$ for Propane Dehydrogenation. *J. Catal.* **1986**, *98*, 235−244.
(239) Wang, H.-Z.; Zhang, W.; Jiang, J.-W.; Sui, Z.-J.; Zhu, Y.-A.; Ye, G.-H.; Chen, D.; Zhou, X.-G.; Yuan, W.-K. The Role of H_2S Addition on Pt/Al_2O_3 Catalyzed Propane Dehydrogenation: A Mechanistic Study. *Catal. Sci. Technol.* **2019**, *9*, 867−876.
(240) Clark, P. D.; Dowling, N. I.; Liu, S. Ethylene Manufacture by Partial Oxidation with Sulfur. *J. Sulfur Chem.* **2010**, *31*, 479−491.
(241) Adams, C. R. Catalytic Oxidations with Sulfur Dioxide I. Exploratory Studies. *J. Catal.* **1968**, *11*, 96−112.
(242) Ushkov, S. B.; Osipova, Z. G.; Sokolovskii, V. D. Propane Dehydrogenation by SO_2 in the Presence of Carbon. *React. Kinet. Catal. Lett.* **1988**, *36*, 97−102.
(243) Osipova, Z. G.; Ushkov, S. B.; Sokolovskii, V. D.; Kalinkin, A. V. Selective Catalytic Oxidation of Propane By Sulphur Dioxide. *Stud. Surf. Sci. Catal.* **1990**, *55*, 527−535.
(244) Danilova, I. G.; Ivanova, A. S. Role of Silica-Alumina Catalyst Texture in the Reaction of Propane Oxidative Dehydrogenation in the Presence of Sulfur Dioxide. *Kinet. Catal.* **2000**, *41*, 566−571.
(245) Danilova, I. G.; Paukshtis, E. A.; Kalinkin, A. V.; Chuvilin, A. L.; Litvak, G. S.; Altynnikov, A. A.; Anufrienko, V. F. Catalytic and Physicochemical Properties of Oxidative Condensation Products in the Oxidative Dehydrogenation of Propane by Sulfur Dioxide on SiO_2. *Kinet. Catal.* **2002**, *43*, 698−710.
(246) Zichittella, G.; Hemberger, P.; Holzmeier, F.; Bodi, A.; Perez-Ramirez, J. Operando Photoelectron Photoion Coincidence Spectroscopy Unravels Mechanistic Fingerprints of Propane Activation by Catalytic Oxyhalogenation. *J. Phys. Chem. Lett.* **2020**, *11*, 856−863.
(247) Scharfe, M.; Zichittella, G.; Paunović, V.; Pérez-Ramírez, J. Ceria in Halogen Chemistry. *Chin. J. Catal.* **2020**, *41*, 915−927.
(248) Zhang, H.-M.; Fan, Q.-Y.; Zhang, Q.-H.; Kang, J.-C.; Wang, Y.; Cheng, J. Understanding Catalytic Mechanisms of Alkane Oxychlorination from the Perspective of Energy Levels. *J. Phys. Chem. C* **2020**, *124*, 6070−6077.
(249) Zichittella, G.; Aellen, N.; Paunovic, V.; Amrute, A. P.; Perez-Ramirez, J. Olefins from Natural Gas by Oxychlorination. *Angew. Chem., Int. Ed.* **2017**, *56*, 13670−13674.
(250) Paunovic, V.; Lin, R.; Scharfe, M.; Amrute, A. P.; Mitchell, S.; Hauert, R.; Perez-Ramirez, J. Europium Oxybromide Catalysts for

Efficient Bromine Looping in Natural Gas Valorization. *Angew. Chem., Int. Ed.* **2017**, *56*, 9791−9795.
(251) Paunovic, V.; Zichittella, G.; Moser, M.; Amrute, A. P.; Perez-Ramirez, J. Catalyst Design for Natural-Gas Upgrading through Oxybromination Chemistry. *Nat. Chem.* **2016**, *8*, 803−809.
(252) Zichittella, G.; Scharfe, M.; Puertolas, B.; Paunovic, V.; Hemberger, P.; Bodi, A.; Szentmiklosi, L.; Lopez, N.; Perez-Ramirez, J. Halogen-Dependent Surface Confinement Governs Selective Alkane Functionalization to Olefins. *Angew. Chem., Int. Ed.* **2019**, *58*, 5877−5881.
(253) Schweizer, A. E.; Jones, M. E.; Hickman, D. A. Oxidative Halogenation and Optional Dehydrogenation of C_{3+} Hydrocarbons. US 0158110 A1, 2004.
(254) Testova, N. V.; Shalygin, A. S.; Kaichev, V. V.; Glazneva, T. S.; Paukshtis, E. A.; Parmon, V. N. Oxidative Dehydrogenation of Propane by Molecular Chlorine. *Appl. Catal., A* **2015**, *505*, 441−446.
(255) Kumar, C. P.; Gaab, S.; Müller, T. E.; Lercher, J. A. Oxidative Dehydrogenation of Light Alkanes on Supported Molten Alkali Metal Chloride Catalysts. *Top. Catal.* **2008**, *50*, 156−167.
(256) Gärtner, C. A.; van Veen, A. C.; Lercher, J. A. Oxidative Dehydrogenation of Ethane: Common Principles and Mechanistic Aspects. *ChemCatChem* **2013**, *5*, 3196−3217.
(257) Sugiyama, S.; Fukuda, N.; Hayashi, H. Effect of Tetrachloromethane on Redox Behaviors of Copper(II) Oxide in the Oxidative Dehydrogenation of Propane. *Catal. Lett.* **2002**, *78*, 139−143.
(258) Sugiyama, S.; Iizuka, Y.; Nitta, E.; Hayashi, H.; Moffat, J. B. Role of Tetrachloromethane as a Gas-Phase Additive in the Oxidative Dehydrogenation of Propane over Cerium Oxide. *J. Catal.* **2000**, *189*, 233−237.
(259) Sugiyama, S.; Kastuma, K.; Fukuda, N.; Shono, T.; Moriga, T.; Hayashi, H. Effect of the Phase Transition of Iron (III) Oxide on the Oxidative Dehydrogenation of Propane in the Presence and Absence of Tetrachloromethane. *Catal. Commun.* **2001**, *2*, 285−290.
(260) Kim, G. H.; Jung, K.-D.; Kim, W.-I.; Um, B.-H.; Shin, C.-H.; Oh, K.; Koh, H. L. Effect of Oxychlorination Treatment on the Regeneration of Pt-Sn/Al_2O_3 Catalyst for Propane Dehydrogenation. *Res. Chem. Intermed.* **2016**, *42*, 351−365.
(261) Nager, M. Dehydrogenation Process. US 3080435, 1963.
(262) Nager, M. Manufacture of Aromatic Hydrocarbons. US 3168584, 1965.
(263) Upham, D. C.; Gordon, M. J.; Metiu, H.; McFarland, E. W. Halogen-Mediated Oxidative Dehydrogenation of Propane Using Iodine or Molten Lithium Iodide. *Catal. Lett.* **2016**, *146*, 744−754.
(264) Dahl, I. M.; Grande, K.; Jens, K.-J.; Rytter, E.; Slagtern, A. Oxidative Dehydrogenation of Propane in Lithium Hydroxide Lithium Iodide Melts. *Appl. Catal.* **1991**, *77*, 163−174.
(265) Huang, C.; Kristoffersen, H. H.; Gong, X.-Q.; Metiu, H. Reactions of Molten LiI with I_2, H_2O, and O_2 Relevant to Halogen-Mediated Oxidative Dehydrogenation of Alkanes. *J. Phys. Chem. C* **2016**, *120*, 4931−4936.
(266) Latimer, A. A.; Aljama, H.; Kakekhani, A.; Yoo, J. S.; Kulkarni, A.; Tsai, C.; Garcia-Melchor, M.; Abild-Pedersen, F.; Norskov, J. K. Mechanistic Insights into Heterogeneous Methane Activation. *Phys. Chem. Chem. Phys.* **2017**, *19*, 3575−3581.
(267) Tyo, E. C.; Yin, C.; Di Vece, M.; Qian, Q.; Kwon, G.; Lee, S.; Lee, B.; DeBartolo, J. E.; Seifert, S.; Winans, R. E.; Si, R.; Ricks, B.; Goergen, S.; Rutter, M.; Zugic, B.; Flytzani-Stephanopoulos, M.; Wang, Z. W.; Palmer, R. E.; Neurock, M.; Vajda, S. Oxidative Dehydrogenation of Cyclohexane on Cobalt Oxide (Co_3O_4) Nanoparticles: The Effect of Particle Size on Activity and Selectivity. *ACS Catal.* **2012**, *2*, 2409−2423.
(268) Schwarz, H. Chemistry with Methane: Concepts Rather than Recipes. *Angew. Chem., Int. Ed.* **2011**, *50*, 10096−10115.
(269) Latimer, A. A.; Kulkarni, A. R.; Aljama, H.; Montoya, J. H.; Yoo, J. S.; Tsai, C.; Abild-Pedersen, F.; Studt, F.; Norskov, J. K. Understanding Trends in C-H Bond Activation in Heterogeneous Catalysis. *Nat. Mater.* **2017**, *16*, 225−229.
(270) Fu, H.; Liu, Z.-P.; Li, Z.-H.; Wang, W.-N.; Fan, K.-N. Periodic Density Functional Theory Study of Propane Oxidative Dehydrogenation over V_2O_5(001) Surface. *J. Am. Chem. Soc.* **2006**, *128*, 11114−11123.
(271) Fung, V.; Tao, F.; Jiang, D.-e. Understanding Oxidative Dehydrogenation of Ethane on Co_3O_4 Nanorods from Density Functional Theory. *Catal. Sci. Technol.* **2016**, *6*, 6861−6869.
(272) Kwon, S.; Deshlahra, P.; Iglesia, E. Dioxygen Activation Routes in Mars-van Krevelen Redox Cycles Catalyzed by Metal Oxides. *J. Catal.* **2018**, *364*, 228−247.
(273) Wang, S.; Li, S.; Dixon, D. A. Mechanism of Selective and Complete Oxidation in La_2O_3-Catalyzed Oxidative Coupling of Methane. *Catal. Sci. Technol.* **2020**, *10*, 2602−2614.
(274) Kwapien, K.; Paier, J.; Sauer, J.; Geske, M.; Zavyalova, U.; Horn, R.; Schwach, P.; Trunschke, A.; Schlogl, R. Sites for Methane Activation on Lithium-Doped Magnesium Oxide Surfaces. *Angew. Chem., Int. Ed.* **2014**, *53*, 8774−8778.
(275) Schwach, P.; Hamilton, N.; Eichelbaum, M.; Thum, L.; Lunkenbein, T.; Schlögl, R.; Trunschke, A. Structure Sensitivity of the Oxidative Activation of Methane over MgO Model Catalysts: II. Nature of Active Sites and Reaction Mechanism. *J. Catal.* **2015**, *329*, 574−587.
(276) Fan, H.; Feng, J.; Li, X.; Guo, Y.; Li, W.; Xie, K. Ethylbenzene Dehydrogenation to Styrene with CO_2 over V_2O_5 (001): A Periodic Density Functional Theory Study. *Chem. Eng. Sci.* **2015**, *135*, 403−411.
(277) Cheng, Z.; Sherman, B. J.; Lo, C. S. Carbon Dioxide Activation and Dissociation on Ceria (110): A Density Functional Theory Study. *J. Chem. Phys.* **2013**, *138*, 014702.
(278) Yan, B.; Yao, S.; Kattel, S.; Wu, Q.; Xie, Z.; Gomez, E.; Liu, P.; Su, D.; Chen, J. G. Active Sites for Tandem Reactions of CO_2 Reduction and Ethane Dehydrogenation. *Proc. Natl. Acad. Sci. U. S. A.* **2018**, *115*, 8278−8283.
(279) Yan, B.; Yang, X.; Yao, S.; Wan, J.; Myint, M.; Gomez, E.; Xie, Z.; Kattel, S.; Xu, W.; Chen, J. G. Dry Reforming of Ethane and Butane with CO_2 over PtNi/CeO_2 Bimetallic Catalysts. *ACS Catal.* **2016**, *6*, 7283−7292.
(280) Myint, M.; Yan, B.; Wan, J.; Zhao, S.; Chen, J. G. Reforming and Oxidative Dehydrogenation of Ethane with CO_2 as a Soft Oxidant over Bimetallic Catalysts. *J. Catal.* **2016**, *343*, 168−177.
(281) Zuo, Z.; Liu, S.; Wang, Z.; Liu, C.; Huang, W.; Huang, J.; Liu, P. Dry Reforming of Methane on Single-Site Ni/MgO Catalysts: Importance of Site Confinement. *ACS Catal.* **2018**, *8*, 9821−9835.
(282) Porosoff, M. D.; Myint, M. N.; Kattel, S.; Xie, Z.; Gomez, E.; Liu, P.; Chen, J. G. Identifying Different Types of Catalysts for CO_2 Reduction by Ethane through Dry Reforming and Oxidative Dehydrogenation. *Angew. Chem., Int. Ed.* **2015**, *54*, 15501−5.
(283) Kattel, S.; Chen, J. G.; Liu, P. Mechanistic Study of Dry Reforming of Ethane by CO_2 on A Bimetallic PtNi(111) Model Surface. *Catal. Sci. Technol.* **2018**, *8*, 3748−3758.
(284) Gomez, E.; Nie, X.; Lee, J. H.; Xie, Z.; Chen, J. G. Tandem Reactions of CO_2 Reduction and Ethane Aromatization. *J. Am. Chem. Soc.* **2019**, *141*, 17771−17782.
(285) Yamamoto, H.; Chu, H. Y.; Xu, M.; Shi, C.; Lunsford, J. H. Oxidative Coupling of Methane over a Li^+/MgO Catalyst Using N_2O as An Oxidant. *J. Catal.* **1993**, *142*, 325−336.
(286) Thum, L.; Rudolph, M.; Schomäcker, R.; Wang, Y.; Tarasov, A.; Trunschke, A.; Schlögl, R. Oxygen Activation in Oxidative Coupling of Methane on Calcium Oxide. *J. Phys. Chem. C* **2019**, *123*, 8018−8026.
(287) Cornu, D.; Guesmi, H.; Krafft, J.-M.; Lauron-Pernot, H. Lewis Acido-Basic Interactions between CO_2 and MgO Surface: DFT and DRIFT Approaches. *J. Phys. Chem. C* **2012**, *116*, 6645−6654.
(288) Polfus, J. M.; Yildiz, B.; Tuller, H. L.; Bredesen, R. Adsorption of CO_2 and Facile Carbonate Formation on $BaZrO_3$ Surfaces. *J. Phys. Chem. C* **2018**, *122*, 307−314.
(289) Dasireddy, V. D. B. C.; Huš, M.; Likozar, B. Effect of O_2, CO_2 and N_2O on Ni-Mo/Al_2O_3 Catalyst Oxygen Mobility in *n*-Butane Activation and Conversion to 1,3-Butadiene. *Catal. Sci. Technol.* **2017**, *7*, 3291−3302.

(290) Vitillo, J. G.; Bhan, A.; Cramer, C. J.; Lu, C. C.; Gagliardi, L. Quantum Chemical Characterization of Structural Single Fe(II) Sites in MIL-Type Metal-Organic Frameworks for the Oxidation of Methane to Methanol and Ethane to Ethanol. *ACS Catal.* **2019**, *9*, 2870−2879.
(291) Mahyuddin, M. H.; Shiota, Y.; Staykov, A.; Yoshizawa, K. Theoretical Investigation of Methane Hydroxylation over Isoelectronic $[FeO]^{(2+)}$- and $[MnO]^{(+)}$-Exchanged Zeolites Activated by N_2O. *Inorg. Chem.* **2017**, *56*, 10370−10380.
(292) Barona, M.; Ahn, S.; Morris, W.; Hoover, W.; Notestein, J. M.; Farha, O. K.; Snurr, R. Q. Computational Predictions and Experimental Validation of Alkane Oxidative Dehydrogenation by Fe_2M MOF Nodes. *ACS Catal.* **2020**, *10*, 1460−1469.
(293) Pascucci, B. M.; Otero, G. S.; Belelli, P. G.; Branda, M. M. Understanding the Effects of Metal Particle Size on the NO_2 Reduction from A DFT Study. *Appl. Surf. Sci.* **2019**, *489*, 1019−1029.
(294) Gao, X.; Du, X.-s.; Jiang, Y.; Zhang, Y.; Luo, Z.-y.; Cen, K.-f. A DFT Study on the Behavior of NO_2 in the Selective Catalytic Reduction of Nitric Oxides with Ammonia on A V_2O_5 Catalyst Surface. *J. Mol. Catal. A: Chem.* **2010**, *317*, 46−53.
(295) Bai, Y.; Mavrikakis, M. Mechanistic Study of Nitric Oxide Reduction by Hydrogen on Pt(100) (I): A DFT Analysis of the Reaction Network. *J. Phys. Chem. B* **2018**, *122*, 432−443.
(296) Annamalai, L.; Liu, Y.; Deshlahra, P. Selective C−H Bond Activation via NO_x-Mediated Generation of Strong H-Abstractors. *ACS Catal.* **2019**, *9*, 10324−10338.
(297) Zhang, X.; You, R.; Wei, Z.; Jiang, X.; Yang, J.; Pan, Y.; Wu, P.; Jia, Q.; Bao, Z.; Bai, L.; Jin, M.; Sumpter, B.; Fung, V.; Huang, W.; Wu, Z. Radical Chemistry and Reaction Mechanisms of Propane Oxidative Dehydrogenation over Hexagonal Boron Nitride Catalysts. *Angew. Chem., Int. Ed.* **2020**, *59*, 8042−8046.
(298) Zhu, Q.; Wegener, S. L.; Xie, C.; Uche, O.; Neurock, M.; Marks, T. J. Sulfur as A Selective 'Soft' Oxidant for Catalytic Methane Conversion Probed by Experiment and Theory. *Nat. Chem.* **2013**, *5*, 104−109.
(299) Paunović, V.; Pérez-Ramírez, J. Catalytic Halogenation of Methane: A Dream Reaction with Practical Scope? *Catal. Sci. Technol.* **2019**, *9*, 4515−4530.
(300) Ovsitser, O.; Kondratenko, E. V. Similarity and Differences in the Oxidative Dehydrogenation of C_2-C_4 Alkanes over Nano-sized VO_x Species Using N_2O and O_2. *Catal. Today* **2009**, *142*, 138−142.
(301) Woods, M. P.; Mirkelamoglu, B.; Ozkan, U. S. Oxygen and Nitrous Oxide as Oxidants: Implications for Ethane Oxidative Dehydrogenation over Silica-Titania-Supported Molybdenum. *J. Phys. Chem. C* **2009**, *113*, 10112−10119.
(302) Held, A.; Kowalska, J.; Nowińska, K. Nitrous Oxide as An Oxidant for Ethane Oxydehydrogenation. *Appl. Catal., B* **2006**, *64*, 201−208.
(303) López Nieto, J. M.; Dejoz, A.; Vazquez, M. I.; O'Leary, W.; Cunningham, J. Oxidative Dehydrogenation of *n*-Butane on MaO-Supported Vanadium Oxide Catalysts. *Catal. Today* **1998**, *40*, 215−228.
(304) Gomez, E.; Yan, B.; Kattel, S.; Chen, J. G. Carbon Dioxide Reduction in Tandem with Light-Alkane Dehydrogenation. *Nat. Rev. Chem.* **2019**, *3*, 638−649.
(305) Zhu, X.; Imtiaz, Q.; Donat, F.; Müller, C. R.; Li, F. Chemical Looping beyond Combustion—A Perspective. *Energy Environ. Sci.* **2020**, *13*, 772−804.
(306) Wu, T.; Yu, Q.; Roghair, I.; Wang, K.; van Sint Annaland, M. Chemical Looping Oxidative Dehydrogenation of Propane: A Comparative Study of Ga-based, Mo-based, V-based Oxygen Carriers. *Chem. Eng. Process.* **2020**, *157*, 108137.
(307) Neal, L. M.; Yusuf, S.; Sofranko, J. A.; Li, F. Oxidative Dehydrogenation of Ethane: A Chemical Looping Approach. *Energy Technol.* **2016**, *4*, 1200−1208.
(308) Pati, S.; Dewangan, N.; Wang, Z.; Jangam, A.; Kawi, S. Nanoporous Zeolite-A Sheltered Pd-Hollow Fiber Catalytic Membrane Reactor for Propane Dehydrogenation. *ACS Appl. Nano Mater.* **2020**, *3*, 6675−6683.
(309) Wang, Z.; Xu, J.; Pati, S.; Chen, T.; Deng, Y.; Dewangan, N.; Meng, L.; Lin, J. Y. S.; Kawi, S. High H_2 Permeable SAPO-34 Hollow Fiber Membrane for High Temperature Propane Dehydrogenation Application. *AIChE J.* **2020**, *66*, No. e16278.
(310) Wang, Z.; Chen, T.; Dewangan, N.; Li, Z.; Das, S.; Pati, S.; Li, Z.; Lin, J. Y. S.; Kawi, S. Catalytic Mixed Conducting Ceramic Membrane Reactors for Methane Conversion. *React. Chem. Eng.* **2020**, *5*, 1868−1891.
(311) Wang, Z.; Bian, Z.; Dewangan, N.; Xu, J.; Kawi, S. High-Performance Catalytic Perovskite Hollow Fiber Membrane Reactor for Oxidative Propane Dehydrogenation. *J. Membr. Sci.* **2019**, *578*, 36−42.

https://dx.doi.org/10.1021/acscatal.0c03999
ACS Catal. 2021, 11, 2182−2234